REPUBLIC OF TÜRKİYE
YILDIZ TECHNICAL UNIVERSITY
GRADUATE SCHOOL OF SCIENCE AND ENGINEERING

DEVELOPMENT OF LIPOSOMAL HYDROGEL HYBRID SYSTEMS FOR ENCAPSULATION OF PROPOLIS

Öznur SAROĞLU

DOCTOR OF PHILOSOPHY THESIS

Department of Food Engineering

Program of Food Engineering

Supervisor

Assoc. Prof. Dr. Ayşe KARADAĞ

June, 2025

REPUBLIC OF TÜRKİYE

YILDIZ TECHNICAL UNIVERSITY

GRADUATE SCHOOL OF SCIENCE AND ENGINEERING

DEVELOPMENT OF LIPOSOMAL HYDROGEL HYBRID SYSTEMS FOR ENCAPSULATION OF PROPOLIS

A thesis submitted by Öznur SAROĞLU in partial fulfillment of the requirements for the degree of **DOCTOR OF PHILOSOPHY** is approved by the committee on 12.06.2025 in Department of Food Engineering, Food Engineering Program.

Assoc. Prof. Dr. Ayşe KARADAĞ
Yildiz Technical University
Supervisor

Approved By the Examining Committee

Assoc. Prof. Dr. Ayşe KARADAĞ, Supervisor
Yildiz Technical University _____

Prof. Dr. Salih KARASU, Member
Yildiz Technical University _____

Assist. Prof. Dr. Canan Yağmur KARAKAŞ, Member
Yildiz Technical University _____

Prof. Dr. Esra ÇAPANOĞLU GÜVEN, Member
İstanbul Technical University _____

Assoc. Prof. Dr. Gülay ÖZKAN, Member
İstanbul Technical University _____

I hereby declare that I have obtained the required legal permissions during data collection and exploitation procedures, that I have made the in-text citations and cited the references properly, that I haven't falsified and/or fabricated research data and results of the study and that I have abided by the principles of the scientific research and ethics during my Thesis Study under the title of "Development of liposomal hydrogel hybrid systems for encapsulation of food propolis" supervised by my supervisor, Assoc. Prof. Dr. Ayşe KARADAĞ. In the case of a discovery of false statement, I am to acknowledge any legal consequence.

Öznur SAROĞLU

Signature

This work was supported by the project no 120O315 of the Scientific and Technological Research Council of Türkiye (TÜBİTAK).

Dedicated to my family,

ACKNOWLEDGEMENTS

I would like to express my sincere gratitude to my advisor, Assoc. Prof. Dr. Ayşe Karadağ, for her invaluable guidance, profound knowledge, constant support, and encouragement throughout every stage of this thesis. Knowing that I had her support at every difficult moment gave me the strength to continue and complete this study.

I am also deeply grateful to the members of my thesis monitoring committee, Prof. Dr. Esra Çapanoğlu Güven and Prof. Dr. Salih Karasu, for their valuable guidance, constructive feedback, and academic insight throughout the thesis process.

I would like to extend my heartfelt thanks to my dear friend and research assistant, Duygu Özmen, whose emotional support, motivation, and encouragement were invaluable to me. Without her support, completing this thesis would have been much more difficult.

I would like to express my sincere gratitude to Dr. Ruşen Metin Yıldırım for her valuable support and guidance during the thesis. I also wish to thank my colleagues in the KMB-116 laboratory for their help and assistance throughout the experimental work. Furthermore, I would like to sincerely thank my fellow research assistants in the department for their continuous support: Fidan Özge Tıkıloğlu, Hatice Bekiroğlu, Selma Kayacan Çakmakoğlu, Perihan Kübra Akman, Afranur Mitaf, Kader Korkmaz Ediş, Sevda Dere, and Dora Mutlu.

Finally, I am profoundly thankful to my family for their endless support and encouragement, especially to my mother and father, who have always stood by me with unconditional love and patience.

Öznur SAROĞLU

TABLE OF CONTENTS

LIST OF SYMBOLS viii
LIST OF ABBREVIATIONS ix
LIST OF FIGURES xi
LIST OF TABLES xiii
ABSTRACT xiv
ÖZET xvi
1 INTRODUCTION 1
1.1 Propolis 1
1.2 Liposome 4
1.3 Hydrogel 5
1.4 Liposomal Hydrogel Hybrid System 6
1.5 Bioaccessibility and Bioavailability of Bioactive Compounds 9
1.6 Hypothesis 10
1.7 Objective of the Thesis 10
2 MATERIAL AND METHODS 12
2.1 Material 12
2.2 Methods 12
2.2.1 Preparation of Liposomes 12
2.2.2 Mean Particle Size and Zeta Potential Measurements 13
2.2.3 Encapsulation Efficiency of PE in Liposomes 13
2.2.4 Morphology of Samples by SEM, Cryo-TEM, and TEM 14
2.2.5 Preparation of Salep-Xanthan Gum Hydrogel and Liposomal Gel 15
2.2.6 Rheological Properties 16
2.2.7 Texture Profile Analysis (TPA) 18
2.2.8 DSC and FTIR Spectroscopy Analysis 18
2.2.9 Determination of Mucoadhesive Property of Liposomal Gels 18
2.2.10. *In Vitro* Simulated Digestion Analysis 19

2.2.11. Total Phenolic Contents (TPC), Total Flavonoid Contents (TFC), and Antioxidant Activity Assays 20
2.2.12. Analysis of Phenolic Compounds by LC-MS/MS 22
2.2.13. Statistical Analysis 22
3 RESULTS AND DISCUSSION **24**
3.1 Formulation and Characterization of Xanthan-gum Salep Hydrogels and Liposomal Gels 24
3.1.1 Characterization of Liposomes and Liposomal Gels: Particle Size, Zeta Potential, and PDI Analysis 24
3.1.2 Morphological Characterization of Liposomes, Hydrogels, and Liposomal Gels Through TEM, cryo-TEM, and SEM Analysis 26
3.1.3 Rheological Characterization of Hydrogels and Liposomal Gel 30
3.1.4 Texture Profile Analysis 39
3.1.5 Fourier Transform Infrared Spectroscopic (FTIR) Evaluation of Hydrogel and Liposomal Gel Systems 43
3.2 Propolis Incorporation into Liposomes: Formulation Strategy, Characterization 45
3.2.1 Characterization of PE-Loaded Liposomes: Particle Size, Zeta Potential, Morphology, and Encapsulation Efficiency 45
3.3 Liposomal PE-Loaded Xanthan–Salep Hydrogels: Preparation, Characterization, and Bioaccessibility of Phenolics 49
3.3.1 Morphological Characterization of Liposomal Gel Samples 49
3.3.2 Structural and Thermal Characterization of Liposomal Gels by DSC and FTIR 52
3.3.3 Flow Behaviour of Liposomal Gels 55
3.3.4 *In Vitro* Mucoadhesive Properties 59
3.3.5 *In Vitro* Digestion Analysis of Free PE, PE-Loaded Liposome, and Liposomal PE-Loaded Gel 60
4 CONCLUSION **78**
REFERENCES **80**
PUBLICATIONS FROM THE THESIS **98**

LIST OF SYMBOLS

pKa	Acid Dissociation Constant
ω	Angular Velocity
~	Approximately
°C	Celsius
G*	Complex Modulus
K'	Elastic Coefficient
n	Flow Behavior Index
g	Gram
G_0	Initial Storage Modulus
kV	Kilovolt
G''	Loss Modulus
mA	Milliampere
mL	Milliliter
mV	Millivolt
min	Minute
nm	Nanometer
%	Percent
Deff%	Percent Deformation Values
n'	Power Law Exponent
n''	Power Law Exponent
s	Second
G'	Storage Modulus
Ge	The Ratio of The Equilibrium Storage Modulus
k	Thixotropic Rate Constant
K''	Viscous Coefficient

LIST OF ABBREVIATIONS

3-ITT	Three-Interval Thixotropy Test
AMP	Ammonium Phosphatide
ANOVA	Analysis of Variance
BI	Bioaccessibility Index
CAPE	Caffeic Acid Phenethyl Ester
CE	Catechin Equivalent
cryo-TEM	Cryogenic Transmission Electron Microscopy
DLS	Dynamic Light Scattering
DPPH	2,2-diphenyl-1-picrylhydrazyl
DSC	Differential Scanning Calorimetry
EE	Encapsulation Efficiency
FC	Folin-ciocalteu
FRAP	Ferric Reducing Antioxidant Power
FTIR	Fourier-Transform Infrared Spectroscopy
HG	Hydrogel
K	Xanthan Gum
kDA	Kilodalton
LG	Liposomal Gel
LVR	Linear Viscoelastic Region
mm-Hg	Millimetres Of Mercury
PDI	Polydispersity Index
PE	Propolis Extract
rpm	Revolutions Per Minute
S	Salep
SEM	Scanning Electron Microscopy
SGF	Simulated Gastric Fluid

SIF	Simulated Intestinal Fluid
SSF	Simulated Salivary Fluid
T80	Tween 80 (polyoxyethylene Sorbitan Monooleate)
TE	Trolox Equivalent
TEM	Transmission Electron Microscopy
TFC	The Total Flavonoid Content
TPA	Texture Profile Analysis
TPC	Total Phenolic Content
v/v	Volume/volume
w/v	Weight/volume
w/w	Weight/weight

LIST OF FIGURES

Figure 1.1 Chemical structures of main phenolics in poplar-type propolis.....2

F**igure 1.2** Schematic representation of liposome formation(W. Liu, Ye, & Singh, 2015) 4

F**igure 1.3** Illustration of bioactive-loaded liposome integration into hydrogel matrix and subsequent release.....7

F**igure 1.4** Schematic representation of the three key factors determining oral bioavailability: bioaccessibility, absorption, and transformation (J. Chen & Hu, 2020).....9

Figure 2.1 Schematic of the hydrogel and liposomal gel production process 16

Figure 2.2 The schematic diagram of the *in vitro* simulated digestion procedure 20

Figure 3.1 Images of xanthan-salep hydrogels (A) and liposomal gels (B) 25

Figure 3.2 TEM images of liposomes, scale bar = 100 nm. 26

Figure 3.3 SEM images of xanthan-salep hydrogel (A) and liposomal gels (B) ..28

Figure 3.4 Cryo-TEM images of the hydrogel (A) and the liposomal gel (B). 29

Figure 3.5 TEM images of liposomal gels, scale bar = 200 nm 30

Figure 3.6 Viscosity profiles of hydrogels (A) and liposomal gels (B) depending on xanthan-salep concentration.....31

Figure.**3.7**.Dynamic rheological behavior of hydrogels at varying polymer concentrations 32

Figure 3. 8 Dynamic rheological behavior of hydrogels (A) and liposomal gels (B) at varying xanthan-salep concentrations 34

Figure 3.9 3-ITT rheological properties of hydrogels (A) and liposomal gels (B) at varying xanthan-salep concentrations 36

Figure 3.10 Complex modulus of hydrogel (A, B) and liposomal gel (C, D) during heating (10–45°C) and cooling (45–10°C) phases, respectively. 39

Figure 3.11 FTIR spectra of the individual components (lecithin, xanthan gum, salep) and gel systems (hydrogel and liposomal gel). 45

Figure 3.12 Images of empty and PE-loaded (2%, w/v) liposomes.....45

Figure 3.13 TEM images of empty liposomes (L1 and L2; B and D) and PE-loaded liposomes (L1-PE2 and L2-PE2; A and C), formulated with T80 and AMP, respectively.....49

Figure 3.14 PE-loaded and empty liposomal gels incorporated with AMP (A: PE-loaded, B: empty) and T80 (C: PE-loaded, D: empty).....50

Figure 3.15 SEM images of PE-loaded AMP liposomal gel (A-B) and PE-loaded T80 liposomal gel (C-D).....51

Figure 3.16 Cryo-TEM images of PE-loaded (A) and empty (B) AMP-liposomal gels. Scale bar: 100 nm 52

Figure 3.17 FTIR spectra of individual components and liposomal gels: 1. PE, 2. Lecithin, 3. Empty T80-liposomal gel, 4. PE-loaded T80-liposomal gel, 5. Empty AMP-liposomal gel, 6. PE-loFaded AMP-liposomal gel....53

Figure 3.18 DSC thermograms of PE and liposomal gels: 1. PE; 2. PE-loaded AMP- liposomal gel; 3. Empty AMP-liposomal gel; 4. Empty T80-liposomal gel; 5. PE-loaded T80-liposomal gel.....55

Figure 3.19 Viscosity curves of (A) AMP-liposomal gels, (B) T80-liposomal gels. 56

Figure 3.20 Dynamic rheological properties of PE-loaded AMP-(A), T80- (B) liposomal gels, and empty AMP- (C) and T80- (D) liposomal gels...58

Figure 3.21 TEM images of gastric (A) and intestinal (B) digesta of PE-loaded AMP liposomal gel. 75

Figure 3.22 Heat maps showing the concentration profiles of individual phenolic compounds during *in vitro* digestion including the gastric (A) and intestinal (B) phases, as well as their BI (%) values (C).....76

LIST OF TABLES

Table 1.1 Summary of recent studies on liposomal hydrogel systems incorporating bioactive compounds 8

Table 3.1 Mean particle size, zeta potential, and PDI values of liposomes and liposomal gels 24

Table 3.2 Power Law model parameters for hydrogels and liposomal gels 33

Table 3.3 Second-order structural kinetic model parameters for 3-ITT 37

Table 3.4 Texture profile analysis (TPA) results of hydrogel and liposomal gel formulations 41

Table 3.5 Encapsulation efficiency (%), particle size distribution, surface charge (zeta potential), and PDI values of the liposomal formulations..... 47

Table 3.6 Rheological parameters (K′, K″, n′, n″) obtained from the Power Law model for PE-loaded and unloaded liposomal gel formulations..... 57

Table 3.7 *In vitro* mucoadhesion results of liposomal gels..... 60

Table 3.8 LC-MS/MS analysis of phenolic compounds in PE and PE-loaded liposome..... 62

Table 3.9 Effect of *in vitro* digestion on the phenolic compounds of free PE and liposomal PE 65

Table 3.10 Changes in TPC, TFC, and antioxidant activity of free PE and liposomal PE gel during *in vitro* digestion 70

Table 3.11 Changes in individual phenolic compounds of liposomal gel during *in vitro* gastrointestinal digestion..... 72

ABSTRACT

Development of Liposomal Hydrogel Hybrid Systems for Encapsulation of Propolis

Öznur SAROĞLU

Department of Food Engineering

Doctor of Philosophy Thesis

Supervisor: Assoc. Prof. Dr. Ayşe KARADAĞ

Liposomes are widely used as biocompatible and non-toxic carriers for bioactive compounds; however, their low colloidal stability and limited gastrointestinal resistance restrict their efficiency. To address these limitations, a hybrid delivery system was developed by incorporating propolis extract (PE)-loaded liposomes into xanthan gum–salep hydrogels. PE was characterized by LC-MS/MS, identifying major phenolics such as pinocembrin (18.64 ± 0.54 mg/g), galangin (14.36 ± 1.48 mg/g), pinobanksin (14.06 ± 0.98 mg/g), and CAPE (12.66 ± 0.74 mg/g). Liposomes were prepared using phosphatidylcholine with or without food-grade surfactants, polyoxyethylene sorbitan monooleate (T80) and ammonium phosphatide (AMP), and PE was encapsulated at a 2% (w/w) concentration, achieving encapsulation efficiencies ranging from 70.27% to 75.49%. PE loading increased vesicle size from 47.18 nm to 103.41 nm and from 80.97 nm to 179.30 nm for T80- and AMP-based liposomes, respectively. Liposomal gels were produced using various xanthan gum:salep ratios (1:1–3:1, w/w), and their rheological, textural, morphological, thermal (DSC), and chemical (FTIR) properties were evaluated. The K1S3 formulation with surfactant-free

liposomal gel showed an increase in storage modulus (K′) from 47.60 to 70.89 Pa.s^n and in hardness from 317.58 to 353.49 g compared to hydrogel counterparts. AMP-based PE-loaded liposomal gels further increased K′ to 100.74 Pa.s^n. All formulations exhibited solid-like and shear-thinning behavior. The mucoadhesion value was higher in AMP-based liposomal gels (13.38-2.87 g.mm) than in T80-based liposomal gels (8.77-1.51 g.mm), and was further enhanced by PE incorporation. SEM, TEM, and Cryo-TEM confirmed spherical, homogeneously distributed vesicles without aggregation. FTIR analysis revealed interactions between xanthan gum–salep and lecithin. The total bioaccessibility of free PE increased from 1.72% to 185.90% (liposome) and 286.52% (liposomal gel). Vesicles retained their structural integrity in gastric fluid but were disrupted in intestinal fluid. These results demonstrate that liposomal hydrogels effectively overcome the aqueous stability limitations of liposomes and offer a promising strategy to enhance bioactive delivery in functional food and nutraceutical applications.

Keywords: Propolis, liposome, liposomal hydrogel, xanthan gum, salep

ÖZET

Propolis Enkapsülasyonu İçin Lipozomal Hidrojel Hibrit Sistemlerinin Geliştirilmesi

Öznur SAROĞLU

Gıda Mühendisliği Anabilim Dalı

Doktora Tezi

Danışman: Doç. Dr. Ayşe KARADAĞ

Lipozomlar, biyolojik olarak uyumlu ve toksik olmayan yapıları sayesinde biyoaktif bileşenlerin taşınmasında yaygın olarak kullanılan taşıyıcı sistemlerdir; ancak, düşük kolloidal stabiliteleri ve sınırlı gastrointestinal dayanıklılıkları etkinliklerini kısıtlamaktadır. Bu sınırlamaların üstesinden gelmek amacıyla, propolis ekstraktı (PE) yüklü lipozomların ksantan gam–salep hidrojel matrisine entegre edilmesiyle hibrit bir taşıyıcı sistem geliştirilmiştir. PE, LC-MS/MS yöntemiyle karakterize edilmiş ve başlıca fenolik bileşikler olarak pinosembrin (18.64 ± 0.54 mg/g), galangin (14.36 ± 1.48 mg/g), pinobanksin (14.06 ± 0.98 mg/g) ve CAPE (12.66 ± 0.74 mg/g) tanımlanmıştır. Lipozomlar, polietilen glikol sorbitan monooleat (T80) ve amonyum fosfatid (AMP) gibi gıda sınıfı yüzey aktif maddeler ile veya bu maddeler olmadan fosfatidilkolin kullanılarak hazırlanmış ve PE, %2 (w/w) oranında enkapsüle edilmiştir. Enkapsülasyon verimi %70.27 ile %75.49 arasında değişmiştir. PE yüklemesi, T80 bazlı lipozomlar için 47.18 nm'den 103.41 nm'ye, AMP bazlı lipozomlar için ise 80.97 nm'den 179.30 nm'ye olmak üzere vezikül boyutlarını artırmıştır. Lipozomal jeller, çeşitli ksantan gam:salep oranları (1:1–3:1, w/w) ile hazırlanmış ve reolojik,

tekstürel, morfolojik, termal (DSC) ve kimyasal (FTIR) özellikleri değerlendirilmiştir. Yüzey aktif madde içermeyen lipozomal jel içeren K1S3 formülasyonu, karşılık gelen hidrojele kıyasla depolama modülünde (K′) 47.60'tan 70.89 Pa.s^n'ye ve sertlik değerinde 317.58'den 353.49 g'a artış göstermiştir. AMP bazlı PE yüklü lipozomal jellerde bu değer 100.74 Pa.s^n'ye kadar yükselmiştir. Tüm formülasyonlar katı benzeri ve kesme incelmesi gösteren bir reolojik davranış sergilemiştir. Mukoadhezyon değeri, AMP bazlı lipozomal jellerde (13.38-2.87 g.mm), T80 bazlı jellere (8.77-1.51 g.mm) kıyasla daha yüksek bulunmuş ve PE ilavesi ile daha da artmıştır. SEM, TEM ve Cryo-TEM analizleri, küresel şekilli, homojen dağılmış ve agregasyon göstermeyen veziküllerin varlığını doğrulamıştır. FTIR analizi, ksantan gam–salep ve lesitin arasında moleküller arası etkileşimleri ortaya koymuştur. Serbest PE'nin toplam biyoerişilebilirliği %1.72 iken, bu oran lipozomal formülasyonda %185.90'a, lipozomal jelde ise %286.52'ye yükselmiştir. Veziküller mide sıvısında yapısal bütünlüğünü korurken, bağırsak sıvısında bozulmuşlardır. Bu bulgular, lipozomal hidrojel sistemlerinin lipozomların sulu ortamlardaki stabilite sınırlamalarını etkin şekilde aşabildiğini ve biyoaktif bileşenlerin fonksiyonel gıda ve nutrasötik uygulamalarında taşınımı için umut vadeden bir strateji sunduğunu göstermektedir.

Anahtar Kelimeler: Propolis, lipozom, lipozomal hidrojel, ksantan gum, salep

1
INTRODUCTION

1.1 Propolis

Propolis is a naturally occurring resinous complex produced by honeybees (*Apis mellifera L.*) through the collection of plant-derived materials such as exudates and bud secretions, which are then mixed with pollen and salivary enzymes (Tavares et al., 2022). The word "propolis" comes from the Greek terms pro (defense) and polis (city), emphasizing its natural function as a protective material utilized by bees to safeguard the hive (Alvarenga et al., 2021). In addition to acting as a physical barrier by sealing cracks and smoothing the hive interior, bees also use propolis for its antiseptic properties to prevent microbial contamination and help regulate the internal hive temperature. (Anjum et al., 2019). The chemical composition of propolis is highly complex, comprising roughly 50% resin and plant-derived balsam, 30% wax, 10% essential and aromatic oils, 5% pollen, and other organic materials (Balasubramaniam et al., 2025). More than 420 chemical constituents have been identified in propolis samples worldwide, representing a wide range of compounds (Balasubramaniam et al., 2025). Among these, phenolic compounds, particularly flavonoids and phenolic acids, as well as xanthones and terpenoids, have received the greatest attention due to their notable bioactive properties (Tavares et al., 2022). Notably, the phenolic composition of propolis may vary depending on climatic conditions. Temperate propolis, also referred to as poplar-type propolis, is high in aglycone flavonoids, phenolic acids, and their esters, but tropical propolis contains prealkylated derivatives including *p*-coumaric acid and acetophenone, as well as diterpenes and lignans. Furthermore, neotropical propolis has unique chemicals such as polyisoprenyl benzophenones, while Brazilian green

propolis is especially high in artepillin C and chlorogenic acid (Alvarenga et al., 2021). In addition to climatic influences, propolis can also be categorized into seven distinct types according to plant sources and major chemical components: Poplar, Pacific, Green (alecrim), Red, Birch, Clusia, and Mediterranean (Irigoiti et al., 2021).

Poplar-type propolis is characterized by a rich diversity of flavonoids and phenolic acids. The typical flavonoids identified in this type of propolis include flavones and flavonols such as chrysin, tectochrysin, galangin, luteolin, apigenin, quercetin, kaempferol, and isorhamnetin. Additionally, flavanones and flavanoles are also abundant, with representative compounds including pinocembrin, pinostrobin, pinobanksin, and its various esters such as pinobanksin-3-O-acetate, pinobanksin-3-O-propionate, pinobanksin-3-O-butyrate, and pinobanksin-3-O-pentanoate. Other notable flavanones and flavanoles present are 3,7-dihydroxy-5-methoxyflavanone, naringenin, taxifolin, and liquiritigenin.

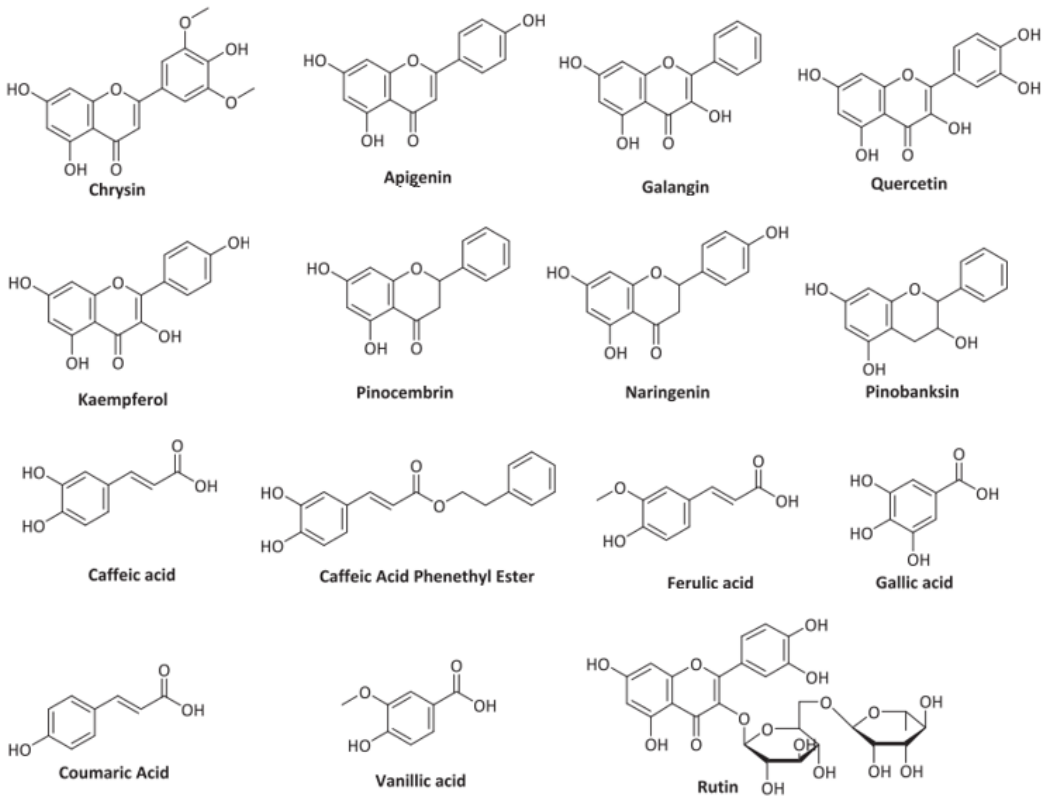

Figure 1. 1 Chemical structures of main phenolics in poplar-type propolis

Regarding phenolic acids and their derivatives, poplar-type propolis typically contain hydroxybenzoic acid derivatives, including gallic acid, gentisic acid, protocatechuic acid, salicylic acid, and vanillic acid. Hydroxycinnamic acid derivatives and their esters are also prevalent, with compounds such as cinnamic acid, caffeic acid, ferulic acid, and *p*-coumaric acid. Furthermore, several caffeic acid esters have been identified, including, caffeic acid phenethyl ester, 3-methyl-2-butenylcaffeate, 2-methyl-2-butenylcaffeate, benzylcaffeate, phenethylcaffeate, cinnamylcaffeate, and p-methoxy-cinnamic acid cinnamyl ester, along with rosmarinic acid (Ghallab et al., 2025).

The rich phenolic composition of propolis contributes to a broad spectrum of biological activities, including antioxidant (Abduh et al., 2024), anti-microbial (Çelekli et al., 2024), anti-proliferative (Russo et al., 2004), anti-cancer (Mariana Kustiawan et al., 2024), anti-tumoral (Díaz-Carballo et al., 2008), anti-inflammatory (Arung et al., 2023), anti-angiogenic (Iqbal et al., 2019), anti-cariogenic (Kouidhi et al., 2010), anti-hyperglycemic (Nna et al., 2018) and immunomodulatory (Mendez-Pfeiffer et al., 2021), wound healing (Ghallab et al., 2025) hepatoprotective effects (Alvarenga et al., 2021). Although propolis exhibits a wide range of biological activities and therapeutic potential, its direct use is limited by several factors. These include low water solubility, poor bioavailability, and rapid degradation during digestion, particularly in the gastrointestinal tract (Mendez-Pfeiffer et al., 2021; Tavares et al., 2022). Its solubility is mainly in alcohol. Furthermore, its strong and distinctive odor, along with its intense taste, can negatively affect sensory properties, further limiting its incorporation into food products. (Busch et al., 2017; Shakoury et al., 2022).

To address these limitations, encapsulation methods have emerged as a promising strategy to protect the bioactivity of propolis and to minimize its undesirable sensory characteristics. Various encapsulation techniques have been reported in the literature, including nanoparticles (Shakoury et al., 2022), spray drying (Busch et al., 2017), freeze drying (Šturm et al., 2019), liposomes (Aytekin et al., 2020; Ramli et al., 2021), complex coacervation (Nori et al., 2011), nanofiber (Mirbagheri et al., 2023), hydrogels (Ferreira et al., 2024), solid lipid nanoparticles (Shahab-Navaei & Asoodeh, 2023), nanoemulsions (Seibert et al., 2019). While encapsulation serves as an effective approach to overcome the solubility limitations of propolis, careful

selection of carrier materials is required to ensure they are non-toxic, biodegradable, and biocompatible for safe use in food and pharmaceutical applications (Karakas et al., 2023).

1.2 Liposome

"Liposome" comes from the Greek terms lipo (fat) and soma (structure) and refers to a spherical vesicle formed by the self-assembly of amphiphilic molecules, mainly phospholipids. Liposomes are composed of one or more phospholipid bilayers that surround an internal aqueous core. The bilayers encapsulate hydrophilic compounds within the aqueous core, while hydrophobic molecules are embedded within the lipid bilayers (W. Liu, Ye, & Singh, 2015). Liposomes, which can be derived from natural substances, exhibit non-toxic, biocompatible, biodegradable, and non-immunogenic properties. Their bilayer membranes typically consist of phosphatidylglycerol, phosphatidylcholine, distearoylphosphatidylcholine, and dipalmitoylphosphatidylcholine, as well as cholesterol, stearylamine, and dicetylphosphate (Maja et al., 2020). The size of liposomes, which can range from 20 nm up to 1000 nm, is influenced by the number of bilayers (Pasarin et al., 2023). Liposomes are classified based on their membrane structure into multivesicular vesicles (MVVs, greater than 1 μm), multilamellar vesicles (MLVs, greater than 400 nm), and unilamellar vesicles (ULVs, greater than 20 nm) (W. Liu et al., 2012).

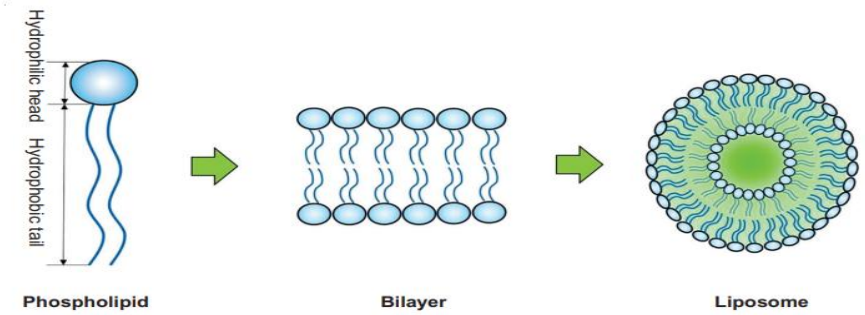

Figure 1. 2 Schematic representation of liposome formation(W. Liu, Ye, & Singh, 2015)

Throughout liposome preparation, mechanical forces promote phospholipid aggregation and subsequent self-assembly into bilayer formations (Chai & Park, 2024). Liposomes have been produced using various methods, including conventional techniques like thin film rehydration, ethanol injection, detergent removal, heating, and extrusion, as well as advanced methods such as supercritical

fluid technology, ultrasonication, and microfluidic systems, which have been developed to enhance the effectiveness of liposome production (Ajeeshkumar et al., 2021).

Liposomes are highly versatile delivery systems capable of encapsulating both hydrophilic and lipophilic compounds, making them suitable for a wide range of applications. Liposomal encapsulation offers numerous advantages for food bioactives, including enhanced stability, controlled release, improved bioactivity, and increased bioavailability. In addition, liposomal applications in food products enhance sensory attributes and overall quality (Pamunuwa & Karunaratne, 2022). Despite these benefits, their use is limited by their short circulation half-life, vulnerability to degradation, and high production costs. Their stability is further affected by exposure to gastric pH, bile salts, enzymatic hydrolysis, and environmental factors such as temperature, light, lipid peroxidation, and pH variations (Maja et al., 2020; Pasarin et al., 2023). Thus, further improvements in liposome stability are essential to maximize their potential in food and pharmaceutical applications.

1.3 Hydrogel

Hydrogels are hydrophilic polymer networks with a three-dimensional structure that can retain large quantities of water, resulting in a gel-like matrix (Edo et al., 2025). Hydrogels can absorb water several thousand times their dry mass, depending on the hydrophilic nature of the polymer and the structural characteristics of the network, leading to the formation of chemically stable or biodegradable gels (J. Li et al., 2021). The hydrophilic character of hydrogels results from the presence of functional groups, such as sulfonic ($–SO_3H$), carboxyl (–COOH), hydroxyl (–OH), amide (–CONH, $–CONH_2$), and amine ($–NH_2$) groups within the polymer chains (Gul et al., 2022).

Although hydrogels can be synthesized from either synthetic or natural polymers, natural polymers are preferred due to their safety and environmental compatibility. Examples include proteins (e.g., gelatin, soy protein, whey protein), polysaccharides (e.g., chitosan, alginate, pectin), and protein–polysaccharide complexes, which are commonly used in biopolymer-based hydrogel systems. (Klein & Poverenov, 2020).

Two fundamental conditions are required for hydrogel formation. First, the polymer molecules must have hydrophilic groups on their main or side chains. Second, sufficient cross-linking strength must be established between the molecules to create a stable gel network. Based on the mechanisms of gel formation, hydrogels can be categorized into four groups: physical crosslinking (including electrostatic interactions and hydrogen bonding), chemical crosslinking, multi-crosslinking systems, and enzymatic crosslinking (J. Li et al., 2021).

The porous structure of hydrogels enables them to act as effective carriers for the protection and delivery of bioactive compounds (Nascimento et al., 2020). Hydrogels are capable of swelling, degrading, or disintegrating when exposed to environmental stimuli like pH, ionic strength, and temperature, and utilize diffusion, swelling, and degradation as major release mechanisms in targeted delivery systems (Yang et al., 2023). In this context, hydrogel-based encapsulation offers several advantages, including biocompatibility, protection of sensitive compounds, controlled release, and responsiveness to environmental triggers, while combining the characteristics of both solids and liquids (Lin et al., 2022). However, hydrogels have several disadvantages, including low mechanical strength, burst release, and sensitivity to environmental changes, which can alter their swelling or shrinkage behavior, thereby limiting their broader applications (Ahmed, 2015; Lin et al., 2022; Paun et al., 2016).

1.4 Liposomal Hydrogel Hybrid System

In recent years, considerable progress has been made in the independent development of liposomes and hydrogels. By combining the unique advantages of each, a new emerging class of delivery systems, liposomal hydrogel hybrid systems, has been developed. These systems can be applied to various fields, including immunomodulation, drug delivery, detoxification, tissue engineering, and encapsulation of food bioactives. A liposomal hydrogel system is typically formed by uniformly dispersing nanoliposomes within a hydrogel matrix, enabling not only the continuous release of high concentrations of therapeutic agents at the target site but also enhancing permeability and therapeutic efficacy (Tu et al., 2025). In such systems, a two-stage controlled release can be achieved, where liposomes are initially released from the hydrogel structure, followed by the gradual release of the

active substances from the liposomes. (Y. Liu & Liang, 2011). The incorporation of liposomes into hydrogel systems offers potential benefits, including better solubility of hydrophobic molecules in aqueous environments, extended compound stability, controlled multi-phase release, and enhanced mucoadhesion (Alinaghi et al., 2013; Jøraholmen et al., 2020).

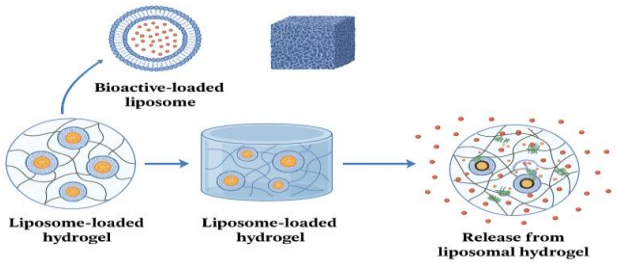

Figure 1. 3 Illustration of bioactive-loaded liposome integration into hydrogel matrix and subsequent release.

Table 1. 1 Summary of recent studies on liposomal hydrogel systems incorporating bioactive compounds

Bioactive Compounds	**Polymers**	**Results**	**References**
Quercetin	Gelatin, Chitosan	Compared to the liposomes without embedding in hydrogels, the liposomal hydrogels showed a better protective effect of quercetin	(W. Liu et al., 2020)
Curcumin	*Alyssum homocarpum* seed gum, Alginate	Improving stability, enabling controlled release, and increasing bioaccessibility	(Mousavi et al., 2025)
Quercetin	Carboxymethyl cellulose, Carbomer	Improvement of quercetin bioavailability and enhancement of its dermal delivery efficiency.	(C. Liu et al., 2023)
Resveratrol	Chitosan	The delivery system enhanced the bioactivity and applicability of resveratrol.	(Jøraholmen et al., 2020)
A-tocopherol	Chitosan	Achieving sustained drug release, improving retention time, and enhancing drug efficacy.	(Qu et al., 2019)
Caffeic acid	Carbopol 940	Modification of adhesion and interaction forces within the three-dimensional carbomer-based hydrogel network upon incorporation of caffeic acid-loaded liposomes.	(Dejeu et al., 2022)
Tea polyphenol	Poloxamer 407	Efficient inhibition of bacterial growth and modulation of inflammation,	(Shen et al., 2025)

1.5 Bioaccessibility and Bioavailability of Bioactive Compounds

Before a bioactive compound can be absorbed and reach target tissues, it must be released from the food matrix and/or broken down by digestive or microbial enzymes. This process is influenced by food composition, physical form, and matrix structure (Grundy et al., 2025). To properly understand potential health benefits of bioactive compounds, it is crucial to evaluate two key concepts: bioaccessibility and bioavailability. Bioaccessibility refers to the fraction of a compound that becomes available for absorption, whereas bioavailability describes the portion that is effectively absorbed, utilized, or stored by body tissues and organs (Jia et al., 2024). For this reason, determining bioaccessibility constitutes the initial step in the evaluation of bioavailability (Ubeyitogullari et al., 2022). In the assessment of oral bioavailability, three main factors are typically considered: the bioaccessibility, absorption, and transformation of biomolecules (Dima et al., 2020).

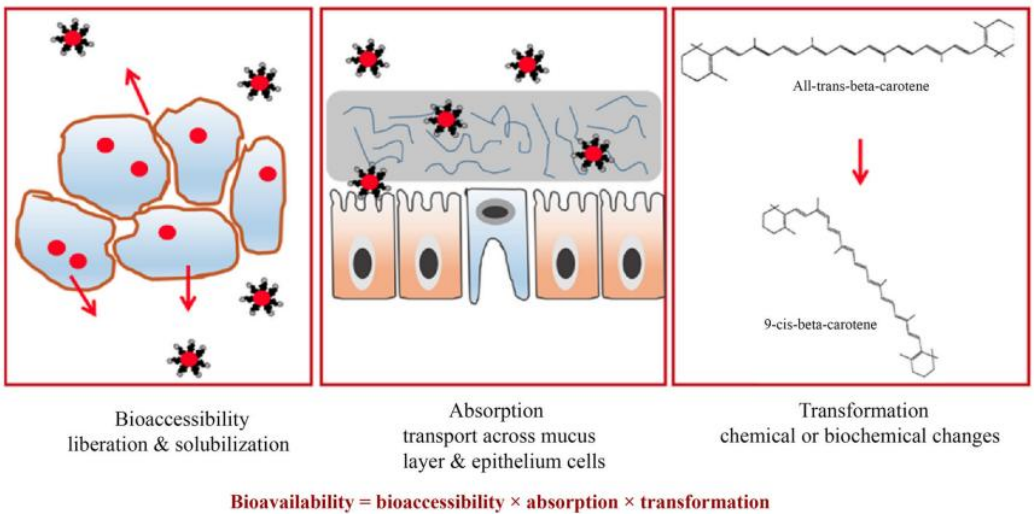

Figure 1. 4 Schematic representation of the three key factors determining oral bioavailability: bioaccessibility, absorption, and transformation (J. Chen & Hu, 2020).

Several methods, including *in vitro* digestion models, cellular uptake assays, and *in vivo* digestion studies, are employed to assess the bioaccessibility of dietary bioactive compounds. *In vitro* digestion models are favored for their cost-effectiveness. These models mimic the digestive processes in the oral, gastric, and intestinal phases, taking into account thermal and enzymatic effects, changes in pH and temperature, the movement of the digestive tract, and the fermentation

processes carried out by microorganisms (Jia et al., 2024). *In vitro* methods offer several benefits, including speed, cost-effectiveness, reduced labor, the absence of ethical concerns, reproducibility, controlled conditions, and ease of sampling. These advantages allow for high-throughput screening of numerous samples and make *in vitro* models highly suitable for evaluating the digestion behavior and bioaccessibility of bioactive compounds (Minekus et al., 2014). *In vitro* digestion models are generally classified as static, semi-dynamic, or dynamic systems (Calero et al., 2024). In static *in vitro* digestion models, the different stages of human digestion are simulated under consistent conditions within closed systems. Samples are combined with simulated digestive fluids and incubated at a controlled temperature, enzyme activity, and pH for a specific duration. To promote uniformity across research, the INFOGEST network established a standardized static digestion protocol in 2014 (Minekus et al., 2014). In contrast, dynamic models better reproduce the complexity of physiological digestion by incorporating continuous flow, automated pH adjustment, regulated enzyme addition, peristaltic movements, and gastric emptying (Calero et al., 2024). While dynamic systems offer a more realistic representation of digestion, they are more complex, demand larger quantities of enzymes and samples, are more expensive, and require specialized equipment not typically found in standard laboratories (Xavier & Mariutti, 2021).

1.6 Hypothesis

Liposomal hydrogel systems are promising carriers for enhancing the stability, release, and delivery efficiency of bioactive compounds. Based on this premise, it is hypothesized that encapsulating propolis phenolic compounds in a liposomal hydrogel using a mucoadhesive polymer can prolong the release period, enable controlled release under specific conditions, and enhance the effective delivery of these compounds. This approach aims to provide better protection and targeted release of propolis phenolics.

1.7 Objective of the Thesis

Nowadays, colloidal delivery systems have gained increasing attention across various fields, including pharmaceuticals, dietary supplements, and the food

industry, due to their ability to encapsulate bioactive compounds, enhance stability, and control release (Z. Zhang et al., 2016). The use of hybrid encapsulation systems, which combine different methods, has demonstrated better performance compared to traditional single-carrier systems, particularly in delivering food bioactive compounds. Among these carriers, liposomes have attracted considerable interest due to their biocompatibility and low toxicity, making them favorable for food and pharmaceutical applications. However, liposomal systems face certain challenges, such as low colloidal stability, gradual leakage of encapsulated compounds, and structural vulnerability under gastrointestinal conditions. Similarly, hydrogel systems are limited by their low mechanical strength, burst release behavior, and sensitivity to environmental changes.

The purpose of this thesis is to develop a hybrid liposomal hydrogel system by loading propolis phenolics into liposomes and embedding them into a hydrogel network made of mucoadhesive polymers such as salep and xanthan gum. This system aims to overcome the limitations of liposomes and hydrogels, improve stability, achieve controlled and responsive release, and enhance the delivery of propolis phenolic compounds for potential applications in food systems.

The main layout of the thesis consists of:

- Production of liposomal gel templates: hydrogels loaded with empty (surfactant-free) liposomes using mucoadhesive polysaccharides (xanthan gum and salep).
- Production and characterization of empty liposomes (surfactant free).
- Production and characterization of empty and PE-loaded liposomes incorporated with AMP and T80.
- Integration of PE-loaded liposomes into the hydrogel matrix to form hybrid liposomal PE gels..
- Characterization of the rheological, textural, mucoadhesiveness, thermal properties, chemical structure, and morphology of the liposomal gels.
- The change of phenolics at in vitro digestion stages, including oral, gastric, and intestinal phases for free PE, liposomal PE, and liposomal PE loaded gels.

2
MATERIAL AND METHODS

2.1 Material

Lipoid S75 (70% phosphatidylcholine) was obtained from Lipoid (Ludwigshafen, Germany). Ethanol (99.5%) and sodium benzoate were purchased from Tekkim (Istanbul, Turkey). Amylase (A1031), mucin (M2378), pepsin (P7012), pancreatin (P7545), bile (B3883), polyoxyethylene sorbitan monooleate (Tween 80), Amicon® membrane ultra-centrifugal filter (50 kDa), and analytical standards for propolis phenolics were supplied by Sigma-Aldrich Ltd. (Steinheim, Germany). Ammonium phosphatide (AMP 4455) was kindly provided by Palsgaard A/S (Istanbul, Turkey). The ethanolic extract of propolis (PE) was donated by Balparmak (Altıparmak Gıda, Istanbul, Turkey). Salep was obtained from Baldo (Istanbul, Turkey), while xanthan gum (Grindsted xanthan) was provided by DuPont (Istanbul, Turkey).

2.2 Methods

2.2.1 Preparation of Liposomes

Empty liposomes were produced by the thin-film hydration technique as described by Ramli et al. (2021), with certain modifications. Soy lecithin (Lipoid S75, 2% w/v) was dissolved in ethanol, and the solvent was evaporated under vacuum (40 °C, 70 mmHg) using a rotary evaporator (Buchi-R-210, Germany). The resulting dry lecithin film was rehydrated with pure water (2% w/v) and homogenized with an Ultra-Turrax (IKA T-18, Germany) at 10,000 rpm for 5 min. The mixture was then sonicated for 5 min at 60% amplitude and 0.5 cycles using an ultrasonic processor (UP400S, Hielscher, Germany). Propolis extract (PE)-loaded liposomes were produced by dissolving soy lecithin (Lipoid S75), Tween 80 (T80), ammonium phosphatide (AMP), and propolis extract (PE) in ethanol. The aim was to reduce surfactant content while enhancing PE loading in the final liposome

without inducing precipitation. The lecithin-to-surfactant ratio (AMP or T80) of 5:1 (w/w) was chosen as it inhibited PE precipitation in the final liposomes for both surfactants. The solvent was removed utilizing a rotary evaporator (Buchi-R-210, Essen, Germany) under vacuum conditions (40 °C, 70 mmHg). The resulting dry film was rehydrated in distilled water, homogenized with an Ultra-Turrax (IKA T-18, Staufen, Germany) at 10,000 rpm for 5 min, then subjected to sonication for 7 min at 60% amplitude and 0.5 cycles using an ultrasonic processor (UP400S, Hielscher, Berlin, Germany). The final liposomal dispersions comprised 4% (w/v) lecithin, with PE incorporated at a concentration of 2% (w/v).

2.2.2 Mean Particle Size and Zeta Potential Measurements

A dynamic light scattering (DLS) device (Nano ZS, Malvern, Worcestershire, UK) was used to assess the zeta potential and z-average particle diameter of the liposomes and liposomal gel samples. Lecithin and water have refractive index values of 1.44 and 1.33, respectively. All samples were diluted 100-fold (v/v) for liposome samples and 1000-fold (v/v) for liposomal hydrogel samples with distilled water to reduce multiple scattering effects. The results were presented as the mean ± standard deviation based on three repeat measurements at 25°C.

2.2.3 Encapsulation Efficiency of PE in Liposomes

The encapsulation efficiency (EE) of PE-loaded liposomes was assessed by separation of free PE from the encapsulated form with centrifugation at 4000 g for 40 min at 4 °C, utilizing an Amicon ultra-centrifugal filter with a 50 kDa membrane (Karakas et al., 2023). A 1 mL aliquot of liposome suspension was introduced into the upper chamber of the filter, allowing free PE to migrate into the permeate (lower section). In contrast, PE-loaded liposomes were retained in the retentate (upper section). Due to the potentially low concentration of free PE in the permeate, both phases were analyzed to ensure an accurate determination of EE. After mixing the PE with ethanol and centrifuging it at 4000 g for 30 min at 4 °C, which precipitated the lecithin, the PE in the retentate was measured. The amount of PE in the supernatant was then examined. In spectrophotometric tests, unloaded liposomes (without PE) were used as blanks after undergoing the same processing. EE was estimated using the free PE in the permeate, and PE recovered from the retentate phase was used to cross-check the results. EE was calculated using equation (2.1),

and the PE content was measured using the total phenolic content (TPC), which has been determined by the Folin-Ciocalteu (FC) method (Singleton & Rossi, 1965).

$$\text{EE\%} = \frac{\text{Initial PE (TPC) loading} - \text{Free PE (TPC) content}}{\text{Initial PE (TPC) content}} \quad (2.1)$$

2.2. 4 Morphology of Samples by SEM, Cryo-TEM, and TEM

Scanning Electron Microscope (SEM) Analysis

The surface morphology of hydrogel, empty, and PE-loaded liposomal hydrogel samples was analyzed using scanning electron microscopy (SEM) (Carl Zeiss EVO 10, Köln, Germany) operated at acceleration voltages of 7 kV and 10 kV (W. Liu et al., 2020). Prior to analysis, the hydrogel and liposomal hydrogel samples were subjected to freeze-drying. The samples were affixed to aluminum pin stubs, which were subsequently coated with a gold layer in three cycles at 40 mA for 100 s per cycle, utilizing an argon gas purge.

Transmission Electron Microscopy (TEM) Analysis

Liposomes, liposomal gels, and gastric and intestinal digesta samples of liposomal gels were analyzed using transmission electron microscopy (TEM) with the negative staining technique detailed by Ruozi et al. (2011). Samples were diluted with deionized water, and a drop of the resultant suspension was placed onto 200-mesh copper grids. Following the adherence of the samples, the grids were stained with a 2% (w/v) aqueous solution of uranyl acetate and permitted to dry at ambient temperature. The prepared grids were then examined using a TEM (Hitachi HT7800, Tokyo, Japan) operated at an acceleration voltage of 100 kV.

Cryogenic Transmission Electron Microscopy (cryo-TEM) Analysis

Cryogenic electron microscopy (cryo-TEM) analysis was conducted on hydrogel and liposomal gel samples in accordance with the protocol established by (Martín-Saavedra et al. (2017), with modifications. The samples were first diluted with deionized water, and a small droplet was applied to a TEM grid. The grid and the sample were rapidly frozen in liquid ethane and subsequently stored in liquid nitrogen to maintain the cryogenic conditions. The prepared grids were then examined using a cryo-TEM (Hitachi HT7800, Tokyo, Japan) operating at an acceleration voltage of 100 kV.

2.2.5 Preparation of Salep-Xanthan Gum Hydrogel and Liposomal Gel

Xanthan gum, salep hydrogels, and liposomal gels were prepared following the modified method of Acar and Kurt (2020). For hydrogel preparation, xanthan gum, salep, and 0.01% (w/v) sodium benzoate were dissolved in water, mixed at 80 °C for 15 min at 300 rpm, and stored at 4 °C overnight. Prior to analysis, the samples were equilibrated to room temperature. Liposomal gels were prepared using the same protocol, except the polymers were dissolved in liposomal dispersions instead of water. The total polymer concentration (xanthan gum + salep) was maintained at 1% (w/v), with xanthan gum-to-salep ratios of 1:1, 1:2, 1:3, 2:1 and 3:1 (w/w), resulting in five different hydrogel and five liposomal gel formulations. The same procedure was followed for the preparation of PE-loaded xanthan gum-salep liposomal gels, where the total polymer concentration remained 1% (w/w), and the xanthan gum-to-salep ratios were set at 1:1, 1:3, and 3:1 (w/w). The final PE loading in the liposomal gels was determined to be 1.98% (w/w).

Additionally, a preliminary study was conducted to evaluate the dynamic rheological behavior of hydrogels, where the total polymer concentration ranged from 0.375% to 0.875% (w/v), and the xanthan gum-to-salep ratios varied between 1:1 and 3:1 (w/w). A schematic representation of the liposomal gel formation process was provided in Figure 2.1.

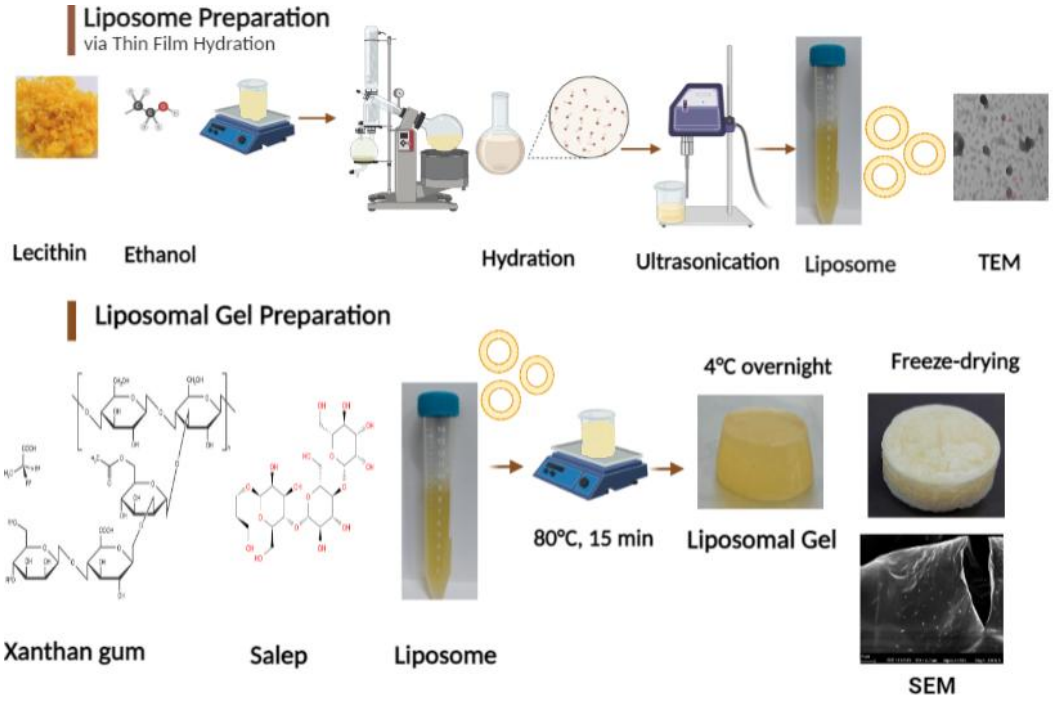

Figure 2. 1 Schematic of the hydrogel and liposomal gel production process

2.2.6 Rheological Properties

The rheological properties of hydrogels and surfactant-free empty liposomal gels were analyzed through viscosity, frequency sweep, three-interval thixotropy test (3-ITT), and temperature sweep measurements, whereas PE-loaded liposomal gels were characterized by using viscosity and frequency sweep tests. A stress- and strain-controlled rheometer (Anton Paar, MCR 302, Austria) equipped with a Peltier system was employed for all measurements. A parallel plate (PP50) geometry with a 50 mm diameter and a 1.0 mm gap height was utilized. All rheological experiments were conducted in triplicate at 25°C, with samples equilibrated at this temperature for 1 min before testing. The steady shear viscosity of hydrogels and liposomal gels was measured across a shear rate range of 0.1–100 s^{-1}.

A frequency sweep test was used for dynamic rheological analysis. Prior to oscillatory measurements, an amplitude (stress) sweep test at 0.1% strain was performed to determine the linear viscoelastic region (LVR). Within this region, the frequency sweep test was carried out over an angular velocity (ω) range of 0.1–64 s^{-1}. The storage modulus (G′) and loss modulus (G″) were calculated as functions

of angular velocity, and the dynamic rheological parameters were estimated using the power-law model and nonlinear regression as follows:

$$G' = K'\gamma n' \tag{2.2}$$

$$G'' = K''\gamma n'' \tag{2.3}$$

where G′ (Pa) represents the storage modulus, G″ (Pa) denotes the loss modulus, ω (s^{-1}) is the angular velocity, and K′ and K″ ($Pa.s^n$) correspond to the consistency indices, while n′ and n″ represent the flow behavior indices.

The Three-Interval Thixotropy Test (3-ITT) was performed to assess the degree of structural recovery after deformation. The 3-ITT properties were determined at constant and variable shear rates of 0.5 s^{-1} and 150 s^{-1}, respectively. The LVR was taken into account when selecting these values, and the test was concluded at 50 s^{-1}. The experiment comprised three phases: (i) application of a low shear rate (0.5 s^{-1}) for 100 s, (ii) exposure to a high shear rate (150 s^{-1}) for 40 s, and (iii) reapplication of the initial low shear rate (0.5 s^{-1}) to evaluate structural recovery. The extent of recovery was assessed by monitoring changes in G′, and the solid-like behavior of the samples in the third interval was modeled using a second-order structural kinetic model:

$$\left[\frac{G' - G_e}{G_0 - G_e}\right]^{1-n} = (n-1)kt + 1 \tag{2.4}$$

The parameter k represents the thixotropic rate constant, G_0 denotes the initial storage modulus (Pa) in the third interval, and G_e corresponds to the equilibrium storage modulus, indicating complete structural recovery of the product.

The three-interval thixotropy test was performed with some modifications to the standard method to assess the dynamic oscillatory behavior of the samples (Toker et al., 2015). Temperature sweep measurements were conducted over a range of 45 to 10 °C and 10 to 45 °C, with a heating/cooling rate of 1.0 °C/min. The storage modulus (G′), loss modulus (G″), and tan δ (G″/G′) values were determined through temperature sweep tests at a strain of 0.5% and a frequency of 1 Hz. The temperature at which G′ and G″ intersected was identified as the gelling or melting point of the samples.

2.2.7 Texture Profile Analysis (TPA)

The textural properties of hydrogels and empty liposomal gels, including hardness, adhesiveness, springiness, cohesiveness, gumminess, chewiness, and resilience, were assessed using a texture analyzer (TA, HD Plus, Stable Micro System, United Kingdom) with slight modifications to the method described by Liu et al. (2020). For the analysis, cylindrical samples with a diameter of 40 mm and a height of 20 mm were utilized. The pre-test, test, and post-test speeds were set at 1 mm/sec, while the strain value was maintained at 10%. A P/36-R probe and a 5 kg load cell were employed, with a trigger force of 5 g and a residence time of 5 s.

2.2.8 DSC and FTIR Spectroscopy Analysis

Freeze-dried liposomal gels were first finely ground. Their thermal properties were analyzed with a TA Q100 DSC (Thermo Q2, New Castle, USA). The powdered samples were heated from 20°C to 200°C at a rate of 10°C/min in an alumina crucible under a nitrogen flow of 20 mL/min.

FTIR spectra of lecithin, xanthan gum, salep, PE, hydrogel, and liposomal gels were examined using ATR-FTIR spectroscopy (Bruker Tensor 27, Karlsruhe, Germany). Spectra were recorded within the range of 4000 to 600 cm^{-1}, with a resolution of 2 cm^{-1} and an average of 100 scans.

2.2.9 Determination of Mucoadhesive Property of Liposomal Gels

The *in vitro* mucoadhesion of liposomal gels was evaluated using a texture analyzer (Stable MicroSystems TA-XT/Plus) in adhesive mode with a 5-kg load cell. Mucin enzyme served as a substrate following the method described by Thirawong et al. (2007).

Mucin disks were prepared by compressing mucin powder with a hydraulic press (10 tons for 30 s) and were affixed to a P/10 probe (10 mm) using double-sided tape. The gel samples were placed on the metallic holder at the lower platform.

Before testing, mucin disks were pre-moistened with phosphate buffer (0.1 M, pH 7.4) for 1 min, and the excess solution was removed with absorbent paper. The probe holding the mucin disk was lowered at a speed of 0.5 mm/s until it made contact with the liposomal gel samples under a force of 5 g, maintaining contact for

100 s in the *in vitro* test. The probe was then retracted at the same speed (0.5 mm/s) to detach the mucin disk from the gel samples.

Six measurements were performed for each sample. The work of adhesion (g.mm), defined as the area under the force-displacement curve, was determined using the built-in software.

2.2.10 *In Vitro* Simulated Digestion Analysis

The *in vitro* simulated digestion assay was performed following the method described by Brodkorb et al. (2019) and Minekus et al. (2014) (Figure 2.2).

The samples were combined in a 1:1 ratio (w/v) with simulated salivary fluid (SSF), α-amylase (75 U/mL), and $CaCl_2$ (0.75 mM), then vortexed for 2 min at 37 °C (pH 7.0). The resulting oral bolus was mixed with simulated gastric fluid (SGF) in a 1:1 ratio (v/v), containing $CaCl_2$ (0.075 mM) and pepsin (2000 U/mL), and incubated for 2 hours at 37 °C with continuous shaking at 100 rpm (pH 3.0). Subsequently, the gastric chyme was diluted with simulated intestinal fluid (SIF) (1:1, v/v), supplemented with $CaCl_2$ (0.3 mM), pancreatin (100 U/mL), and fresh bile (10 mM), followed by a 2-hour incubation under the same conditions (37 °C, 100 rpm, pH 7.0). At each digestion stage, test tubes were centrifuged at 2480 g for 10 min at 4 °C, and the obtained supernatants (0.45 µm filtered) were immediately frozen in liquid nitrogen and lyophilized. A blank sample containing only digestion fluids, without any test material, was also analyzed. The lyophilized supernatants from the oral, gastric, and intestinal phases were reconstituted in 80% aqueous methanol acidified with 0.1% HCl (v/v). All experiments were performed in triplicate. The bioaccessibility index (BI) was calculated using the following equation (2.5).

$$\text{BI } \% = \frac{C_{intestinal}}{C_{initial}} \times 100 \qquad (2.5)$$

Here, $C_{intestinal}$ refers to the concentration of the compound present in the intestinal phase, whereas $C_{initial}$ indicates its initial concentration in the undigested control sample.

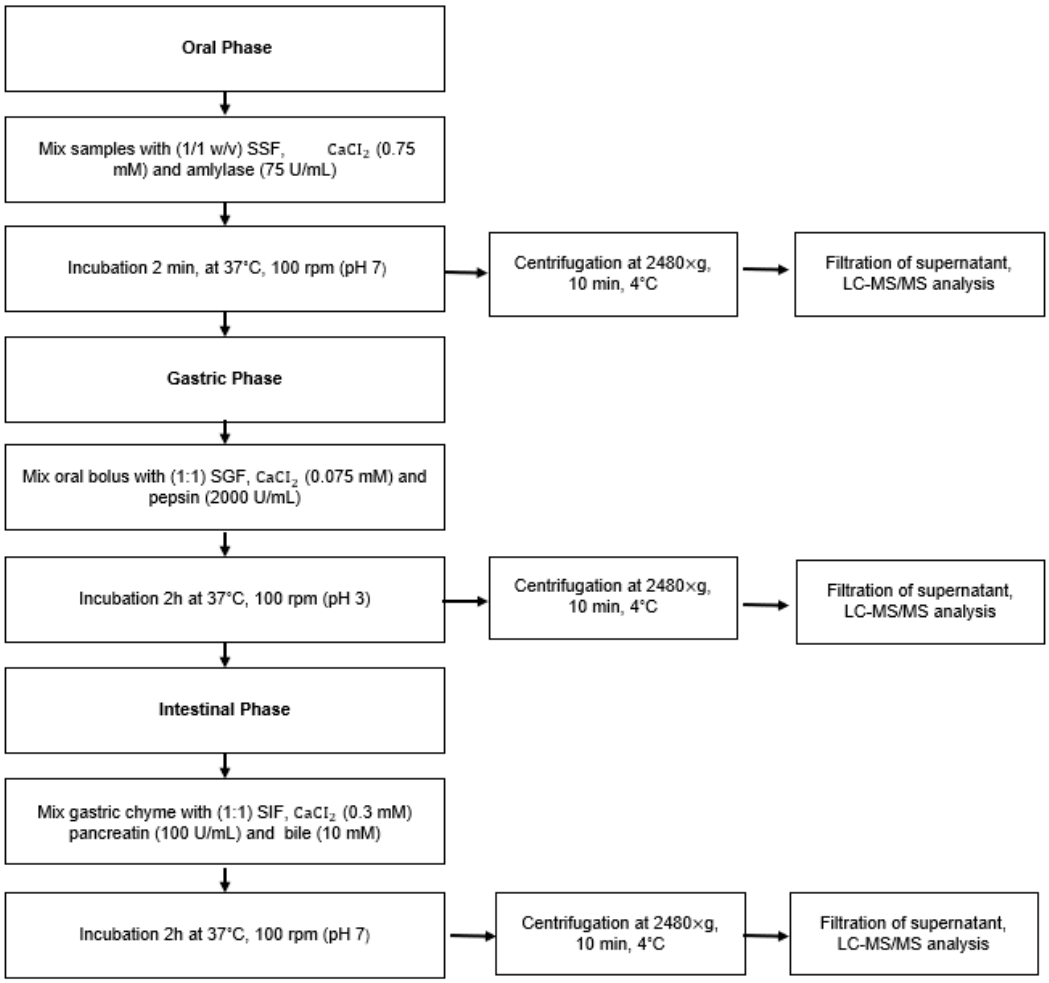

Figure 2. 2 The schematic diagram of the *in vitro* simulated digestion procedure

2.2.11 Total Phenolic Contents (TPC), Total Flavonoid Contents (TFC), and Antioxidant Activity Assays

Total Phenolic Content (TPC): The TPC of the samples was evaluated utilizing the Folin-Ciocalteu (FC) reagent in accordance with the procedures established by Singleton and Rossi (1965). Gallic acid was used as the reference standard. A 0.5 mL aliquot of the sample was mixed with 2.5 mL of FC reagent (0.2N) and 2 mL of Na_2CO_3 (2%). Subsequently, the mixture was incubated in a dark environment at ambient temperature for 30 min, following which its absorbance was measured at 760 nm utilizing a Shimadzu 150 UV-1800 spectrophotometer (Kyoto, Japan). The results were expressed as µg gallic acid equivalent (GAE)/g.

The Total Flavonoid Content (TFC): TFC was determined using the method described by Zhishen et al. (1999). A 1 mL sample was combined with 4 mL of distilled water, 0.3 mL of $NaNO_2$ (5%), and 0.3 mL of $AlCl_3$ (10%) solution, and

left to stand for 6 min. Following this, 2 mL of NaOH (1 M) was added, and the final volume was adjusted to 10 mL with distilled water. The absorbance was then measured at 510 nm using a Shimadzu 150 UV-1800 spectrophotometer. The results were expressed as µg catechin equivalent (CE)/g.

Antioxidant Activity Assays:

The DPPH (2,2-Diphenyl-1-picrylhydrazyl) Assay: The DPPH assay was conducted following the method described by Brand-Williams et al. (1995). A 0.1 mL aliquot of the diluted sample was mixed with 4.9 mL of DPPH solution (6×10^{-5} M in methanol) and incubated in the dark at room temperature for 20 min. The absorbance was then recorded at 517 nm using a Shimadzu UV-1800 spectrophotometer. The results were expressed as micrograms of Trolox equivalent (TE) per gram. The results were expressed as µg Trolox equivalent (TE)/g.

The ABTS Assay: The ABTS radical scavenging assay was conducted following the method of Re et al. (1999). The ABTS radical cation was generated by combining a 7 mM ABTS solution with 2.45 mM potassium persulfate and allowing the mixture to incubate in the dark at room temperature for 12–16 hours. Prior to analysis, the stock solution was diluted with distilled water to achieve an absorbance of 0.700 at 734 nm. For the measurement, 2 mL of the ABTS solution was added to 0.1 mL of the extract and incubated in the dark for 6 min. The absorbance was then recorded at 734 nm using a Shimadzu UV-1800 spectrophotometer. The results were expressed as micrograms of Trolox equivalent (TE) per gram.

The FRAP Assay (Ferric Reducing Antioxidant Power): The FRAP assay (ferric reducing antioxidant power) was conducted following the method of Benzie and Strain (1996). The FRAP reagent was freshly prepared by combining 300 mM acetate buffer (pH 3.6), 10 mM TPTZ solution (dissolved in 40 mM HCl), and 20 mM $FeCl_3\times6H_2O$ in a 10:1:1 (v/v/v) ratio. For the assay, 100 µL of the sample was mixed with 900 µL of distilled water and 2 mL of FRAP reagent, followed by incubation in the dark at room temperature for 30 min. The absorbance was then recorded at 593 nm using a spectrophotometer. The results were expressed as micrograms of Trolox equivalent (TE) per gram.

2.2.12 Analysis of Phenolic Compounds by LC-MS/MS

The analysis was carried out using a Waters® Xevo LC-MS/MS system (Waters Corporation, Milford, MA, USA) equipped with a binary pump, an autosampler, a temperature-controlled column compartment, and a triple-quadrupole (TQ) mass spectrometer with an electrospray ionization (ESI) source according to the method of Guzelmeric et al. (2023). Phenolic compound separation was achieved using a Cortecs T3 analytical column (1.6 µm, 2.1 × 150 mm, Waters Corporation, Milford, USA).

A gradient elution program was employed with two mobile phases: phase A (acidified water containing 0.01% acetic acid, v/v) and phase B (a mixture of acetonitrile and methanol in an 80:20 ratio, v/v) at a flow rate of 0.25 µL/min. The gradient profile was as follows: 2% B (0–1.30 min), increasing to 55% B (1.30–35 min), further increasing to 95% B (35–37 min), rapidly decreasing to 2% B (37–37.01 min), and maintaining 2% B until 40 min. The autosampler and column temperatures were set at 10 °C and 30 °C, respectively, with an injection volume of 5 µL.

Stock standard solutions (2 mg/mL) were prepared in methanol, and calibration curves were generated at 50, 100, 250, 500, and 1000 µg/L concentrations. Quantitative analysis of targeted compounds was performed in multiple reaction monitoring (MRM) mode.

The LC-eluted compounds were analyzed using an ESI-MS/MS system operating under optimized conditions: an ion source temperature of 150 °C, a desolvation temperature of 450 °C, a capillary voltage of 2 kV, and gas flows set to 850 L/h for desolvation and 50 L/h for cone gas. LC-MS/MS data processing was carried out using Waters® MassLynx software with the TargetLynx program.

2.2.13 Statistical Analysis

All experiments were performed at least in triplicate. The data were presented as mean values ± standard deviation (SD). Statistical analyses were carried out using SPSS Statistics Software (IBM version 20, Armonk, NY, USA) and Statistica software (StatSoft Inc., Tulsa, UK). A one-way analysis of variance (ANOVA) was used to compare the means, and Tukey's post hoc test was applied to identify

differences that were statistically significant ($p < 0.05$). An independent-sample t-test was used when making specific comparisons between two samples.

Statistica software was employed for nonlinear regression analysis in addition to ANOVA to determine the parameters of the power-law and second-order structural kinetic models. GraphPad Prism 5 software (GraphPad Software Inc.; San Diego, CA, USA) was used to further enhance the visualization of the data. A heat map was generated to show how the phenolic compounds changed during different stages of digestion, along with the bioaccessibility % (BI) values for each sample.

3
RESULTS AND DISCUSSION

3.1 Formulation and Characterization of Xanthan-gum Salep Hydrogels and Liposomal Gels

3.1.1 Characterization of Liposomes and Liposomal Gels: Particle Size, Zeta Potential, and PDI Analysis

The z-average particle size, zeta potential, and polydispersity index (PDI) values of liposomes and liposomal gels incorporating xanthan gum (K) and salep (S) polymers are shown in Table 3.1. Representative images of the prepared liposomal gels are presented in Figure 3.1.

Table 3. 1 Mean particle size, zeta potential, and PDI values of liposomes and liposomal gels

Samples	Z-average size (nm)	Zeta potential (mV)	PDI
Liposome	94.21±0.57^{d}	-37.40±3.05^{a}	0.26±0.01^{b}
LG-K1S1	111.20±0.85^{b}	-29.47±0.23^{b}	0.28±0.02^{b}
LG-K2S1	103.97±3.04^{c}	-30.63±0.49^{b}	0.27±0.02^{b}
LG-K3S1	110.10±2.62^{b}	-30.47±0.51^{b}	0.30±0.04^{b}
LG-K1S2	97.84±1.13^{d}	-29.73±1.25^{b}	0.26±0.00^{b}
LG-K1S3	116.83±1.97^{a}	-28.53±0.81^{b}	0.42±0.00^{a}

Values in the same column with different superscript letters show a significant difference ($p < 0.05$). LG refers to liposomal gel, K and S represent xanthan gum and salep, respectively.

The mean particle size of the liposomes was 94.21±0.57 nm. The integration of liposomes into xanthan gum and salep hydrogels increased the particle size. K1S1, K2S1, and K3S1 liposomal gels exhibited particle sizes of 111.20, 103.97, and 110.10 nm, respectively. K1S2 liposomal gel had a size closest to the initial

liposome (94.21 nm), while K1S3 liposomal gel exhibited the largest particle size (116.83 nm).

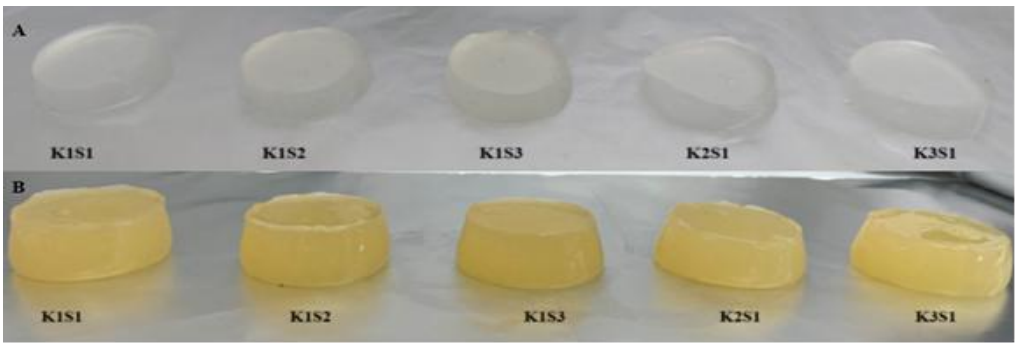

Figure 3. 1 Images of xanthan-salep hydrogels (A) and liposomal gels (B)

The polydispersity index (PDI) indicates particle size distribution, with values under 0.3 signifying a narrow dispersion. The liposome exhibited a PDI of 0.26, which indicates a relatively monodisperse system (Danaei et al., 2018). The PDI values of the xanthan gum-salep liposomal gels ranged from 0.26 to 0.42. The formulation with the greatest salep content had a notably increased PDI of 0.42. A higher PDI indicates increased heterogeneity, which may result from aggregation dynamics and interactions between polymers and lipids (Karaz et al., 2022). Zeta potential reflects the surface charge of the particles and provides insight into their stability (Midekessa et al., 2020). The initial surface charge of liposomes was -37.40±3.05 mV. Liposomes that exhibit zeta potentials of ±30 mV or higher are regarded as stable, as they are able to withstand aggregation (Németh et al., 2022). However, their integration into the polymer hydrogels resulted in a notable decrease, varying from -28.53 to -30.63 mV. A decrease in the magnitude of zeta potential (becoming less negative) generally indicates reduced electrostatic repulsion. The data suggest that polymers may have interacted with the surfaces of liposomes. In this study, polymers were dispersed in the liposomal solution, and salep exhibited greater solubility challenges than xanthan gum. As a result, its interaction with liposomal surfaces was probably more pronounced, greatly influencing particle size, zeta potential, and PDI values of liposomes. Consistent with other studies, it was proposed that interactions between liposomes and polymeric micelles facilitated micelle aggregation, resulting in an enlargement of liposomes (Cao et al., 2019).

3.1.2 Morphological Characterization of Liposomes, Hydrogels, and Liposomal Gels Through TEM, cryo-TEM, and SEM Analysis

Uranyl acetate was employed to negatively stain the samples, which binds to the phosphate groups in phospholipids, thereby enhancing the visualization of vesicle structures and providing contrast (Figure 3.2). The TEM image reveals that the liposomes are small (~ <100 nm), well-defined, spherical vesicles. The size measurements from the image are consistent with the Z-average size values obtained from zetasizer. This agreement between DLS and TEM confirms the accuracy of the particle size measurements and indicates that the liposome formulation maintains a relatively homogeneous size distribution.

The observed morphology is indicative of well-formed vesicular structures, which is advantageous for maintaining encapsulation efficiency and stability (Yun et al., 2021). Additionally, the absence of large aggregates suggests that the liposomal dispersion remains stable, likely supported by the negative zeta potential (-37.40 mV), which prevents particle aggregation through electrostatic repulsion.

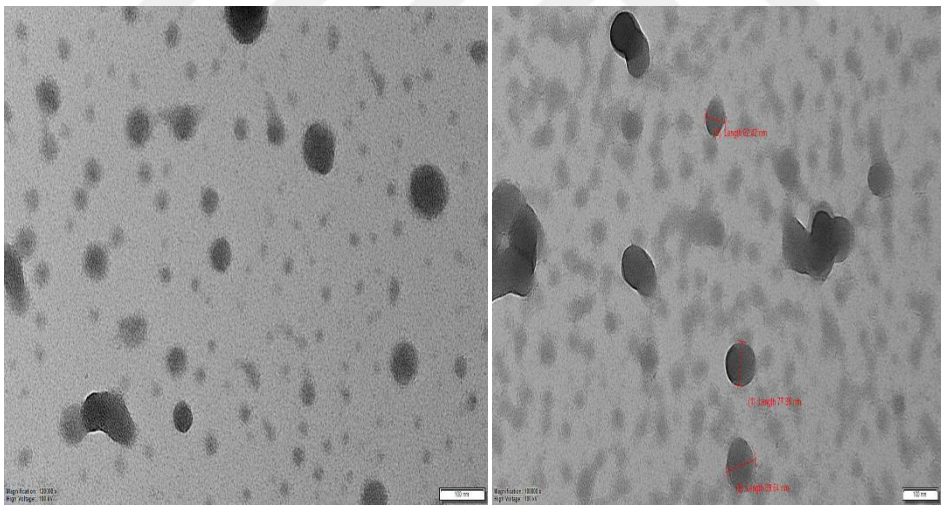

Figure 3. 2 TEM images of liposomes, scale bar = 100 nm.

In this study, the liposomal gel system was successfully produced, the presence of dispersed liposomes embedded within the hydrogel was confirmed by SEM, TEM and Cryo-TEM analysis. This is crucial for controlled release applications, as hydrogel matrices must preserve the structural integrity of liposomes while preventing their degradation and aggregation (Alinaghi et al., 2013; Grijalvo et al., 2016). The hypothesis that the hydrogel serves as a stabilizing environment,

preventing excessive coalescence or leakage, must be supported by the uniform dispersion of liposomes within the gel.

The presence of liposomes in hydrogel formulations was verified through SEM images (Figure 3.3). The xanthan-salep hydrogel (A) has a highly porous and layered structure in the low-magnification SEM image, which is consistent with the structure of biopolymer-based hydrogels (Chandrika et al., 2016). Hydrocolloids with such porous structures are particularly valuable because of their numerous applications in controlled delivery, structured food formulations, and other functional uses. Xanthan gum plays a crucial role in modifying the microstructure of the hydrogel by forming a porous network with thicker walls, thereby enhancing the structural strength of the hydrogel during swelling. The layered surface of the hydrogel, characterized by numerous open pores, further improves water absorption (Naji-Tabasi et al., 2023). This porous structure is typically formed during the freeze-drying process, where water removal leaves behind a well-defined polymeric network (Annabi et al., 2010). The interconnected porous structure could make the scaffolds well-suited for facilitating cell adhesion (Kadri et al., 2020), as well as liposome vesicles. A distinct difference between hydrogels and liposomal gels is visible in the SEM images, particularly in Figure 3.3 A-B, where liposomes appear to be uniformly embedded within the polymer matrix. The white arrows in the high-magnification images highlight liposomal vesicles distributed on the gel surface, confirming their homogeneous entrapment within the matrix.

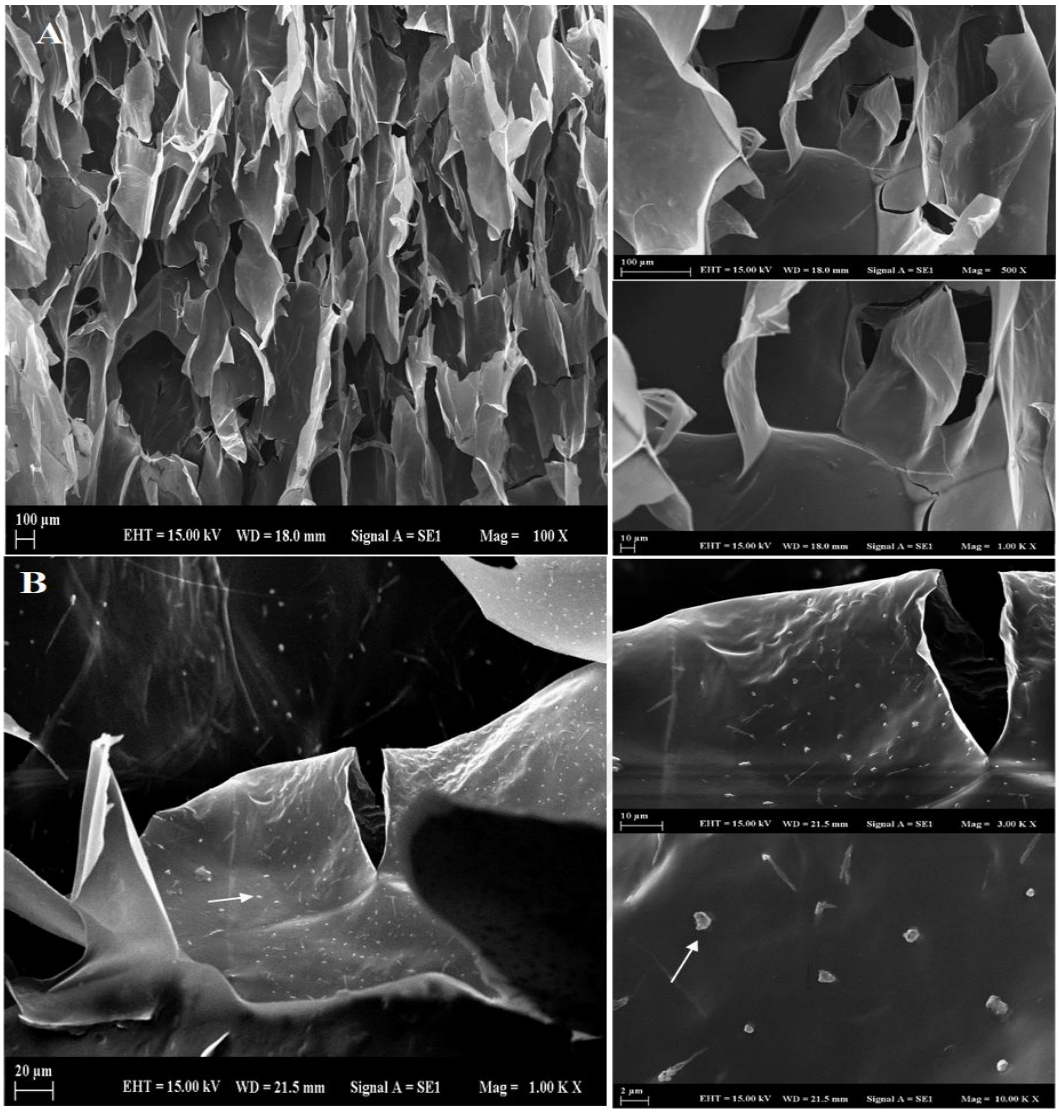

Figure 3. 3 SEM images of xanthan-salep hydrogel (A) and liposomal gels (B)

Cryo-TEM images of hydrogels and liposomal gels at different magnifications were presented in Figure 3.4. When compared to the morphology of the hydrogel structure, the presence of liposomes in the liposomal gel was indicated by relatively spherical, darker particles, marked by white arrows. These findings were consistent with previous research demonstrating that liposomes appear as well-defined, darker structures in Cryo-TEM due to their phospholipid bilayer composition, in contrast to the hydrogel network (Almgren et al., 2000). The Cryo-TEM images further verify that liposomes remain well-dispersed within the hydrogel matrix, without significant aggregation.

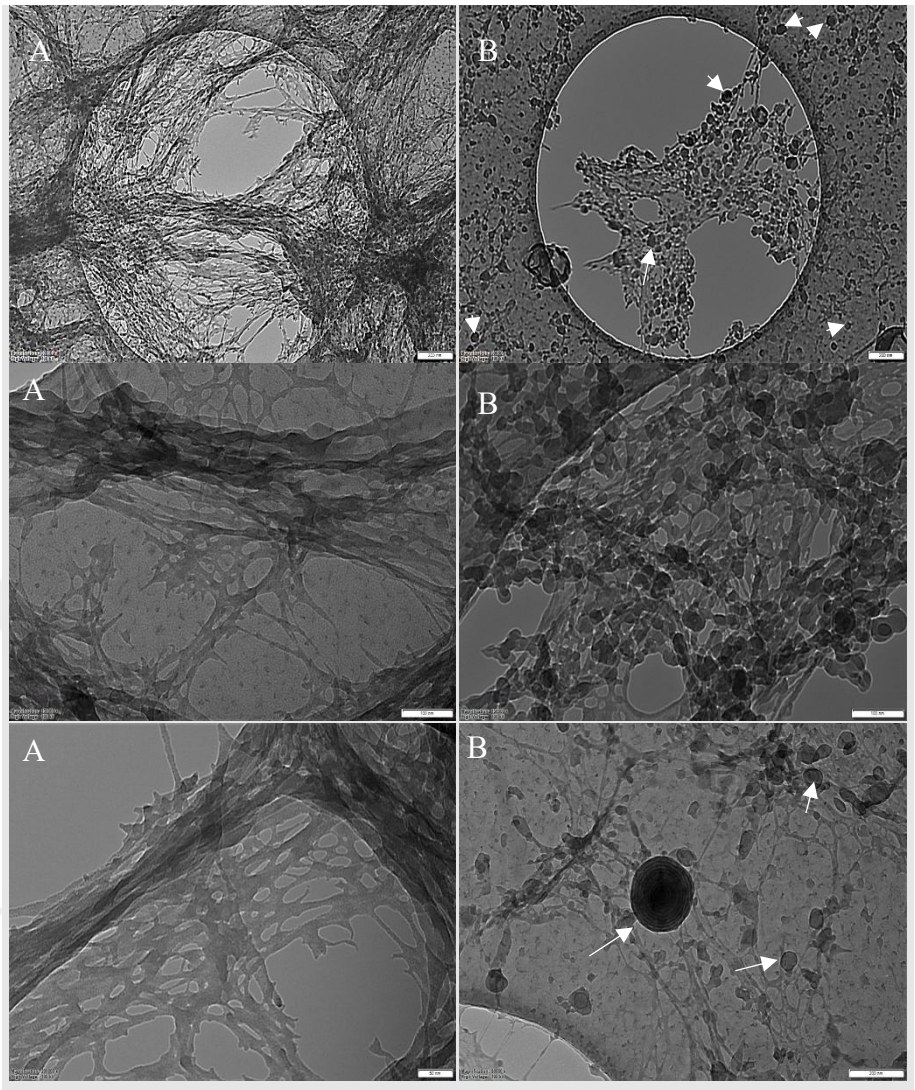

Figure 3. 4 Cryo-TEM images of the hydrogel (A) and the liposomal gel (B).

The presence of liposomes incorporated into the hydrogel structure during liposomal gel production was also confirmed through TEM analysis (Figure 3.5). The size of the observed vesicular structures is consistent with previously measured Z-average values, confirming the stability and uniform distribution of liposomes within the gel network.

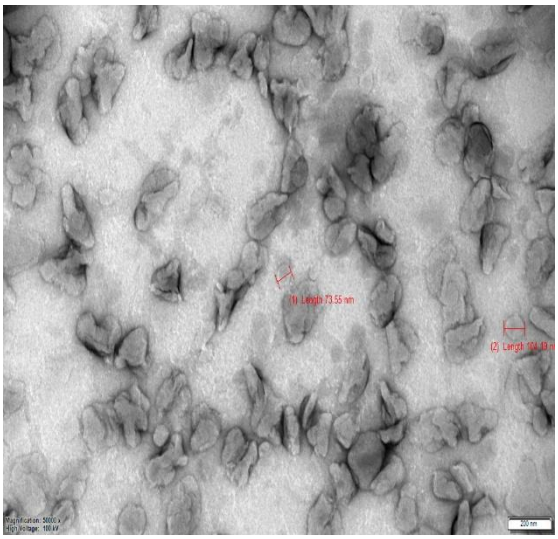

Figure 3. 5 TEM images of liposomal gels, scale bar = 200 nm

3.1.3 Rheological Characterization of Hydrogels and Liposomal Gel

Flow Behavior Properties

The rheological properties and flow behavior of hydrogels and liposome-loaded hydrogels (liposomal gels) were analyzed across a shear rate range of 0.1 to 100 s^{-1}, as given in Figure 3.6. The results indicate that viscosity decreased in all samples as the shear rate increased, demonstrating shear-thinning behavior, a characteristic of non-Newtonian fluids. Mourtas et al. (2008) previously reported that gel-based systems generally exhibit shear-thinning properties, gradually approaching Newtonian behavior at extremely low shear rates. The presence of liposomes in the hydrogel structure did not alter the overall flow characteristics, as all samples exhibited a decline in viscosity with increasing shear rate, a trend typical for polysaccharide-gel formulations (Araújo et al., 2016; Ortan et al., 2011).

In polysaccharide-rich hydrogels with high water content, polysaccharide-polysaccharide and polysaccharide-water interactions significantly influence viscosity formation. Similar findings were reported by Nair and Roy Choudhury (2020), who demonstrated that a levan-gellan composite hydrogel exhibited shear-thinning behavior along with self-recovery properties. Furthermore, an examination of the relationship between shear stress and viscosity in hydrogels and liposomal gels revealed a rapid decrease in viscosity as stress increased, stabilizing around a shear rate of 20 s^{-1}.

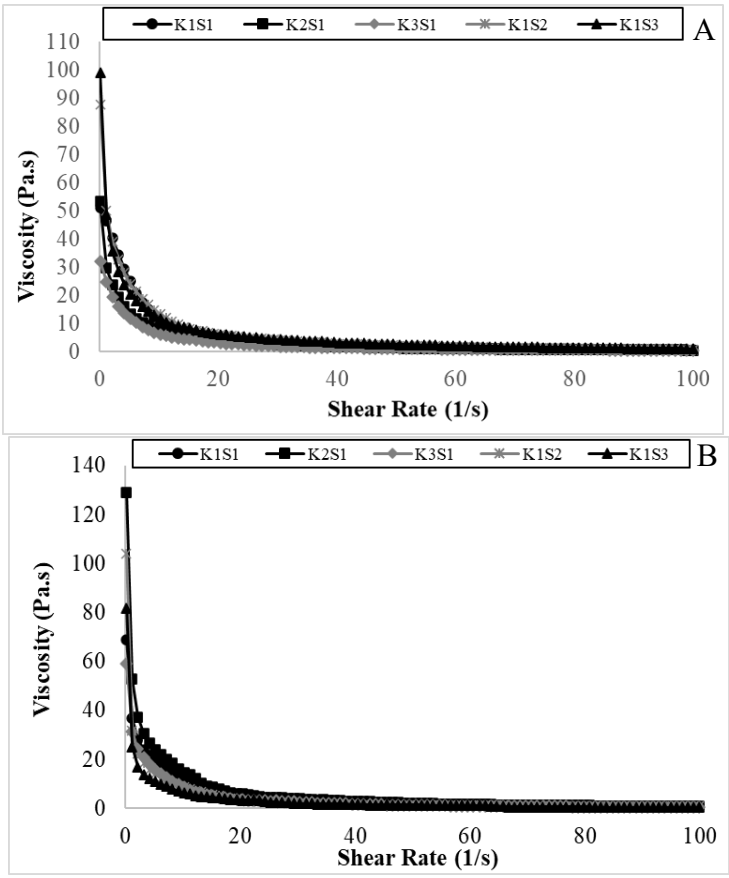

Figure 3. 6 Viscosity profiles of hydrogels (A) and liposomal gels (B) depending on xanthan-salep concentration

Dynamic Rheological Properties

The frequency sweep test was conducted to evaluate the gel characteristics and interactions between the gel components. Xanthan gum and salep, widely used as thickening agents in the food industry, tend to form highly viscous but mechanically weak gels when used individually. These weak gels exhibit low deformation resistance and are highly sensitive to external mechanical forces. Therefore, it was aimed to develop stronger hydrogel structures by utilizing the synergistic effect of xanthan gum and salep. During preliminary experiments, optimizing the total polymer concentration was a key consideration in hydrogel formulation, as the ratio of polymer components significantly impacts gel strength and stability.

As shown in Figure 3.7, the storage modulus (G') values (black dots) were consistently higher than the loss modulus (G") values (gray dots) across the entire frequency range, confirming that all samples exhibited viscoelastic solid behavior.

Despite the dominant solid-like character, a significant increase in G' with rising frequency further indicated the weak gel properties of the samples. This effect was especially pronounced at higher frequencies, where a sharp increase in the graph slope was observed. In rheological analysis, high-frequency values simulate process conditions, while low-frequency values represent deformation behavior during consumption. The findings in Figure 3.7 suggest that these gels are highly deformable under processing conditions. Additionally, at low-frequency values, the G' and G" values were relatively close, reinforcing the notion that these formulations exhibit limited structural strength. Although the increase in slope was not as drastic as in the high-frequency range, a noticeable rise was still evident. These results indicate that polymer concentrations between 0.375% and 0.875% (w/v) may not be sufficient for developing a strong hydrogel, leading to an adjustment to 1% (w/v) polymer content for improved gel strength.

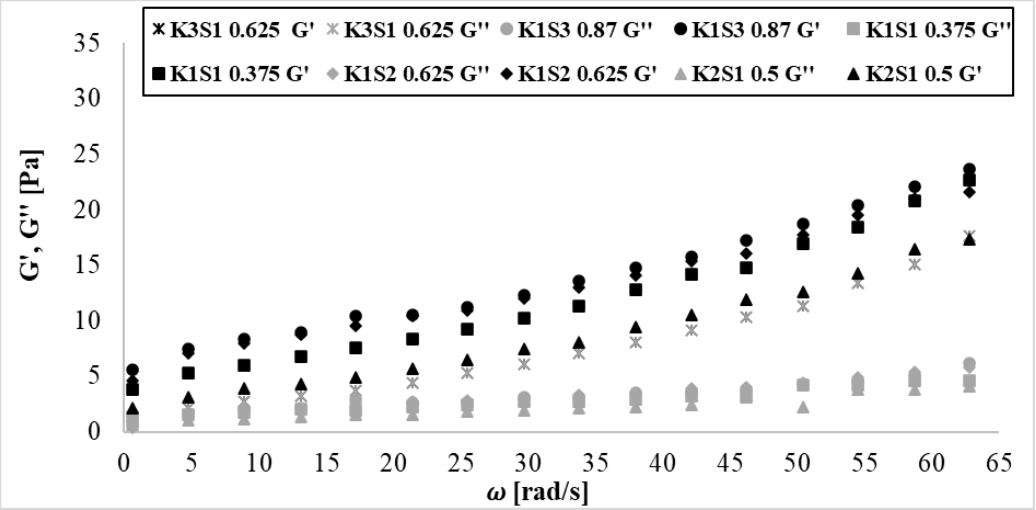

Figure 3. 7 Dynamic rheological behavior of hydrogels at varying polymer concentrations

The frequency sweep test results in Figure 3.8 highlight significant differences between G' and G" values, which are characteristic of hydrogel structures (Acar & Kurt, 2020; Kurt, 2018). Across the entire frequency range, the G' remained higher than the G", confirming the formation of a strong gel network. At all xanthan gum–salep ratios, a robust gel structure was observed, suggesting that these polymers interacted strongly. The variation in G' with increasing frequency was relatively limited; the increase was more pronounced at lower frequencies but became less

significant at higher frequencies. This behavior indicates that these gels can withstand processing and consumption conditions with considerable durability. Furthermore, when the salep content was increased, the samples exhibited higher G' values, producing firmer gels. Among all formulations, K1S3 displayed the highest G' values, attributed to its stronger viscous properties. In contrast, K3S1 exhibited a structure between a highly concentrated biopolymer solution and a well-developed gel network, making it a weak gel system. The weaker viscous response (G") observed in K1S2 and K1S3 suggested stronger gelation properties, which can be attributed to the formation of permanent chain entanglements and enhanced macromolecular interactions between xanthan gum and salep glucomannan. These interactions provide increased resistance against high shear rates, reinforcing the stability of the gel network (Kurt, 2018).

To further analyze the rheological behaviour, the frequency sweep test data were fitted to the power-law model. The high R^2 values (>0.93) obtained in Table 3.2 suggest that the power-law model effectively describes the dynamic rheological behaviour of the hydrogels. The K' values of all samples were significantly higher than K" values, indicating a strong gel structure. The n' and n" values, being close to zero, further confirmed the dominant solid-like properties of the samples. The K' values ranged from 16.06 to 47.60 $Pa \cdot s^n$, with the highest K' recorded in K1S3 (1:3 xanthan gum-salep mixture), identifying it as the strongest hydrogel, which could serve as a model system for liposome production.

Table 3. 2 Power Law model parameters for hydrogels and liposomal gels

Sample	K'	K"	n'	n"	R^2
HG-K1S1	30.97 ± 0.65^{c}	8.78 ± 0.31^{b}	0.19 ± 0.00^{c}	0.12 ± 0.02^{c}	>0.95
HG-K2S1	20.55 ± 0.39^{d}	5.71 ± 0.11^{c}	0.21 ± 0.01^{b}	0.15 ± 0.00^{b}	>0.93
HG-K3S1	16.06 ± 0.00^{d}	4.78 ± 0.32^{c}	0.23 ± 0.00^{a}	018 ± 0.02^{a}	>0.98
HG-K1S2	40.05 ± 0.05^{b}	10.52 ± 0.60^{b}	0.18 ± 0.00^{d}	0.13 ± 0.01^{d}	>0.99
HG-K1S3	47.60 ± 2.46^{a}	13.04 ± 0.37^{a}	0.18 ± 0.00^{d}	0.11 ± 0.00^{e}	>0.95
LG-K1S1	63.84 ± 2.05^{ab}	8.32 ± 0.75^{bc}	0.09 ± 0.00^{d}	0.15 ± 0.00^{b}	>0.91
LG-K2S1	37.44 ± 3.23^{c}	6.77 ± 1.04^{bc}	0.18 ± 0.00^{b}	0.15 ± 0.00^{b}	>0.95
LG-K3S1	20.41 ± 1.53^{d}	5.27 ± 0.31^{c}	0.21 ± 0.01^{a}	0.23 ± 0.01^{a}	>0.99
LG-K1S2	52.79 ± 3.81^{b}	10.19 ± 0.76^{b}	0.14 ± 0.00^{c}	0.10 ± 0.01^{c}	>0.95
LG-K1S3	70.89 ± 2.21^{a}	15.44 ± 0.61^{a}	0.14 ± 0.01^{c}	0.07 ± 0.00^{d}	>0.93

Values in the same column with different superscript letters indicate a statistically significant difference ($p < 0.05$). HG, LG, K and S stand for hydrogel, liposomal gel, xanthan gum and salep, respectively

When comparing liposomal gels with hydrogels at the same polymer concentration, G' values were significantly higher in all liposomal gel samples (Figure 3.8). Similarly, the K' values in liposomal gels exceeded those of hydrogels, while n' values were lower (Table 3.2), suggesting a stronger solid structure and higher deformation resistance. However, previous studies have indicated that liposome incorporation can slightly reduce the storage modulus of hydrogel matrices (Han et al., 2020). This discrepancy might be attributed to differences in the liposomal gel preparation methods. In the study by Han et al. (2020), liposomes were mixed with equal volumes of polymer solutions (1–2 wt%), whereas in the present study, polymers were directly dissolved in liposome solutions, resulting in a higher solid content compared to conventional hydrogels.

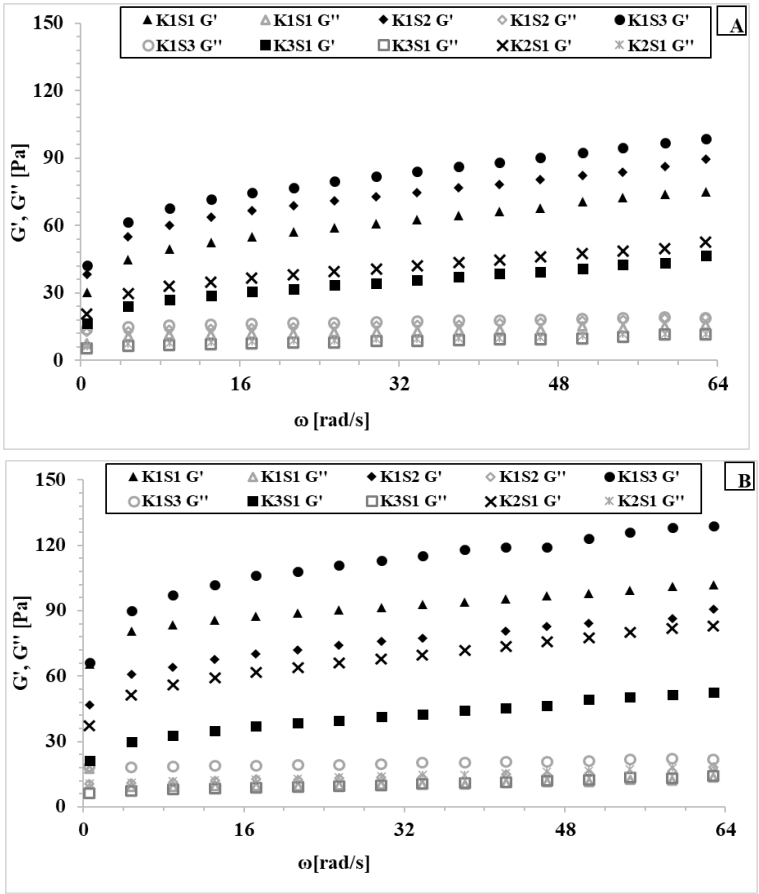

Figure 3. 8 Dynamic rheological behavior of hydrogels (A) and liposomal gels (B) at varying xanthan-salep concentrations

Three Interval Thixotropy Test (3 ITT) Rheological Properties

The 3-ITT test was employed to assess the structural recovery of hydrogels and liposomal gels following exposure to sudden and nonlinear deformation. This test

provides an accurate representation of the rheological changes that a product may undergo when subjected to external stress (Toker et al., 2015). The 3-ITT curves of hydrogels and liposomal gels at varying xanthan-salep concentrations were illustrated in Figure 3.9. The sudden deformation applied in the second time interval of all samples resulted in a decrease in the G' value, as illustrated in the Figure 3.9. All of the samples exhibited a specific degree of recovery during the third time interval. The only hydrogel sample that exhibited a tendency to recover entirely was the K3S1 sample, while none of the liposomal gel samples exhibited complete recovery. The thixotropic characteristic of the samples cannot be adequately assessed based on this result. In the initial interval, liposomal gels exhibited higher G' values than hydrogels. The G' values of all liposomal gels decreased significantly following high shear deformation, and the recovered gels exhibited thixotropic behavior in the third interval. The results were in agreement with those reported by Ramesh et al. (2021) and D'Elía et al. (2020). In part due to the arrangement of the polymer chains along the shear direction, the rate of disentanglement by shearing was slightly higher than the rate of re-entanglement, exhibiting the thixotropic nature characteristic of most hydrogels (Cuomo et al., 2019). It is crucial to ascertain the thixotropic behaviour of liposomal gels, as this is a desirable characteristic of topical semi-solid systems that are easily spreadable materials under shear stress (Ortan et al., 2011).

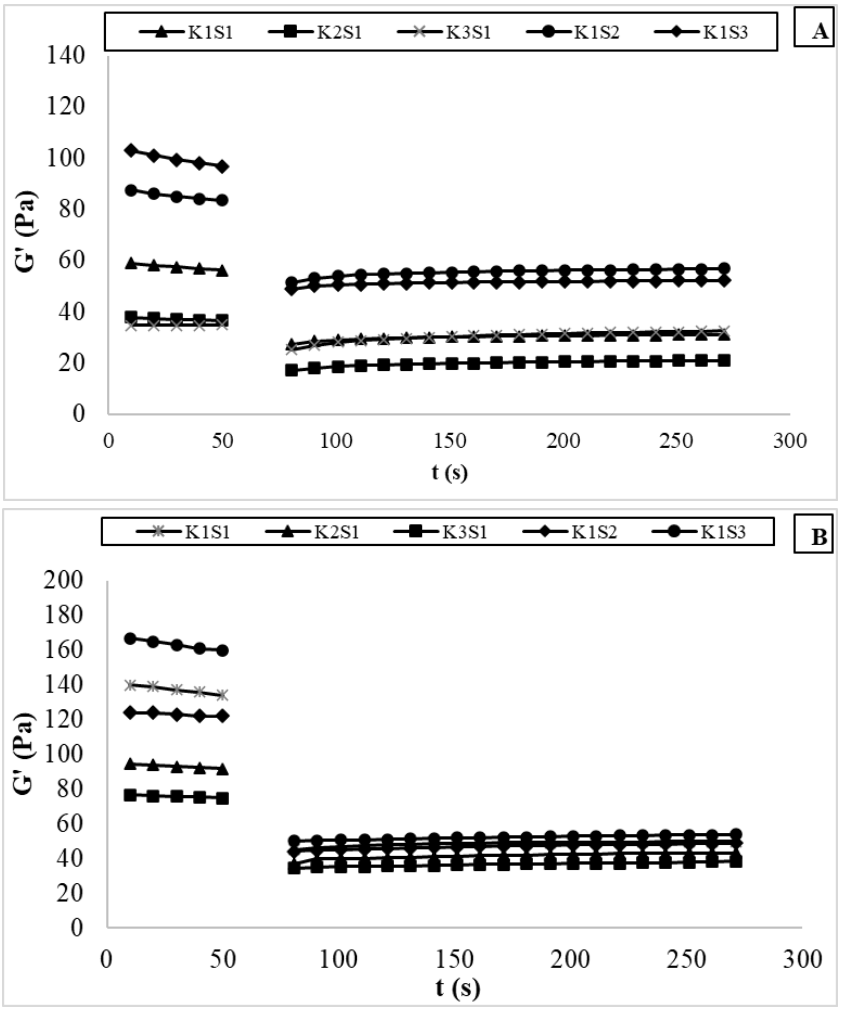

Figure 3. 9 3-ITT rheological properties of hydrogels (A) and liposomal gels (B) at varying xanthan-salep concentrations

To more accurately compare the recovery trends of the samples, it is essential to obtain parameters associated with structural recovery. The third interval data from the 3-ITT test were fitted to a second-order structural kinetic model to assess the recovery characteristics of each sample. To evaluate the recovery capability of each sample, it is necessary to calculate the thixotropic rate constant (k), the ratio of the equilibrium storage modulus (G_e) value and the initial storage modulus (G_0) value as a result of the deformation, and the percent deformation values (D_{eff}%). The second-order structural kinetic model parameters for 3-ITT of hydrogels and liposomal gels were presented in Table 3.3 at varying concentrations of xanthan-salep. The thixotropic rate constant, denoted by k, represents the change in G' value during the third time interval. If this value is high, it indicates that it can recover quickly in the event of abrupt deformation. The k value increased substantially

($p<0.05$) as the salep content of the hydrogel and liposomal gel samples increased. The samples with a higher G' value compared to those with another expression exhibited a stronger gel structure, and consequently, showed higher Def% and k values, as illustrated in Table 3.3. The K3S1 sample, which had a lower G' value, exhibited lower Def% and k values. These findings suggest that gels with a higher salep content exhibit greater recovery potential, accompanied by strong viscoelastic properties. Furthermore, hydrogels demonstrated superior recovery capabilities compared to liposomal gels, which can be attributed to the faster hydrophilic interactions that occur within hydrogels during the recovery phase. The 3-ITT test results confirmed that all samples exhibited some level of structural recovery, and this recovery potential appears to improve as the salep concentration in the formulation increases.

Table 3. 3 Second-order structural kinetic model parameters for 3-ITT

	G_i	G_0	G_e	G_e/G_0	k×1000	R^2	Def%
HG-K1S1	56.3	25.63±0.67^{b}	31.71±0.38^{c}	1.24±0.02^{c}	38.03	0.998	54.480
HG-K2S1	36.5	16.00±0.14^{d}	21.88±0.59^{d}	1.37±0.02^{b}	23.62	0.998	56.154
HG-K3S1	34.8	23.24±0.16^{c}	34.25±0.05^{c}	1.47±0.01^{a}	23.23	0.998	33.205
HG-K1S2	83.4	48.93±0.07^{a}	57.51±0.32^{a}	1.18±0.0^{cd}	41.62	0.996	41.331
HG-K1S3	96.5	47.30±0.32^{a}	52.56±1.16^{b}	1.11±0.02^{d}	47.56	0.995	50.982
LG-K1S1	122.0	40.14±0.14^{c}	45.84±0.84^{c}	1.14±0.02^{a}	15.86	0.998	67.098
LG-K2S1	91.8	37.21±0.81^{cd}	42.1±0.10^{cd}	1.13±0.02^{a}	14.26	0.999	59.466
LG-K3S1	74.9	36.32±0.25^{d}	40.35±0.20^{d}	1.11±0.01^{a}	12.11	0.998	51.506
LG-K1S2	134.0	43.39±0.17^{b}	52.83±0.33^{b}	1.22±0.00^{a}	29.63	0.998	67.618
LG-K1S3	160.0	49.80±0.91^{a}	62.65±1.50^{a}	1.26±0.05^{a}	33.02	0.996	68.876

Values in the same column with different superscript letters indicate a statistically significant difference ($p < 0.05$). HG, LG, K and S stand for hydrogel, liposomal gel, xanthan gum and salep, respectively

Temperature Sweep Analysis

A temperature sweep test was performed to ascertain the kinetics of gel formation, the change in complex modulus (G*), and the mechanical stability of the gel. To assess the thermal behavior of both hydrogel and liposomal gel formulations, a controlled cooling phase was applied from 45 °C to 10 °C, followed by a heating phase that returned to 45 °C (Figure 3.10). Both systems demonstrated comparable

temperature-responsive profiles. Gelation occurred during cooling, whereas the reverse transition gel melting was observed upon reheating. The decline in G* with rising temperature reflected a reduction in the elasticity of gel, indicating a transition toward more fluid-like characteristics (Moreira et al., 2014). The viscosity behavior of water-rich polysaccharide hydrogels is primarily influenced by the interactions between polysaccharide chains and between these chains and water molecules. As the temperature rises, these interactions tend to weaken, leading to a noticeable decrease in viscosity, an expected response for such highly hydrated gel systems. The temperature sweep test provided insight into the thermal sensitivity of the gel network, revealing a distinct decline in G* values across all samples above 25 °C. This significant drop reflects a reduction in gel strength and structural integrity. Such behavior is characteristic of xanthan gum-salep gels, where the high water content and temperature-induced weakening of hydrogen bonds between hydrophilic groups likely contribute to a rapid loss of structural integrity in the gel matrix. As the temperature decreased from 45°C to 10°C, a marked increase in the complex modulus (G*) was detected, indicating the reappearance of gelation. This behavior can be attributed to the re-establishment of molecular interactions between xanthan gum and salep, which had previously weakened at higher temperatures. The cooling facilitated a sol-to-gel transition, likely driven by the entrapment of water between polymer chains. While conventional hydrogels exhibited a similar thermal response pattern during heating and cooling cycles, liposomal gels displayed distinct behavior. In the liposomal systems, a smoother and more pronounced increase in G* was recorded during the cooling phase. The different behavior observed in liposomal gels during the cooling phase may be linked to temperature-induced structural rearrangements that occurred during the initial heating. These changes likely contributed to a more compact distribution of liposomal structures within the aqueous environment, thereby enhancing network organization and facilitating a faster recovery of viscoelastic properties, as indicated by the G* values. Liposomes are known to exhibit a glass transition near 40 °C (Koynova & Caffrey, 1998; Pippa et al., 2018), at which point the membrane undergoes a phase shift into a less ordered state. This disordered phase facilitates lateral movement of phosphatidylcholine molecules within the bilayer, potentially compromising membrane integrity and contributing to observable changes in the gel's mechanical behavior (Ulrich, 2002).

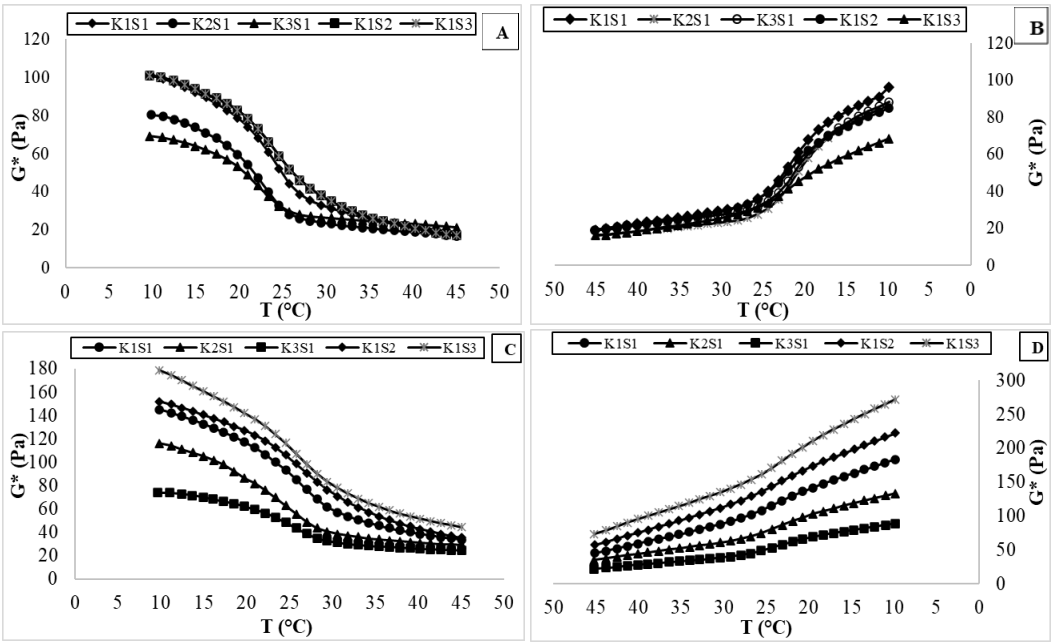

Figure 3. 10 Complex modulus of hydrogel (A, B) and liposomal gel (C, D) during heating (10–45°C) and cooling (45–10°C) phases, respectively.

3.1.4 Texture Profile Analysis

The effects of varying xanthan gum and salep concentrations, along with the inclusion of liposomes, on the mechanical behavior of gel formulations were investigated using texture profile analysis (TPA). Parameters such as hardness, adhesiveness, springiness, cohesiveness, gumminess, chewiness, and resilience were evaluated and are presented in Table 3.4. These mechanical attributes are considered essential for the practical use of gel formulations, particularly in terms of ease of removal from primary packaging, effective application to the target area, and retention at the site of administration (Kaplan et al., 2018). In this context, previous findings have shown that the incorporation of liposomal dispersion (10% w/w) into chitosan hydrogels enhances their texture-related properties, supporting the idea that liposomes may play a functional role in improving the mechanical performance of such systems (Hurler et al., 2013).

Gel matrices exhibit varying degrees of resistance to deformation under compression, and this resistance, referred to as hardness, is typically quantified as the peak force recorded during the initial compression cycle, which is directly associated with the gel's compressive strength (Chandra & Shamasundar, 2015). In the present study, the hardness of hydrogel formulations was found to range from 233.29 to 317.58 g, whereas the liposomal gel formulations demonstrated slightly

higher values, between 270.72 and 353.49 g. This indicates that incorporating liposomes led to increased gel hardness across all samples. Similar results were reported by Aguilar-Zárate et al. (2019), who found that adding 1% soy lecithin to 10% ethylcellulose-based oleogels increased their gel strength by 20 times. The enhanced hardness observed in liposomal gels may be attributed to the increased solid content and the interactions between liposomes and the polymer network. Similarly, Cevher et al. (2008) demonstrated that increasing the chitosan concentration from 2% to 3% (w/v) significantly elevated gel hardness, emphasizing the role of polymer concentration. In our findings, the K1S3 hydrogel sample exhibited the highest hardness value, which increased in parallel with the salep ratio. Conversely, the lowest value was recorded in the K3S1 hydrogel sample. Among liposomal gels, K1S2 and K1S3 formulations displayed increased firmness compared to the others, indicating that textural characteristics are shaped not only by polymer concentration but also by incorporating liposomes. A parallel trend was noted between gel hardness and K' values, with the K1S3 liposomal sample demonstrating the highest K' value of 70.89.

Adhesiveness, which reflects a combination of cohesiveness and gumminess, is considered a critical indicator for evaluating mucoadhesive delivery systems, as it is closely related to the surface characteristics of the material (Xu et al., 2021). Previous studies have also shown that softer gel textures are generally linked with higher adhesiveness values (Chandra & Shamasundar, 2015). The adhesiveness of hydrogel samples varied from −57.98 to −92.01 g.sec, whereas liposomal gels exhibited lower values, changing between −34.76 and −51.35 g.sec. Notably, the K1S3 hydrogel formulation exhibited the highest adhesiveness (−92.01 g·sec), which may be attributed to its relatively softer texture. On the other hand, liposomal gel samples like K1S2 and K1S3 showed the least adhesiveness value, even though they had the highest hardness. These results suggest that the presence of liposomes tends to reduce adhesiveness, potentially by altering surface interactions within the gel matrix. Our results are in agreement with the study by Eren et al. (2019), which similarly reported reduced adhesiveness in liposomal gel formulations containing oleoresin and algal extract when compared to their corresponding hydrogels.

Table 3. 4 Texture profile analysis (TPA) results of hydrogel and liposomal gel formulations

Sample	Hardness (g)	Adhesiveness (g.sec)	Springiness	Cohesiveness	Gumminess	Chewiness	Resilience
HG-K1S1	254.31±1.33^{b}	-58.68±6.10^{b}	0.91±0.05^{a}	0.85±0.10^{a}	251.53±4.86^{a}	230.28±9.98^{a}	0.25±0.01^{a}
HG-K2S1	265.11±21.00^{b}	-62.76±4.32^{b}	0.95±0.01^{a}	0.69±0.03^{b}	183.49±7.37^{b}	174.95±6.00^{b}	0.24±0.00^{a}
HG-K3S1	233.29±13.45^{b}	-57.98±7.43^{b}	0.95±0.00^{a}	0.75±0.01^{ab}	178.60±9.76^{b}	165.73±8.65^{b}	0.25±0.02^{a}
HG-K1S2	268.73±11.98^{b}	-65.09±10.10^{ab}	0.92±0.03^{a}	0.76±0.02^{ab}	206.18±9.77^{b}	189.123±10.88^{b}	0.24±0.03^{a}
HG-K1S3	317.58±12.28^{a}	-92.01±18.66^{a}	0.94±0.02^{a}	0.80±0.05^{ab}	253.06±24.25^{a}	237.072±26.89^{a}	0.20±0.00^{b}
LG-K1S1	299.75±19.17^{abc}	-37.67±1.32^{b}	0.97±0.00^{abc}	0.83±0.06^{a}	249.00±21.51^{ab}	241.03±21.32^{ab}	0.33±0.03^{a}
LG-K2S1	270.72±6.83^{c}	-51.35±0.97^{a}	0.96±0.00^{c}	0.81±0.01^{a}	219.05±3.37^{b}	210.54±3.43^{b}	0.27±0.00^{bc}
LG-K3S1	273.88±11.94^{bc}	-45.78±2.60^{a}	0.97±0.00^{bc}	0.81±0.01^{a}	221.31±11.05^{b}	213.48±10.70^{b}	0.24±0.01^{c}
LG-K1S2	329.38±4.29^{ab}	-34.76±5.04^{b}	0.97±0.01^{ab}	0.80±0.03^{a}	261.86±6.17^{a}	255.10±7.02^{a}	0.30±0.02^{ab}
LG-K1S3	353.49±41.18^{a}	-36.04±0.89^{b}	0.98±0.01^{a}	0.75±0.04^{a}	265.30±18.35^{a}	259.18±17.92^{a}	0.26±0.03^{bc}

Mean values with different superscript letters within the same column indicate statistically significant differences ($p < 0.05$). HG, LG, K and S stand for hydrogel, liposomal gel, xanthan gum and salep, respectively.

Cohesiveness is defined as the amount of work required to deform a sample during the downward movement of the probe in a texture profile analysis (Hurler et al., 2012). A higher cohesiveness value indicates a greater ability of the material to recover its structure after deformation, suggesting enhanced structural integrity (Vargas Villanueva et al., 2019). In this thesis, liposomal gel formulations were found to exhibit higher cohesiveness values than hydrogels in most cases, except for the K1S1 and K1S3 samples, where hydrogels showed slightly greater values. These findings suggest that the inclusion of liposomes may contribute to improved structural recovery and internal stability of the gel network, although this effect appears to be dependent on the specific ratios of xanthan gum and salep used in each formulation.

Springiness, in physical terms, refers to the rate at which a deformed material returns to its original form after the removal of an applied force. From a sensory perspective, it describes the extent to which a product regains its shape after being compressed between the teeth during mastication (Szczesniak, 2002). This property is often considered synonymous with elasticity (Das et al., 2019), and higher springiness indicates that more energy is required during mastication (Rahman & Al-Mahrouqi, 2009). In the present study, the springiness values of the gel formulations ranged between 0.91 and 0.98, reflecting a narrow range of variation among the formulations. The HG-K1S1 formulation exhibited the lowest value (0.91 ± 0.05), while the highest was observed in LG-K1S3 (0.98 ± 0.01). Despite observable variations in measured values, no statistically significant difference was detected among the hydrogel formulations, suggesting a generally uniform elastic behaviour within this group, regardless of polymer ratio.

Chewiness is a texture parameter that reflects the energy required to masticate a solid sample until it reaches a consistency suitable for swallowing. From a physical standpoint, it is considered the product of hardness, cohesiveness, and springiness. In contrast, the sensory definition refers to the time (in seconds) required to reduce the sample to a swallowable state under consistent chewing force (Szczesniak, 2002). In the current formulations, the K1S3 liposomal gel sample exhibited the highest chewiness value (259.18 ± 17.92), suggesting that this gel requires more prolonged and forceful mastication, likely due to its firmer and more elastic texture.

Gumminess is defined as the amount of energy required to break down a semi-solid product to a swallowable state. Physically, it is calculated as the product of hardness and cohesiveness, and is typically associated with semi-solid foods that possess low hardness and high cohesiveness (Chandra & Shamasundar, 2015; Szczesniak, 2002). From a sensory standpoint, gumminess refers to the dense texture that remains throughout mastication and the effort necessary to disintegrate the sample to an ingestible form (Szczesniak, 2002). Although traditionally associated with samples of low firmness and strong cohesion, gumminess can also increase as a result of elevated hardness values (Chandra & Shamasundar, 2015). In this study, K1S2 and K1S3 liposomal gels demonstrated the highest gumminess values (261.86 ± 6.17 and 265.30 ± 18.35, respectively), which may be attributed to their high hardness in combination with adequate cohesiveness. In contrast, the K3S1 hydrogel exhibited the lowest gumminess value (178.60 ± 9.76), indicating a softer structure that breaks down more readily during oral processing.

Resilience is defined as the capacity of a material to undergo reversible deformation without significant energy loss, and it is commonly used to characterize highly elastic systems (Zhu et al., 2017). In gel-based formulations, this parameter reflects the ability of the structure to recover its shape following mechanical deformation (Owczarz et al., 2019). Resilience values for both hydrogel and liposomal gel formulations ranged between 0.20 and 0.33. The highest resilience was recorded in the K1S1 liposomal gel sample (0.33 ± 0.03), while the K1S3 hydrogel formulation exhibited the lowest value (0.20 ± 0.00). These results suggest that liposomal incorporation may enhance the immediate recovery behavior of gel matrices following deformation, although the polymer composition remains a key determinant in this response.

3.1.5 Fourier Transform Infrared Spectroscopic (FTIR) Evaluation of Hydrogel and Liposomal Gel Systems

FTIR spectra of the individual components, including lecithin, xanthan gum, and salep, as well as the gel systems hydrogel and liposomal gel, were evaluated (Figure 3.11). The broad absorption band around 3300 cm^{-1} observed in all samples corresponds to the stretching vibrations of both free and hydrogen-bonded hydroxyl (–OH) groups. In salep, this band appeared at 3322 cm^{-1}, whereas it shifted to 3280 cm^{-1} in the liposomal gel, where lecithin (3283 cm^{-1}) was present, and to 3326 cm^{-1}

in hydrogels that did not contain lecithin. These variations in wavenumber likely result from interactions between the –OH groups of the polymers, ingredients, and the liposomal surface. The bands at 3010 cm^{-1} found in both lecithin and liposomal gel samples are attributed to the asymmetric stretching of CH_3 groups from the triglyceride structure (Adrar et al., 2021). In lecithin, peaks at 2923 and 2853 cm^{-1}, and at 2926 cm^{-1} in salep, correspond to asymmetric and symmetric C–H stretching vibrations (Kuligowski et al., 2008; Kurt & Kahyaoglu, 2017). In hydrogel formulations, this band was slightly shifted to 2920 cm^{-1}, possibly due to interactions involving xanthan gum and salep. A characteristic peak around 1720 cm^{-1} observed in xanthan gum and hydrogels, and at 1737 cm^{-1} in lecithin and liposomal gels, is attributed to C=O stretching vibrations of esters, carboxylic acids, aldehydes, and ketones (Faria et al., 2011). The absorption band at 1638 cm^{-1}, associated with C–O stretching of hydroxyl groups in salep, was no longer present in xanthan gum-based hydrogels (Acar & Kurt, 2020). Additionally, the peak at 1603 cm^{-1}, assigned to the asymmetric stretching of carbonyl groups in xanthan gum (P. Li et al., 2016), shifted to 1605 cm^{-1} in salep xanthan hydrogel and was not detected in liposomal gel formulations. The C=C stretching band in lecithin at 1655 cm^{-1} appeared at 1653 cm^{-1} in the liposomal gel. Furthermore, phosphate group vibrations in lecithin, initially observed at 1239, 1162, and 1055 cm^{-1}, were slightly shifted in the liposomal gel to 1236 and 1169 cm^{-1}, suggesting possible interactions involving the phosphate moieties (Sarabandi et al., 2019; Tantipolphan et al., 2009). The asymmetrical stretching of the choline group at 970 cm^{-1} in lecithin was also present in the liposomal gels. Peaks related to glucose and mannose units in xanthan gum and salep were located at 891 and 869 cm^{-1}, and were shifted to 873 cm^{-1} in the gel formulations (Acemi et al., 2019).

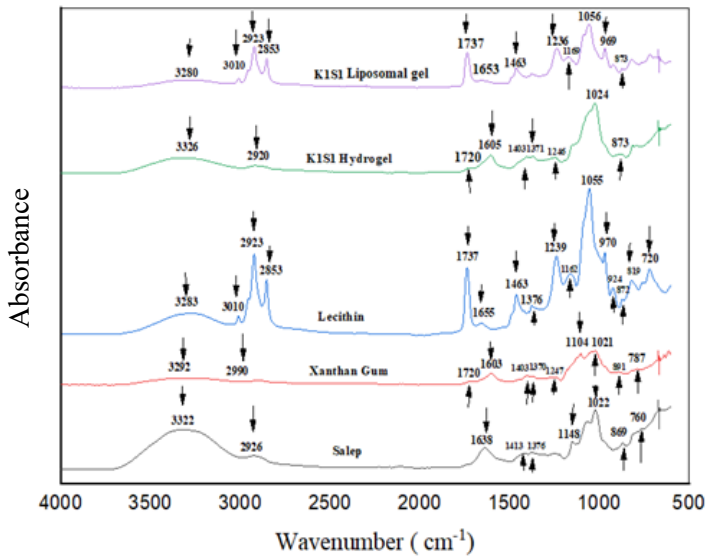

Figure 3. 11 FTIR spectra of the individual components (lecithin, xanthan gum, salep) and gel systems (hydrogel and liposomal gel).

3.2 Propolis Incorporation into Liposomes: Formulation Strategy, Characterization

3.2.1 Characterization of PE-Loaded Liposomes: Particle Size, Zeta Potential, Morphology, and Encapsulation Efficiency

PE loading into plain liposomes ranged between 0.3 and 0.6% (Karakas et al., 2023). Therefore, liposomal formulations containing the food-grade surfactants T80 and AMP were formulated to improve the loading capacity of propolis extract (PE) into liposomes (Figure 3.12). The formulations L1-PE2 and L2-PE2 were loaded with 2% (w/v) propolis extract, while L1 and L2 were empty liposomes with T80 and AMP, respectively.

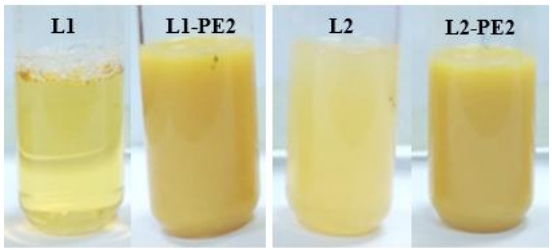

Figure 3. 12 Images of empty and PE-loaded (2%, w/v) liposomes

L1 and L2: empty liposomes containing T80 and AMP. L1-PE2 and L2-PE2: PE-loaded (2%, w/v) liposomes with T80 and AMP respectively.

T80 (E433) and AMP (E442) are both approved food additives (EFSA, 2015; Mortensen et al., 2016). The use of T80 in food supplements is regulated under the "*quantum satis*" principle, indicating it may be used in amounts necessary to achieve the desired technological effect. AMP is a food-grade emulsifier authorized by EFSA with an acceptable daily intake of 30 mg/kg body weight. Its application has not been linked to toxicity, genotoxicity, or adverse reproductive or developmental effects. Both additives can enhance the solubility of bioactive compounds and contribute to modifying the structural characteristics of liposomal membranes. C. Li et al. (2022), Tai et al. (2017), Tan et al. (2014) and Xia & Xu, (2005) have reported that the combination of phospholipids with such surfactants can promote higher loading by reorganizing the bilayer structure, potentially increasing the available space for active compounds during the encapsulation process. In particular, the incorporation of T80 was previously demonstrated to facilitate PE loading at concentrations of 2% and above (Karakas et al., 2023).

The encapsulation efficiency (EE%) of PE was evaluated in liposomal formulations containing two different surfactants, T80 and AMP. In liposomes containing T80 (L1), 2% (w/v) PE was effectively encapsulated (L1-PE2), achieving an encapsulation efficiency of 75.49 ± 1.44%. Likewise, liposomes formulated with AMP (L2) allowed for the incorporation of 2% (w/v) PE (L2-PE2), resulting in an EE% of 70.27 ± 1.13% (Table 3.5). In this thesis, the PE concentration was kept constant at 2% (w/v) to ensure the stability and homogeneity of the liposomal dispersions. The EE% values obtained for both T80 and AMP-based formulations were consistent with previously reported encapsulation efficiencies for PE in phosphatidylcholine-based liposomes, which range between 35% and 82% (Aytekin et al., 2020; Ramli et al., 2021; Refaat et al., 2021).

Table 3. 5 Encapsulation efficiency (%), particle size distribution, surface charge (zeta potential), and PDI values of the liposomal formulations

Sample	Surfactant	EE (%)	z-average size (nm)	Zeta potential (mV)	PDI
L0	-	-	64.61±16.43	-39.23±1.15	0.28 ±0.09
L1	T80	-	47.18±1.31^{b}	-37.00±1.37^{b}	0.36 ±0.02^{c}
L1-PE2		75.49±1.44	103.41±4.09^{a}	-34.33±2.02^{a}	0.46 ±0.02^{a}
L2	AMP	-	80.97±0.99^{b}	-36.53±0.76^{b}	0.44 ±0.01^{a}
L2-PE2		70.27 ±1.13	179.30±2.90^{a}	-33.80±1.28^{a}	0.36 ±0.01^{b}

Values with different superscripts within the same group (L1 or L2) are significantly different ($p < 0.05$). L0: empty liposome without surfactant. L1 and L2: empty liposomes containing T80 and AMP. L1-PE2 and L2-PE2: PE-loaded (2%, w/v) liposomes with T80 and AMP respectively.

The average particle size of empty liposomes varied depending on the type of surfactant incorporated during formulation. The liposomes prepared without the addition of any surfactant (L0) exhibited a particle size of 64.61 ± 16.43 nm. When T80 was included (L1), the particle size was reduced to 47.18 ± 1.31 nm, whereas the inclusion of AMP (L2) resulted in a larger particle size of 80.97 ± 0.99 nm (Table 3.5). These findings suggest that T80 and AMP interact differently with the phospholipid bilayer structure. T80 has a large hydrophilic head group, which may increase membrane curvature (Mkam Tsengam et al., 2022). The reduction in particle size of liposomes upon T80 incorporation may result from steric repulsion among the T80 surfactants present in the outer and inner leaflets of the liposomal bilayer membrane. The T80 surfactants, located in the outer leaflet of the bilayer membrane, enhanced the curvature of liposome particles, while those in the inner leaflet produced the contrary effect. Incorporating T80 surfactant resulted in a reduction of liposomal size, as a higher concentration of T80 was present in the outer leaflet compared to the inner leaflet of the liposomal bilayer membranes (Tasi et al., 2003). On the other hand, AMP might be more strongly associated with the liposome surface, therefore enhancing bilayer thickness. This could be attributed to the ammonium group in AMP, which, due to its higher basicity (Norn, 2014), may show stronger surface interactions. The surface charge of liposomes without surfactant was -39.23 ± 1.15 mV, which slightly decreased upon the inclusion of T80 (-37.00 ± 1.37 mV) and AMP (-36.53 ± 0.76 mV). This decrease in surface charge suggests that both surfactants were more closely associated with the surface of soy lecithin liposomes.

The incorporation of PE into both T80- and AMP-based liposomes resulted in a statistically significant increase in particle size and a decrease in zeta potential compared to their empty counterparts ($p < 0.05$) (Table 3.5). Higher loading of PE in liposomes led to the formation of larger vesicles due to its hydrophobic properties, which were expected to be more accumulated in the bilayers than in the internal aqueous phase of the liposome (Aytekin et al., 2020; Karakas et al., 2023; Ramli et al., 2021). A possible explanation for the lowered zeta potential was that PE interacted with the liposome surface. This is consistent with literature findings showing that phenolic compounds can interact with liposomal membranes through both polar and nonpolar interactions (Gibis et al., 2012; Ramli et al., 2021). The PDI, which measures the uniformity of size in colloidal systems, was also found to depend on the type of surfactant. The PE loading resulted in a broader size distribution in T80-containing liposomes, indicating a decrease in homogeneity. In contrast, liposomes containing AMP exhibited a slight increase in size uniformity following PE encapsulation, as evidenced by a lower PDI value.

The morphological features of empty and PE-loaded liposomes, formulated with T80 (L1, L1-PE2) and AMP (L2, L2-PE2), were visualized by TEM (Figure 3.13). The morphologies of all liposomes varied from near-spherical to spherical, as evidenced by the darker contrast of the vesicles in the TEM images, the incorporation of PE and the use of AMP seemed to enhance the affinity of liposomes for uranyl staining. This increased electron density may be attributed to the interaction between PE, AMP, and the bilayer surface. The empty liposome-T80 formulation (Figure 3.13 B) showed a relatively uniform vesicle size distribution, while the PE-loaded sample (Figure 3.13 A) displayed a broader size distribution, signifying reduced homogeneity. Some vesicles appeared smaller, whereas others exhibited an increase in size.

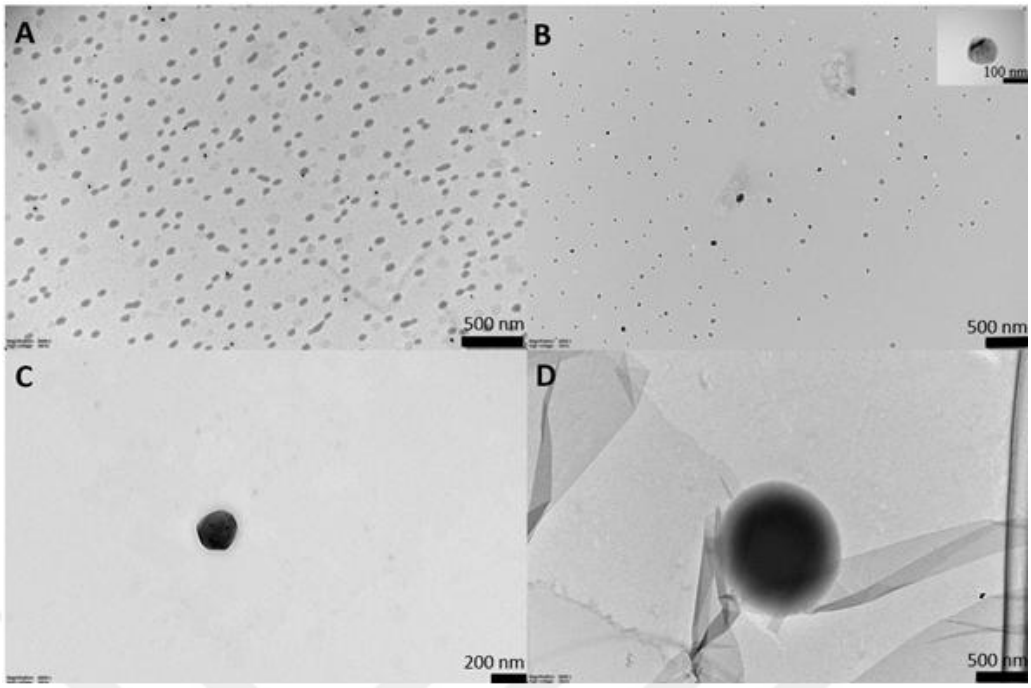

Figure 3. 13 TEM images of empty liposomes (L1 and L2; B and D) and PE-loaded liposomes (L1-PE2 and L2-PE2; A and C), formulated with T80 and AMP, respectively.

3.3 Liposomal PE-Loaded Xanthan–Salep Hydrogels: Preparation, Characterization, and Bioaccessibility of Phenolics

3.3.1 Morphological Characterization of Liposomal Gel Samples

The visual appearances of PE-loaded AMP and T80 liposomal gels were presented in Figure 3.14. Subsequently, their morphology was examined through SEM and cryo-TEM to evaluate the incorporation and structural integrity of the liposomes within the gel matrix, as well as to reveal the effects of AMP and T80 on the overall microstructure and network integrity of the formulations.

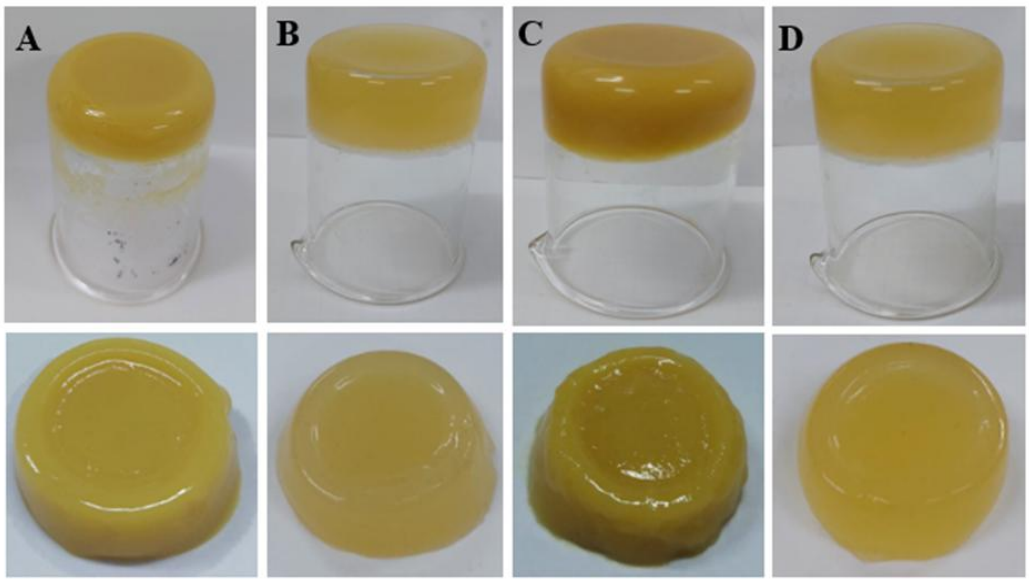

Figure 3. 14 PE-loaded and empty liposomal gels incorporated with AMP (A: PE-loaded, B: empty) and T80 (C: PE-loaded, D: empty).

As presented in Section 3.1.2, SEM analysis of xanthan gum–salep hydrogels without liposomes revealed relatively smooth and uniform surfaces, indicating a homogeneous gel network. In contrast, SEM images of PE-loaded liposomal hydrogels formulated with AMP (Figure 3.15, A–B) and T80 (Figure 3.15, C–D) revealed visible alterations in surface structure. As indicated by the white arrows, the liposomal gel matrix contains spherical or vesicle-like formations, which indicate the successful encapsulation of liposomes within the gel structure. Additionally, a porous morphology resembling a bird net was observed in both T80 and AMP-liposome loaded gels, likely resulting from the interaction between the polysaccharide network and liposomal vesicles. Such porous structures are advantageous for controlled release systems, providing pathways for diffusion of active compounds (Y. Liu et al., 2025).

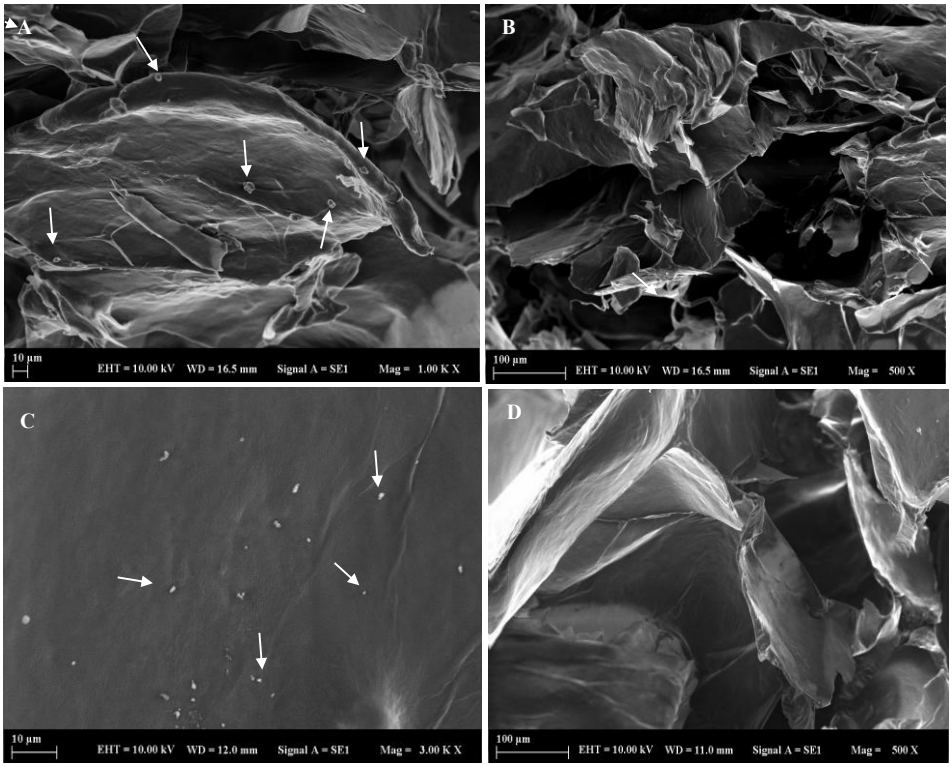

Figure 3. 15 SEM images of PE-loaded AMP liposomal gel (A-B) and PE-loaded T80 liposomal gel (C-D)

To further verify the successful incorporation of those modified liposomes into the hydrogel matrix, cryo-TEM was employed (Figure 3.16). This technique enables direct visualization of liposomes in a vitrified, hydrated state, thereby eliminating the need for negative staining or dehydration processes (Duché et al., 2023). The images demonstrate that both PE-loaded AMP-liposomes (Figure 3.16-A) and empty (Figure 3.16-B) liposomes embedded in the hydrogel maintained their spherical morphology, exhibiting no elongation or structural deformation. This characteristic is crucial for ensuring stable encapsulation and effective delivery of active compounds (Patel & Patel, 2020). Furthermore, PE-loaded liposomes were larger than the empty liposomes, consistent with size measurements obtained through dynamic light scattering (DLS) in aqueous dispersions (Section 3.2.1), which indicated mean diameters of 80.97 nm for the empty liposomes and 179.30 nm for the PE-loaded liposomes.

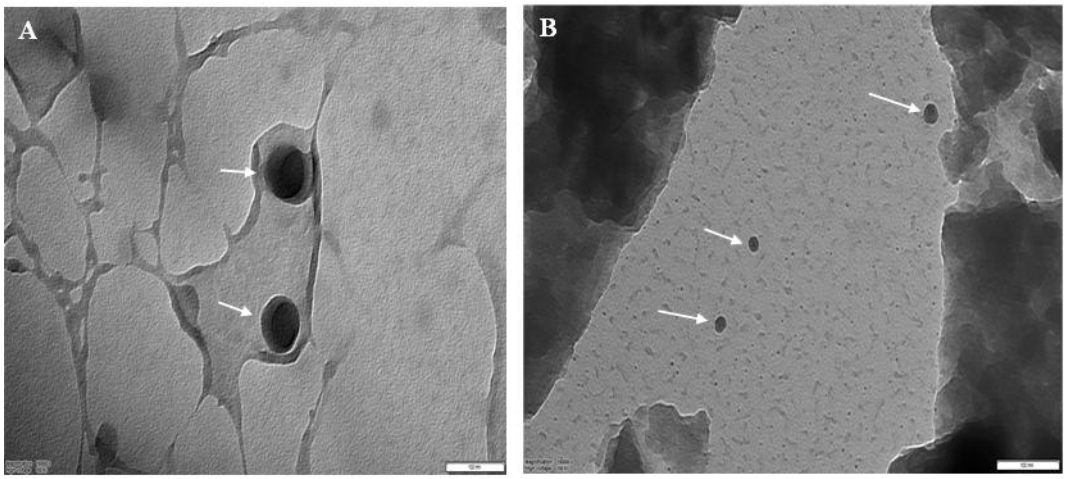

Figure 3. 16 Cryo-TEM images of PE-loaded (A) and empty (B) AMP-liposomal gels. Scale bar: 100 nm

3.3.2 Structural and Thermal Characterization of Liposomal Gels by DSC and FTIR

Figure 3.17 shows the FTIR spectra of the liposomal gel formulations and their corresponding components. Characteristic absorption bands of lecithin were observed at 2922, 2852, and 1737 cm^{-1}, which are consistent with previously reported values (Cai et al., 2023; Saroglu et al., 2022), and were clearly retained in the spectra of the liposomal gels. The peak observed at 1737 cm^{-1}, attributed to the C=O stretching vibration of ester linkages in lipid and triglyceride structures (Jang et al., 2019), was detectable in both empty AMP and T80-based liposomal gels, indicating the presence of lipid vesicles. Additionally, PE displayed specific absorption bands, notably at 1701 cm^{-1} (attributed to –COOH stretching), and at 1635, 1602, and 1454 cm^{-1}, which are linked to the vibrational modes of aromatic C=C, C=O, and/or C–H groups, characteristics commonly associated with phenolic compounds, amino acids, and flavonoids (Karakas et al., 2023). The characteristic PE bands were observed in the spectra of PE-loaded liposomal gels, although with reduced intensity, indicating successful encapsulation of PE within the liposomal matrix and potential interactions with other gel components (Ramli et al., 2021).

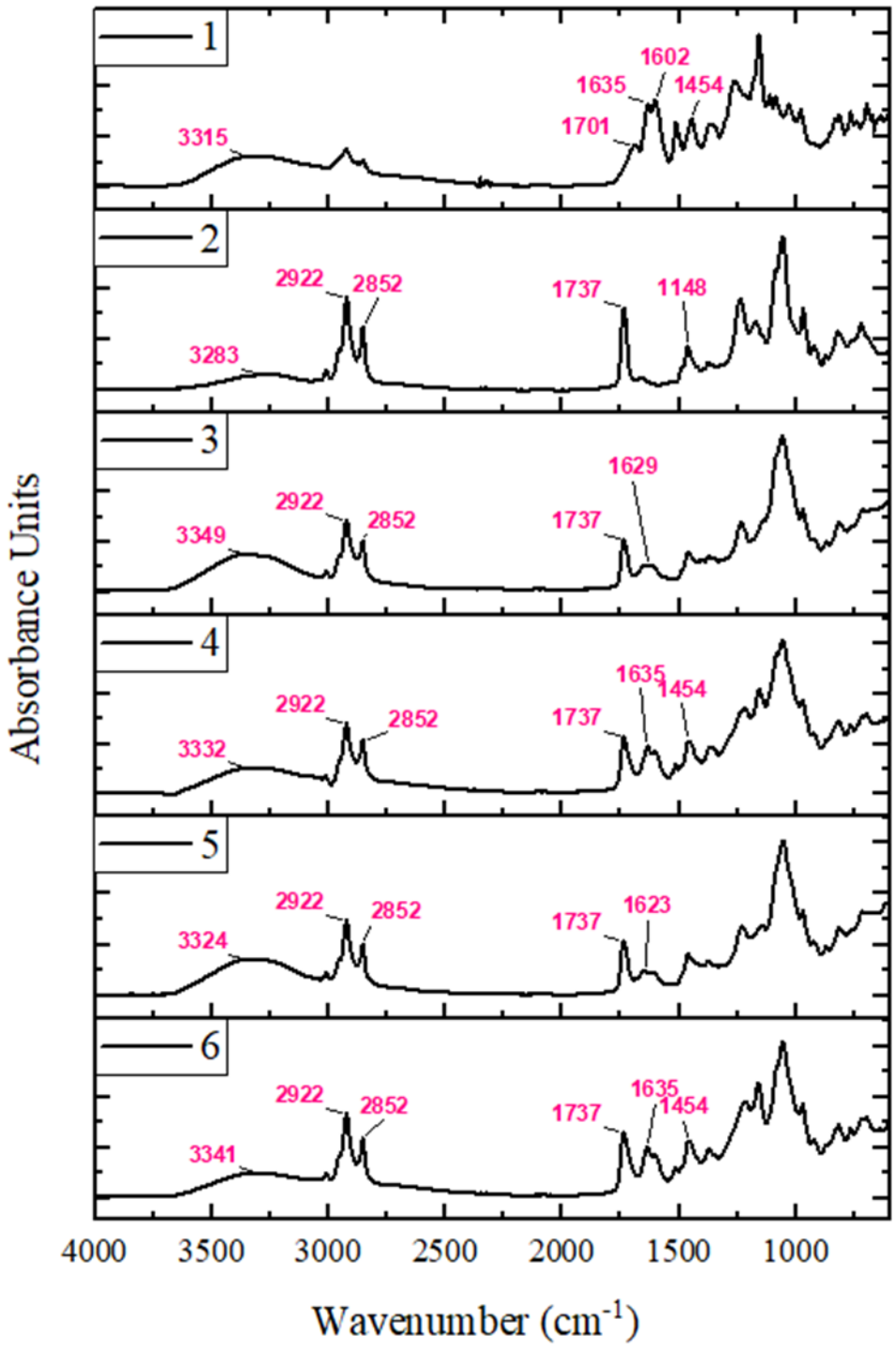

Figure 3. 17 FTIR spectra of individual components and liposomal gels: 1. PE, 2. Lecithin, 3. Empty T80-liposomal gel, 4. PE-loaded T80-liposomal gel, 5. Empty AMP-liposomal gel, 6. PE-loaded AMP-liposomal gel.

DSC is a commonly utilized method in thermal analysis, providing both qualitative and quantitative information about the thermal properties of solid-state materials (Leyva-Porras et al., 2020). It facilitates the evaluation of critical parameters, including melting and degradation points, glass transition, crystallization and

melting enthalpies, latent and specific heats, polymorphic behavior, and the overall purity of substances. Moreover, DSC is commonly used to identify potential molecular interactions (Chiu & Prenner, 2011), particularly among components in complex formulations, such as liposomal gels, thereby enhancing the understanding of structural behavior in multi-component delivery systems. In this study, DSC was applied to evaluate the thermal behavior of the bioactive compound (PE) and to investigate its potential incorporation within the liposomal gel matrix.

Figure 3.18 shows that the DSC thermogram of PE revealed a clear endothermic peak at 179.30 °C, corresponding to the melting of phenolic components. This data corresponds with the melting range of propolis components documented by do Nascimento et al. (2019), which ranges from 145-200 °C. Upon incorporation of PE into the liposomal gel system, this peak shifted to lower temperatures: 150.89 °C in the AMP-based formulation and 155.63 °C in the T80-based formulation, suggesting potential interactions between PE and the gel matrix. Notably, the empty liposomal gels without PE exhibited even lower melting points at 135.91 °C (AMP) and 134.25 °C (T80), indicating structural differences in the absence of the active compound (Figure 3.18). The slightly higher melting point observed in the T80-based liposomal gel compared to AMP-based sample may be attributed to differences in surfactant-lipid interactions. Compared to free PE, the decreased intensity and downward shift of melting peaks in the loaded gels indicate potential entrapment of PE within the formulation (Chen et al., 2012). Similar thermal changes, such as peak shifting, reduced intensity, and broadening, have been associated with encapsulation in previous studies (da Rosa et al., 2013; Gharanjig et al., 2020).

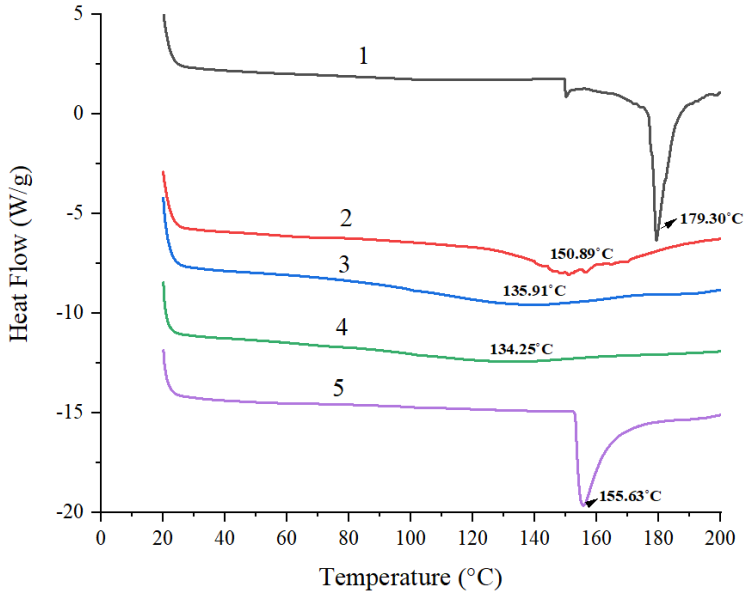

Figure 3. 18 DSC thermograms of PE and liposomal gels: 1. PE; 2. PE-loaded AMP- liposomal gel; 3. Empty AMP-liposomal gel; 4. Empty T80-liposomal gel; 5. PE-loaded T80-liposomal gel

3.3.3 Flow Behaviour of Liposomal Gels

The viscosity of semi-solid formulations has a substantial impact on the release kinetics of active ingredients from delivery systems (Sevinç-Özakar et al., 2022). Liposomes embedded in stiffer gel matrices exhibit slower diffusion into the surrounding medium than those in softer gels (W. Liu et al., 2020). All gel formulations display non-Newtonian, shear-thinning behavior, evidenced by a decrease in viscosity as the shear rate increases. (Figure 3.19). The rheological profile aligns with the established properties of xanthan gum and salep, the polymers utilized in the formulation, which exhibit shear-thinning flow characteristics (Khoobbakht et al., 2024; Xiu et al., 2011). The observed reduction in viscosity under shear is attributed to the disruption of hydrogen bonding interactions between xanthan gum and salep, which weakens the internal network matrix of the gel.

Shear-thinning behaviour was detailed in Section 3.1.3 for liposomal gels prepared with xanthan gum, salep, and surfactant-free liposomes. The incorporation of either empty or PE-loaded T80 and AMP liposomes did not significantly alter the overall flow characteristics of the gel matrix, as all samples exhibited a shear-thinning profile (Figure 3.19).

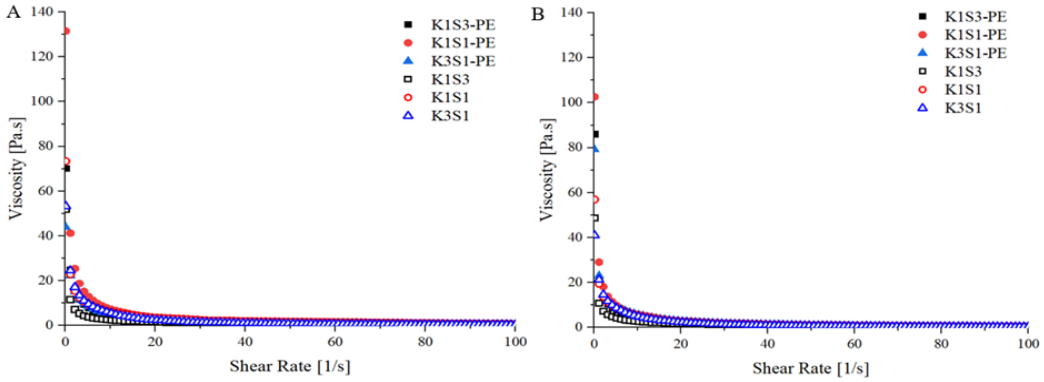

Figure 3. 19 Viscosity curves of (A) AMP-liposomal gels, (B) T80-liposomal gels.

Figure 3.20 illustrates the dynamic rheological behavior of AMP and T80-liposomal gels prepared with varying xanthan gum to salep ratios (1:1, 1:3, and 3:1, w/w). All formulations displayed solid-like viscoelastic properties, with G′ consistently exceeding G″ across the entire frequency range. AMP-based liposomal gels exhibited higher G′ values compared to those formulated with T80, indicating a more significant elastic quality and a more robust gel structure. The incorporation of PE into AMP-liposomal formulations resulted in a further increase in G′ values, suggesting that PE enhanced the mechanical integrity of the gel network. Moreover, both empty and PE-loaded AMP-liposomal gels demonstrated nearly constant G′ values with increasing frequency, indicating a stable elastic response under dynamic conditions. Conversely, T80-liposomal gels loaded with PE demonstrated a frequency-dependent decrease in G′, indicating that the inclusion of PE may have reduced gel strength. Nevertheless, in all instances, G′ values surpassed G″ values, thereby ensuring the preservation of viscoelastic properties.

The Power Law parameters (K′, K″, n′, and n″) calculated for both unloaded and PE-loaded AMP and T80 liposomal gels are shown in Table 3.6. A greater K' value than K" indicates a stronger gel structure in the generated gels. Additionally, values of n' and n" close to zero demonstrate the solid nature of the gels. In AMP-liposomal gels, the K′ values increased from a range of 37.09–65.19 Pa.s^n in the unloaded formulations to 61.14–100.74 Pa.s^n upon PE loading. This suggests that the presence of AMP enhances the gel structure when PE is loaded. The increased

particle sizes of AMP liposomes due to PE loading and the easier packaging of liposomes within the hydrogel have likely influenced the G' value.

Table 3. 6 Rheological parameters (K′, K″, n′, n″) obtained from the Power Law model for PE-loaded and unloaded liposomal gel formulations

	Polymers	K'	K''	n'	n''	R^2
AMP-liposomal gel	K1S3-PE	95.80±0.31^a	21.59±1.22^b	0.17±0.01^b	0.10±0.00^b	>0.99
	K1S1-PE	100.74±5.06^a	27.56±0.85^a	0.17±0.01^b	0.07±0.02^c	>0.99
	K3S1-PE	61.14±1.72^b	17.19±0.26^c	0.21±0.01^a	0.15±0.00^a	>0.99
	K1S3	60.45±1.73^a	10.23±0.23^a	0.16±0.00^b	0.10±0.01^c	>0.97
	K1S1	65.19±5.67^a	6.20±0.48^b	0.14±0.00^c	0.20±0.01^b	>0.95
	K3S1	37.09±0.72^b	5.44±0.13^b	0.21±0.00^a	0.24±0.00^a	>0.94
T80-liposomal gel	K1S3-PE	18.67±1.41^b	7.17±0.13^a	0.38±0.01^a	0.37±0.02^b	>0.97
	K1S1-PE	22.21±0.98^a	5.66±0.20^b	0.33±0.01^b	0.42±0.02^a	>0.97
	K3S1-PE	16.09±0.03^c	4.78±0.05^c	0.37±0.00^a	0.41±0.00^a	>0.96
	K1S3	72.67±5.39^a	14.53±1.45^a	0.18±0.01^b	0.08±0.02^b	>0.99
	K1S1	59.88±1.82^b	10.45±1.11^b	0.16±0.01^c	0.10±0.03^b	>0.98
	K3S1	31.15±0.52^c	5.53±0.04^c	0.21±0.00^a	0.19±0.00^a	>0.95

Different superscript letters in the same column indicate statistically significant differences ($p < 0.05$)

The enhanced solid-like behavior observed in AMP-based gels may be attributed to the molecular characteristics of AMP itself. In the chocolate industry, AMP is frequently used to reduce levels of lecithin and/or cocoa butter without compromising flow-related properties such as viscosity and yield stress. Its superior emulsifying performance compared to lecithin has been linked to the stronger interactions formed between ammonium groups and carbohydrate structures. Due to the basic nature of ammonium groups and the weakly acidic nature of carbohydrates, electrostatic interactions may facilitate the adsorption of ammonium or nitrogen groups (Norn, 2014). In this context, AMP molecules present on the surfaces of liposomes, as well as in their micellar form within the aqueous phase where polysaccharide-based polymers are dispersed, may interact with the surrounding matrix, thereby contributing to the improved rheological behavior of the gel. Additionally, PE, because of its hydrophobic nature, tends to localize at the surface of phospholipid bilayers, which may further interact with surrounding polymer chains, thereby supporting the structural enhancement of the gel network.

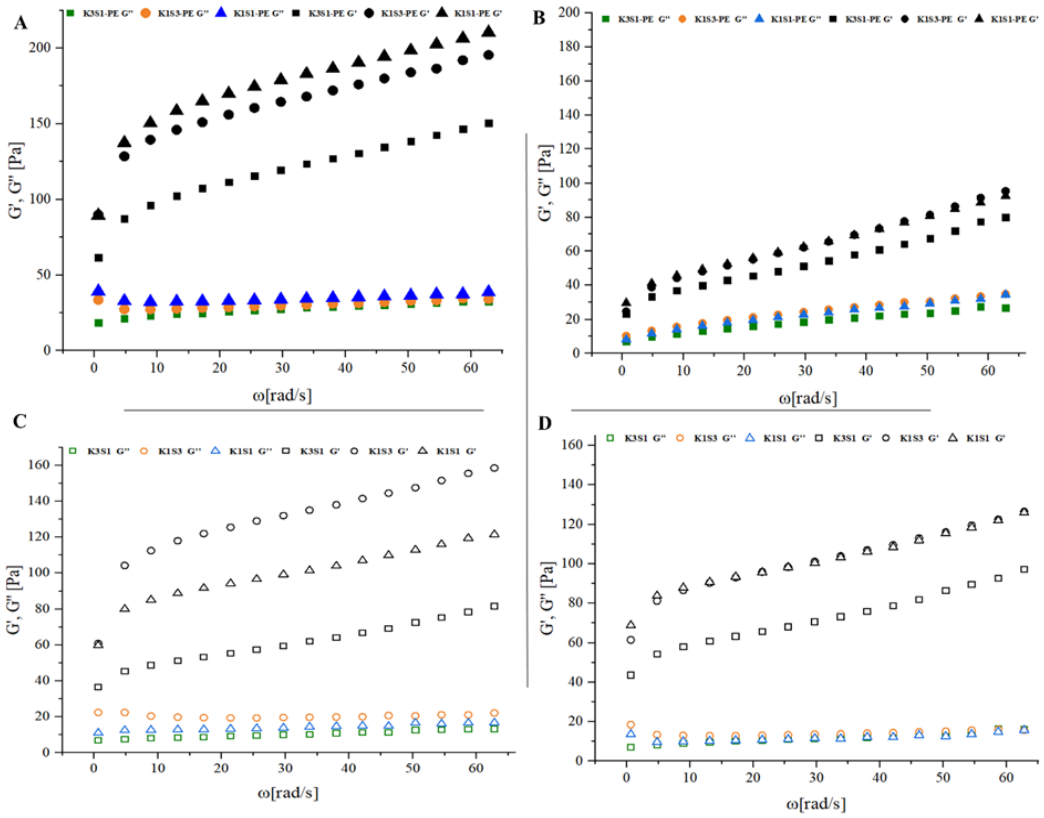

Figure 3. 20 Dynamic rheological properties of PE-loaded AMP-(A), T80- (B) liposomal gels, and empty AMP- (C) and T80- (D) liposomal gels.

Upon incorporating PE, T80-liposomal formulations showed a decrease in K′ values, suggesting reduced gel strength compared to AMP-based gels. This behavior may be linked to the relatively weak interactions between biocompatible hydrogels and specific surfactants, which can influence the rheological profile of microemulsion systems. As noted earlier, incorporating hydrogels into microemulsions might result in systems with altered viscosity and diminished gel-like characteristics (H. Chen et al., 2007). T80, a non-ionic hydrophilic surfactant, is commonly used to enhance the solubility of hydrophobic compounds like PE through liposomal encapsulation. It generates micelles that solubilize these compounds, enabling the micelles to integrate into the liposomal membrane by incorporating the hydrophobic tails into the bilayer while the hydrophilic heads remain in the aqueous phase (Ge & Ge, 2016). Nevertheless, T80 is exceedingly susceptible to temperature fluctuations. The solubility of water is reduced, and the micelle structure eventually releases water as the hydrogen bonds between water molecules and the surfactant diminish with increasing temperature. At a certain temperature, this behavior results in phase separation, commonly defined as the

cloud point temperature. T80 has a cloud point temperature of around 90 °C at its critical micelle concentration in water. This temperature may shift depending on T80 concentration or the presence of other solutes and can drop further when hydrophobic drugs are solubilized in the micelles (Rahman Khan et al., 2019). During gel preparation, liposomal dispersions were exposed to 80°C for 15 min. This thermal process may have influenced the solubility behavior of T80, potentially affecting liposome stability. As a result, previously solubilized PE could have migrated into the aqueous phase or partially precipitated, contributing to a reduction in gel strength. Nevertheless, G′ values remained consistently higher than G″ across all tested frequencies, and K′ values continued to exceed K″, indicating that the gel maintained its elastic characteristics without substantial deterioration of its structure.

3.3.4 *In Vitro* Mucoadhesive Properties

Mucoadhesive properties play a crucial role in developing oral delivery systems, as their interaction with the gastrointestinal mucus layer enhances retention time and promotes the controlled release of encapsulated compounds (Andrews et al., 2009). PE incorporation led to a marked enhancement in mucoadhesion across all xanthan gum to salep ratios for both AMP- and T80-based liposomal gels (Table 3.7). The findings are consistent with prior studies demonstrating enhanced mucoadhesiveness due to the incorporation of PE in hydrogel and fiber-based systems (Berretta et al., 2013; Karakas et al., 2023). Among the PE-loaded formulations, AMP-liposomal gels demonstrated greater mucoadhesion work, with values ranging from 7.39 to 13.38 g.mm, while T80-based gels exhibited values between 4.64 and 8.77 g.mm. This suggests that the presence of AMP significantly influenced gel mucin interactions. The polymer composition strongly influenced mucoadhesion. Formulations with a higher xanthan gum content demonstrated stronger mucoadhesive behavior. Specifically, the K3S1 ratio yielded the highest mucoadhesion values among the PE-loaded gels in both AMP (13.38 g.mm) and T80 (8.25 g·mm) formulations, while the lowest values were observed in PE-loaded K1S3 gels (AMP: 7.39 g.mm; T80: 4.64 g.mm), indicating that increased xanthan gum ratios enhance mucosal interaction. The results support earlier studies indicating that xanthan gum exhibits enhanced mucoadhesive properties relative to other widely used polymers (Nakamura et al., 1996).

Table 3. 7 *In vitro* mucoadhesion results of liposomal gels

Samples	Polymer	PE / Empty	Mucoadhesion work (g.mm)
AMP-liposomal gel	K1S1	PE	9.22 ± 1.50^{b}
		Empty	2.93 ± 0.22^{y}
	K1S3	PE	7.39 ± 0.43^{b}
		Empty	2.87 ± 0.19^{y}
	K3S1	PE	13.38 ± 1.79^{a}
		Empty	4.27 ± 0.04^{x}
T80-liposomal gel	K1S1	PE	8.77 ± 0.10^{a}
		Empty	3.36 ± 0.68^{x}
	K1S3	PE	4.64 ± 0.54^{b}
		Empty	1.51 ± 0.00^{y}
	K3S1	PE	8.25 ± 0.28^{a}
		Empty	3.87 ± 0.27^{x}

Different superscript letters (a–c among PE-loaded; x–z among Empty liposome-loaded gels) in the same column indicate significant differences in T80 and AMP-liposomal gels ($p < 0.05$).

3.3.5 *In Vitro* Digestion Analysis of Free PE, PE-Loaded Liposome, and Liposomal PE-Loaded Gel

The characterization analyses, which included flow behavior analysis and *in vitro* mucoadhesion measurements, indicated that the AMP-based liposomal gel formulation exhibited enhanced structural and functional properties compared to the T80-based formulation. The AMP formulation demonstrated elevated G′ values, indicating increased elasticity and viscoelastic solid-like characteristics, along with enhanced mucoadhesive properties. These attributes are essential for maintaining structural integrity and ensuring localized delivery during gastrointestinal digestion. Consequently, the *in vitro* digestion analysis was performed using the AMP-based liposomal gel system. Additionally, digestion analyses were conducted for free PE and PE-loaded AMP liposomes to facilitate the comparison of change of phenolics at *in vitro* digestion stages and phenolic bioaccessibility between free PE and liposomal encapsulation systems.

***In Vitro* Digestion of Free PE and Liposomal PE**

The phenolic composition of free PE was characterized, and the findings are summarized in Table 3.8. European-type poplar propolis is noted for its complex composition, which includes more than 300 constituents such as free phenolic acids, their esters, flavonoids, glycosides, and phenolic glycerides. The phenolic profile resembled that of poplar-type propolis, featuring a high concentration of cinnamic

acid derivatives, such as *p*-coumaric acid, caffeic acid, *trans*-cinnamic acid, *trans*-ferulic acid, and 3,4-dimethoxycinnamic acid, along with distinctive flavonoids. The compounds identified were flavonols (quercetin, kaempferol, galangin, pinobanksin), flavones (apigenin, luteolin, chrysin), and flavanones (pinocembrin, naringenin). The compounds identified in highest abundance included pinocembrin (18.64 ± 0.54 mg/g), galangin (14.36 ± 1.48 mg/g), pinobanksin (14.06 ± 0.98 mg/g), and CAPE (12.66 ± 0.74 mg/g). The presence of these major constituents is commonly observed in European propolis samples (Guzelmeric et al., 2023; Hegazi et al., 2000; Ozdal et al., 2019).

Table 3. 8 LC-MS/MS analysis of phenolic compounds in PE and PE-loaded liposome

Compounds	Molecular formula	RT (min)	Ionization Mode	Precursor ion (m/z)	Product ion(s) (m/z)	Cone (V)	Collision (eV)	PE	Liposomal PE
								mg/g	µg/mL liposome
3,4 dimethoxy cinnamic acid	$C_{11}H_{12}O_4$	19.1		206.7	102.7	25	20	6.62±0.47	207.72±4.07
Apigenin	$C_{15}H_{10}O_5$	25.0		269	117.3/149/151	40	30/25/25	3.30±0.14	88.21±3.07
Caffeic acid	$C_9H_8O_4$	10.9		179	135	25	20	4.19±1.15	181.76±5.50
CAPE	$C_{17}H_{16}O_4$	32.4		283	179/161/135	25	20	12.66±0.74	306.01±0.66
Chrysin	$C_{15}H_{10}O_4$	30.9		253	225/209/151	25	20	9.31±1.08	212.36±5.44
Trans-ferulic acid	$C_{10}H_{10}O_4$	14.7		193	178/149/134	25	20	1.60±0.21	61.99±4.08
Galangin	$C_{15}H_{10}O_5$	31.9		269	197/213/227	25	20	14.36±1.48	388.33±1.53
Kaempferol	$C_{15}H_{10}O_6$	25.4	ESI(-)	285	93/151/257	25	20	3.68±0.15	98.45±11.57
Luteolin	$C_{15}H_{10}O_6$	22.3		285	133/241/267	25	20	0.94±0.02	29.12±5.08
Naringenin	$C_{15}H_{12}O_5$	24.2		271	145/151	25	20	2.07±0.06	50.03±3.78
p-coumaric acid	$C_9H_8O_3$	13.5		163	93/119/147	25	20	2.14±0.27	90.09±1.85
Pinobanksin	$C_{15}H_{12}O_5$	24.3		271.2	153/225/253	25	20	14.06±0.98	290.66±16.18
Pinocembrin	$C_{15}H_{12}O_4$	31.1		255	151/171/213	25	20	18.64±0.54	608.58±1.47
Quercetin	$C_{15}H_{10}O_7$	22.4		301	150.8/178.9	35	20	1.67±0.18	71.15±2.02
Trans-cinnamic acid	$C_9H_8O_2$	21.1		147	77/102.8	25	20	2.33±0.12	86.44±13.66
Total								**97.56**	**2782.96**

ESI refers to electrospray ionization; RT denotes retention time.

An *in vitro* digestion model simulating oral, gastric and intestinal conditions was employed to assess the change of phenolic content of PE and its liposomal formulation upon digestion. The phenolic composition of each digestion phase was quantified using LC-MS/MS, and the corresponding results are presented in Table 3.9. It is important to note that the digestion process was carried out without the use of alcohol or other solubilizing agents for PE, allowing for a realistic assessment of its bioaccessibility and solubility under physiological conditions.

The limited water solubility of PE restricts its efficacy in oral delivery systems, thereby reducing its bioavailability and functional performance in gastrointestinal environments. Liposomal systems have emerged as promising carriers, enabling the use of food-grade components instead of organic solvents in the delivery of poorly water-soluble compounds like PE. Previous research indicates that liposomal membranes exhibit significant stability in the gastric environment, attributed to the mild effects of pepsin and low pH. In contrast, the enzymatic and surfactant-rich conditions present during the intestinal phase may lead to membrane disruption and an increased release of encapsulated compounds (Saroglu et al., 2022; Zhang et al., 2019). In the gastric phase of digestion, 3,4-dimethoxycinnamic acid and caffeic acid were identified as the most abundant phenolic compounds in both free PE (153.85 and 196.22 µg/g, respectively) and liposomal PE (88.66 and 82.33 µg/mL, respectively) (Table 3.9). Although pinocembrin exhibited the highest concentration in the undigested extract (18.64 mg/g), its levels were lower than those of pinobanksin after gastric treatment. In PE, pinobanksin reached 81.54 µg/g, while pinocembrin remained at 21.96 µg/g; similarly, in liposomal formulation, the values were 61.04 µg/mL and 9.34 µg/mL, respectively. The observed difference can be attributed to the structural properties of pinobanksin, specifically its extra hydroxyl group, which most likely increases its solubility in aqueous environments. Sun et al. (2015) found that pinobanksin concentrations were less influenced by changes in ethanol content, while pinocembrin exhibited greater variability, indicating distinct solubility behaviors between the two flavonoids. In the intestinal phase of digestion, a significant increase in the concentration of most phenolic compounds was observed. Pinobanksin levels increased to 298.60 µg/g in PE and 1440.70 µg/mL in liposomal formulation, whereas pinocembrin levels increased to 292.59 µg/g and 990.80 µg/mL, respectively. Significant increases were also

observed for compounds such as chrysin, 3,4-dimethoxycinnamic acid, and *p*-coumaric acid. The observed increase in phenolic content is in agreement with the findings of Ozdal et al. (2019), who reported a rise in total phenolic and flavonoid levels following intestinal digestion of Turkish propolis extracts.

In the intestinal phase, a reduction in the levels of specific phenolic compounds, such as caffeic acid, *trans*-ferulic acid, and quercetin, was observed in the non-encapsulated PE sample. In contrast, the concentrations of all phenolics were elevated in the liposomal formulation (Table 3.9). The chemical stability of flavonoids in intestinal conditions is associated with distinct structural features, including the hydroxyl group at the C3 position in the C-ring, the presence of a catechol structure on the B-ring, and the C2=C3 double bond, which may affect their degradation under alkaline pH (Jurasekova et al., 2014). Quercetin, with two hydroxyl groups on its B-ring, may exhibit greater susceptibility to intestinal degradation than galangin, which lacks hydroxyl groups on that ring, or kaempferol, which contains only one. Álvarez-Diduk et al. (2013) demonstrated that quercetin degrades more quickly than kaempferol in strongly alkaline conditions (pH > 9), indicating reduced chemical stability. The increase in phenolic concentrations from gastric to intestinal stages in both formulations can be attributed to enhanced solubilization of phenolics, influenced by prolonged exposure time, elevated pH, and the presence of enzymes and bile salts that may facilitate the release of compounds bound to resinous PE matrices. Most phenolics in PE are weak acids, leading to increased solubility at pH values exceeding their respective pKa values. The reported pKa values are 4.43 and 8.69 for caffeic acid (Beltrán et al., 2003); 7.05, 8.88, and 9.92 for kaempferol; 5.87, 7.12, and 8.43 for quercetin (Fuguet et al., 2023); and 6.8 and 9.4 for galangin (Lemańska et al., 2001). These values indicate a tendency for increased solubility in the alkaline conditions of the intestinal phase.

Table 3. 9 Effect of *in vitro* digestion on the phenolic compounds of free PE and liposomal PE

Compounds	PE (µg/g)			Liposomal PE (µg/mL liposome)		
	SGF	SIF	BI%	SGF	SIF	BI%
3,4 dimethoxy cinnamic acid	153.85±13.15^{b}	367.82±66.87^{a}	5.63	88.66±16.89^{b}	586.23±25.95^{a}	282.28
Apigenin	-	-	-	-	90.60±10.32^{a}	102.71
Caffeic acid	196.22±6.85^{a}	122.94±22.52^{b}	3.20	82.33±8.81^{b}	176.37±2.57^{a}	97.03
CAPE	-	3.56±1.19^{a}	0.03	-	205.00±34.64^{a}	66.99
Chrysin	-	56.78±11.75^{a}	0.61	1.92±0.08^{b}	644.90±76.82^{s}	303.68
Trans-ferulic acid	60.35±7.63^{a}	41.68±0.00^{b}	2.64	37.96±8.885^{b}	149.60±40.21^{a}	241.33
Galangin	54.96±18.32^{a}	84.20±17.34^{a}	0.60	9.24±2.13^{b}	81.80±0.69^{a}	21.06
Kaempferol	-	77.48±22.10^{a}	2.09	-	6.40±0.46^{a}	6.50
Luteolin	35.87±11.96^{a}	29.58±9.86^{a}	3.13	7.69±1.66^{b}	52.00±13.89^{a}	178.57
Naringenin	4.54±1.05^{b}	45.38±4.96^{a}	2.19	7.81±1.22^{b}	205.40±5.24^{a}	410.55
p-coumaric acid	62.80±6.29^{b}	103.36±20.56^{a}	4.96	43.72±1.37^{b}	285.90±44.77^{a}	317.35
Pinobanksin	81.54±11.05^{b}	298.60±28.95^{a}	2.12	61.04±4.29^{b}	1440.70±105.01^{a}	495.67
Pinocembrin	21.96±0.42^{b}	292.59±23.50^{a}	1.57	9.34±0.69^{b}	990.80±107.59^{a}	162.81
Quercetin	54.41±11.61^{a}	34.82±7.61^{a}	2.05	5.94±1.22^{b}	41.00±5.00^{a}	57.62
Trans-cinnamic acid	52.24±17.41^{b}	117.76±3.36^{a}	5.06	9.16±1.16^{b}	209.25±16.65^{a}	242.08
Total	*778.73*	*1676.55*	*1.72*	*364.92*	*5173.55*	*185.90*

Values with different superscript letters between digestion stages within each sample differ significantly ($p < 0.05$). BI: Bioaccessibility index (%); SGF: Simulated gastric fluid; SIF: Simulated intestinal fluid; L2-PE2: PE-loaded liposomes with AMP.

The bioaccessibility index (BI%) of phenolic compounds was determined by comparing their concentrations after *in vitro* intestinal digestion (Table 3.9) to those in the corresponding undigested samples (Table 3.8). The non-encapsulated PE exhibited generally low BI% values, indicating restricted solubility and release of phenolics in gastrointestinal conditions. The highest BI% values were recorded for 3,4-dimethoxycinnamic acid (5.63%), *p*-coumaric acid (4.96%), and *trans*-cinnamic acid (5.06%). CAPE (<0.1%), galangin (0.6%), pinobanksin (2.12%), and pinocembrin (1.57%) exhibited low release under intestinal conditions. The encapsulation of PE within liposomes formulated with AMP significantly enhanced the bioaccessibility of all phenolic compounds. The enhancement is due to the structural and protective properties of the liposomal system, which likely improved the dispersion and stability of phenolics during digestion. *p*-coumaric acid demonstrated the highest BI% at 317.4%, followed by 3,4-dimethoxycinnamic acid at 282.3%, trans-cinnamic acid at 242.1%, and trans-ferulic acid at 241.3%. The findings demonstrate the effectiveness of the liposomal delivery system in improving the gastrointestinal bioaccessibility of phenolic compounds derived from propolis.

A previous study indicated that, after *in vitro* digestion, the majority of phenolic compounds in PE extracts dissolved in ethanol and lactic acid, specifically quercetin, kaempferol, apigenin, and luteolin were not detectable at the intestinal stage. Conversely, pinocembrin and trans-cinnamic acid were retained at levels between 43–50% and 62–74%, respectively (Atayoglu et al., 2023).

The liposomal formulation demonstrated significant retention of phenolic compounds after *in vitro* digestion. Compared to the undigested sample, intestinal concentrations of pinocembrin and pinobanksin increased by approximately 1.6-fold and 5-fold, respectively, suggesting improved stability and release within the digestive environment. Among the bioactives, *p*-coumaric acid, *trans*-cinnamic acid, 3,4-dimethoxycinnamic acid, and *trans*-ferulic acid demonstrated BI% values exceeding 240%, while apigenin and CAPE showed recoveries of 103% and 67%, respectively. In contrast, kaempferol (6.5%) and galangin (21.1%) had the lowest bioaccessibility levels. The total phenolics in the liposomal sample presented an overall BI% of 185.9%, indicating that liposomal encapsulation effectively

enhances the solubility and digestive stability of phenolic compounds derived from PE.

Previous studies have emphasized the protective function of liposomal systems in preserving structural integrity during gastrointestinal digestion. The organized bilayer structure of phospholipids has been shown to resist degradation in the gastric environment (Saroglu et al., 2022). The intestinal environment facilitates the enhanced release of phenolic compounds from liposomes, which can be attributed to vesicle swelling, increased membrane permeability resulting from bile salt interaction, and enzymatic hydrolysis of the phospholipid matrix (X. Liu et al., 2020). AMP is thought to contribute to the stability of liposomal vesicles and the improved retention of phenolics throughout digestion. The bioaccessibility of phenolic compounds is influenced by their molecular structure and physicochemical properties. In the study by Toro-Uribe et al. (2018), liposomal encapsulation of phenolic extracts high in cocoa procyanidins enhanced the bioaccessibility of catechins, while no similar effect was noted for alkaloids. The bioaccessibility of Urolithin A and spirulina-derived phenolics has been shown to increase by 4-fold and 1.5-fold, respectively, when utilizing liposomal delivery systems (Hu et al., 2023; Machado et al., 2019).

Variations in the bioaccessibility of PE phenolics are likely influenced by their chemical structure. As highlighted by C. X. Li et al. (2023), phenolic acids generally demonstrate greater bioaccessibility than flavonoids. In particular, among hydroxybenzoic acid derivatives, a higher degree of hydroxylation has been associated with decreased gastrointestinal stability and accessibility. In agreement with these findings, the BI% of caffeic acid was lower than that of *p*-coumaric acid in all sample. Elevated concentrations of phenolic acids following digestion could be attributed to the breakdown of complex phenolic derivatives into simpler forms. Hydroxycinnamic acids, including caffeic, *p*-coumaric, ferulic, and *trans*-cinnamic acids, are typically found in the diet in bound forms such as glycosides or esters of quinic acid. These conjugates can be released through enzymatic hydrolysis during gastrointestinal digestion (Stalmach, 2014). A similar mechanism may account for the increased levels of caffeic acid, potentially resulting from the conversion of CAPE by digestive enzymes. Although direct quantification was not feasible due to the lack of standard references, previous reports have identified significant

amounts of pinobanksin esters, such as pinobanksin-3-acetate, in propolis (Bloor & Mitchell, 2021). Enzymatic activity during digestion likely contributed to the hydrolysis of such esterified forms, leading to the release of free pinobanksin.

***In Vitro* Digestion of PE-Loaded AMP-Liposomal Gel**

In vitro digestion results for TPC, TFC, and antioxidant activities (FRAP, DPPH, and ABTS) of free PE and liposomal PE gel are shown in Table 3.10, which includes values before digestion as well as at simulated oral, gastric, and intestinal stages. The values obtained during the oral phase were lower than the initial concentration values. This observed reduction can be attributed to the limited solubility of PE in simulated saliva and the brief duration of exposure during the oral phase (Ucar & Karadag, 2019). When compared to the oral phase, significant increases were observed only in TFC, ABTS, and DPPH values in free PE during the gastric stage. An increase in TPC, FRAP, and ABTS levels was observed in the intestinal phase for both free PE and its AMP-liposomal gel counterpart. While TFC values increased in both samples, the change was statistically significant only for the liposomal gel formulation ($p < 0.05$). The results align with previous studies indicating that the intestinal environment aids in the release of phenolic compounds (Ozdal et al., 2019; Yesiltas et al., 2014). Although the gastric phase had a longer incubation time, the limited increase in values compared to the oral phase could be linked to its acidic conditions. At low pH levels, phenolic compounds typically experience protonation, leading to decreased polarity and, consequently, reduced solubility in aqueous environments (Yen et al., 2017). Phenolic compounds found in PE exhibit weak acidic properties and tend to become more soluble at pH values above their pKa. Since the pH of the intestinal phase is close to these values, solubility improves at this stage. Additionally, the extended exposure time and the action of intestinal enzymes and bile salts likely contribute to the enhanced release of phenolics. The digestion process resulted in clearly different recovery levels of TPC, TFC, and antioxidant capacity between free PE and the liposomal gel. BI% values for free PE were consistently low, ranging from 0.06% to 0.25%. The lowest value was noted for DPPH, while ABTS had the highest within this range. In contrast, BI% values were markedly improved when PE was encapsulated in the liposomal gel, increasing to a range of 18.57% to 91.41%, with the highest again observed in ABTS. Both sample types were initially dispersed in water without the

use of organic solvents; the liposomal matrix clearly supported improved solubility and retention during digestion. Specifically, the BI% of TPC reached 40.45% in the liposomal PE gel, which aligns with previously reported values for solvent-assisted systems (12–47%) that utilized solvents such as ethanol, propylene glycol, L-arginine, or lactic acid (Mergen Duymaz et al., 2024).

Table 3. 10 Changes in TPC, TFC, and antioxidant activity of free PE and liposomal PE gel during *in vitro* digestion

	Sample	Initial	Oral	Gastric	Intestinal	BI%
		mg/g		µg/g		
TPC[1]	**PE**	312.74±18.74	287.58±5.10^{b}	285.09±28.84^{b}	652.66±56.16^{a}	0.21
	Liposomal gel	6.28±0.22	584.06±48.56^{b}	686.50±14.97^{b}	2605.07±172.75^{a}	40.45
TFC[2]	**PE**	180.93±8.23	81.45±1.94^{b}	138.65±20.36^{a}	183.26±26.18^{a}	0.10
	Liposomal gel	4.20±0.16	316.43±24.75^{b}	321.36±19.56^{b}	782.90±55.42^{a}	18.57
FRAP[3]	**PE**	489.93±31.23	446.28±53.53^{b}	447.49±24.87^{b}	755.54±26.09^{a}	0.16
	Liposomal gel	9.85±1.82	609.40±87.44^{b}	462.94±44.15^{b}	5547.39±848.47^{a}	56.35
ABTS[4]	**PE**	658.35±25.83	439.16±30.59^{c}	701.46±58.08^{b}	1659.59±35.60^{a}	0.25
	Liposomal gel	12.34±0.39	2222.55±331.01^{b}	2257.01±234.38^{b}	11281.43±743.84^{a}	91.41
DPPH[5]	**PE**	428.84±2.38	116.13±14.57^{b}	220.20±43.71^{a}	241.01±22.89^{a}	0.06
	Liposomal gel	8.72±0.11	507.42±98.61^{b}	366.97±40.60^{b}	1691.07±14.00^{a}	19.38

PE: Propolis extract; BI: Bioaccessibility index (%). Different superscript letters in the same row indicate significant differences ($p < 0.05$). TPC: Total phenolic content (µg GAE/g), TFC: Total flavonoid content (µg CE/g), FRAP: Ferric reducing antioxidant power, ABTS: 2,2'-azino-bis (3-ethylbenzothiazoline-6-sulfonic acid), DPPH: 2,2-diphenyl-1-picrylhydrazyl radical scavenging activity. All antioxidant values are expressed as µg TE (Trolox equivalent)/g.

The changes in individual phenolic compounds PE-loaded AMP-liposomal gels during *in vitro* digestion were given in Table 3.11. The total amounts of identified phenolic acids and flavonoids in the non-digested samples were 2.65 mg/g for the liposomal PE gel. The primary flavonoids identified included pinocembrin, galangin, CAPE, pinobanksin, and chrysin. Among the phenolic acids, caffeic acid and 3,4-dimethoxycinnamic acid were found in higher concentrations. Several phenolic acids, including CAPE, may also exist as esters of benzyl, methylbutenyl, phenylethyl, or cinnamyl alcohols (Table 3.11).

While the recovery of phenolic compounds from free PE after intestinal digestion was limited to 1.72% (1676.55 µg/g), it increased to 186% with liposomal PE, as previously discussed in the previous section. In this gel-based delivery system, incorporating PE into a liposomal gel resulted in a recovery rate of 286.52% (7590.02 µg/g) after-digestion (Table 3.11). The additional hydrogel barrier likely contributed to improved protection of phenolics against digestion and facilitated their enhanced release during the intestinal phase.

The *in vitro* bioaccessibility (BI%) of individual phenolic compounds ranged from 6.50% to 495.60% in liposomal PE. When PE was incorporated into a liposomal gel, the BI% values further increased, ranging from 10.13% to 582.75% (Table 3.11). Among the evaluated flavonoids, kaempferol (10.13%), galangin (23.66%), and quercetin (61.08%) demonstrated the lowest BI% values from the liposomal gel. This trend can be attributed to the inadequate alkaline stability of flavonoids containing a hydroxyl group at the C3 position. Conversely, luteolin, which does not possess this functional group, exhibited a notably higher BI% (305.61%), consistent with literature indicating its improved stability under intestinal conditions (Jurasekova et al., 2014). In a previous study, PE was dissolved in ethanol, propylene glycol, and L-arginine prior to digestion, and under these conditions, kaempferol and quercetin were not detected in the intestinal phase, while galangin exhibited a BI% of 0.78–3.33% (Mergen Duymaz et al., 2024).

Table 3. 11 Changes in individual phenolic compounds of liposomal gel during *in vitro* gastrointestinal digestion

	Liposomal PE gel				
	Initial	**Oral**	**Gastric**	**Intestinal**	**BI%**
	Phenolics (µg/g)				
3,4 Dimethoxy cinnamic acid	197.83±3.88	110.88±3.01^{c}	141.47±13.82^{b}	573.49±12.20^{a}	290.04
Apigenin	84.01±2.93	4.05±0.54^{b}	1.70±0.20^{b}	161.00±16.00^{a}	192.20
Caffeic acid	173.11±5.25	75.13±9.15^{c}	146.74±18.56^{b}	714.00±10.00^{a}	412.60
CAPE	291.44±0.63	18.16±1.33^{b}	4.10±0.22^{c}	592.75±3.21^{a}	203.39
Chrysin	202.25±5.18	38.22±0.84^{b}	12.87±1.45^{b}	1003.92±63.10^{a}	497.04
***Trans*-Ferrulic acid**	59.04±3.89	42.44±0.09^{b}	36.81±7.21^{b}	253.03±17.02^{a}	430.12
Galangin	369.83±1.46	6.13±1.63^{b}	8.66±1.03^{b}	87.50±2.09^{a}	23.66
Kaempferol	92.18±5.66	-	-	9.31±1.28^{a}	10.13
Luteolin	27.73±4.83	3.21±0.66^{b}	4.28±0.54^{b}	83.00±1.77^{a}	305.61
Naringenin	47.64±3.60	11.43±0.81^{b}	14.27±1.93^{b}	245.32±28.26^{a}	519.88
***p*-Coumaric acid**	85.80±1.76	36.72±5.00^{b}	46.91±4.03^{b}	443.12±70.32^{a}	516.10
Pinobanksin	276.82±15.41	75.84±3.79^{b}	95.83±9.78^{b}	1604.38±171.31^{a}	582.75
Pinocembrin	579.60±1.40	70.45±3.37^{b}	35.15±2.33^{b}	1613.53±147.71^{a}	278.37
Quercetin	67.76±1.93	3.23±0.11^{b}	3.74±0.85^{b}	41.42±3.85^{b}	61.08
***Trans*-cinnamic acid**	82.33±13.01	13.52±2.11^{b}	19.37±5.32^{b}	150.60±0.32^{b}	185.92
Total	***2650.44***	***509.41***	***574.60***	***7590.02***	***286.52***

BI: Bioaccessibility index (%). Different superscript letters in the same row indicate statistically significant differences ($p < 0.05$).

Similarly, Atayoglu et al. (2023) were unable to detect several flavonoids, including quercetin, kaempferol, and apigenin, following the simulated intestinal digestion of free PE dissolved in a lactic acid solution. An improved recovery of structurally sensitive flavonoids, such as galangin and luteolin, was observed when PE was delivered using liposomal gel.

Apigenin, a flavonoid mainly found in products derived from bees, exhibits limited bioaccessibility in the gastrointestinal tract due to its low solubility in both water and lipid environments. Several delivery systems, such as liposomal carriers, nanocrystals, and self-emulsifying formulations, have been developed to address its poor solubility (Kashyap et al., 2022). According to the previous section, when free PE was directly dispersed into the oral phase, apigenin was not detected at any stage of digestion. When initially dissolved in certain solvents, apigenin became detectable, with its BI% ranging from 29% to 56% (Mergen Duymaz et al., 2024). The inclusion of PE in a liposomal gel led to a significant increase in apigenin concentration during the intestinal phase, resulting in a BI% of 192.20. This enhancement likely results from improved solubilization and some level of protection for apigenin or its metabolites during digestion. Apigenin is often present in propolis in glycosylated forms like isoschaftoside and vicenin-2, which are recognized for their stability under gastric conditions (Kashyap et al., 2022; Righi et al., 2013). Enzymatic cleavage of the C-ring and subsequent reduction of double bonds during the intestinal phase may result in increased levels of free apigenin. (Stevens & Maier, 2016).

CAPE shows limited solubility in water (<10 µg/mL) and is quickly hydrolyzed into caffeic acid and phenethyl alcohol during the digestion (Catchpole et al., 2018; Wang et al., 2020). Its sensitivity to pepsin has also been demonstrated under *in vitro* gastric conditions (Wei et al., 2021). The CAPE levels in the liposomal PE gel decreased from 18.16 µg/g in the oral phase to 4.10 µg/g in the gastric phase during digestion, indicating that the gel is susceptible to gastric conditions. A marked increase in the intestinal phase (592.75 µg/g) may be attributed to improved release.

Among the phenolic compounds evaluated in the liposomal gel, pinobanksin showed the highest bioaccessibility, with a BI% of 582.75. In comparison, its bioaccessibility was only 2.12% when free PE was dispersed in water and varied between 0% and 78% when solubilized using various solvents (Mergen Duymaz et

al., 2024). This value was further elevated to 496% in the AMP-based liposomal system. Though external standards for pinobanksin derivatives were unavailable for direct identification, studies indicate pinobanksin-3-O-ester compounds are naturally present in both honey and propolis (Zheng et al., 2018). Furthermore, in a human study that involved the consumption of European-type propolis, plasma samples only contained conjugated metabolites, including pinobanksin 3-O-acetate (Bloor & Mitchell, 2021). These results indicate that intestinal enzymes and bile salts may have hydrolyzed esterified forms of pinobanksin, resulting in the release of free pinobanksin into the digestion medium.

The bioaccessibility of hydroxycinnamic acids is usually influenced by the number of hydroxyl groups attached to the aromatic ring, with fewer substitutions often resulting in higher BI% values (C. X. Li et al., 2023). The results of liposomal gel support this trend, as *p*-coumaric acid (with two hydroxyl groups) demonstrated a higher BI% (516.10) compared to caffeic acid, which has three hydroxyl groups (412.60). Similarly, ferulic acid, which contains one methoxy group and one hydroxyl group, exhibited a comparable BI% of 430.12, while *trans*-cinnamic acid, lacking hydroxyl substitutions, showed a significantly lower value of 185.92. The increase in these acids during digestion can be associated with the enzymatic breakdown of bound forms, such as glucosides or quinic acid esters, which are usually found in plant matrices and serve a significant role as dietary phenolics (Stalmach, 2014).

The notably high BI% of caffeic acid (412.60%) observed after intestinal digestion of the liposomal gel may be linked to the breakdown of more complex phenolic esters, such as prenyl caffeate, β-phenylethyl caffeate, and isopentyl caffeate into simpler, more bioaccessible forms like caffeoylglycerol and free caffeic acid. Previous studies indicated that, following the digestion of PE, the recovery rates for caffeic acid and its glycerol conjugate achieved levels of 230.7% and 147.5%, respectively (Cea-Pavez et al., 2024). The findings indicate that enzymatic hydrolysis during digestion significantly contributes to the release of these phenolics from their esterified forms, thus improving their bioaccessibility.

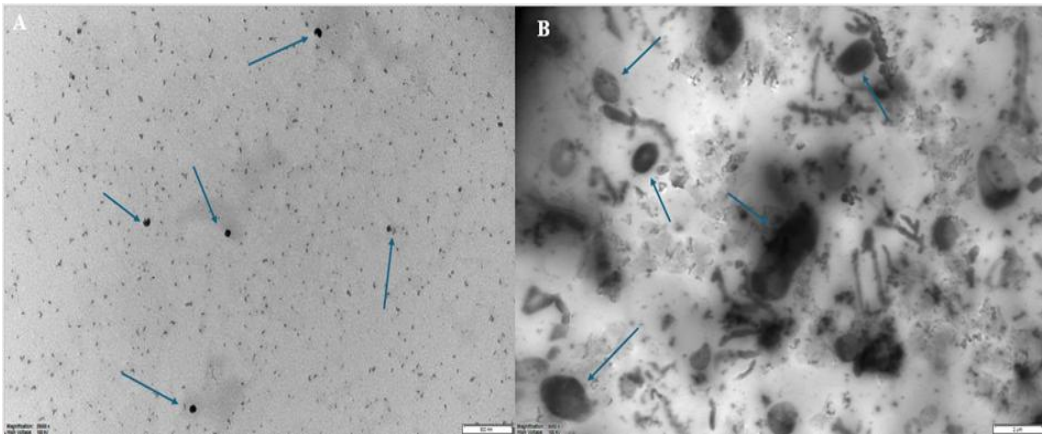

Figure 3. 21 TEM images of gastric (A) and intestinal (B) digesta of PE-loaded AMP liposomal gel.

The main objective of the liposomal gel formulation was to enhance the solubility of PE in digestive fluids, facilitate its targeted release during the intestinal phase, and provide partial protection against challenging digestive conditions. Figure 3.21 shows TEM images of the gastric and intestinal digesta of the PE-loaded liposomal gel. In the gastric environment, vesicles maintained their structural integrity and appeared smaller than those observed after intestinal digestion. After centrifuging the gastric samples, gel components were clearly seen as precipitates at the bottom of the tube, suggesting that a significant amount of the liposomal vesicles remained trapped within the undissolved gel matrix at this stage. The stability of liposomes in acidic conditions results from the organized arrangement of phospholipids in their bilayer structure, which effectively resists degradation during gastric digestion (W. Liu, Ye, Liu, et al., 2015). Conversely, the enlargement of vesicles observed during the intestinal phase is likely attributed to the migration of bile salts and the enzymatic hydrolysis of membrane phospholipids (W. Liu, Ye, Liu, et al., 2015; Saroglu et al., 2022). The process results in the formation of lysophospholipids, which interact with bile salts to form micelles that enhance the effective delivery of lipophilic compounds (X. Xu et al., 2023). The morphological changes identified through TEM were consistent with the increased release of phenolic compounds observed during the intestinal phase, as confirmed by LC-MS/MS analysis (Table 3.11).

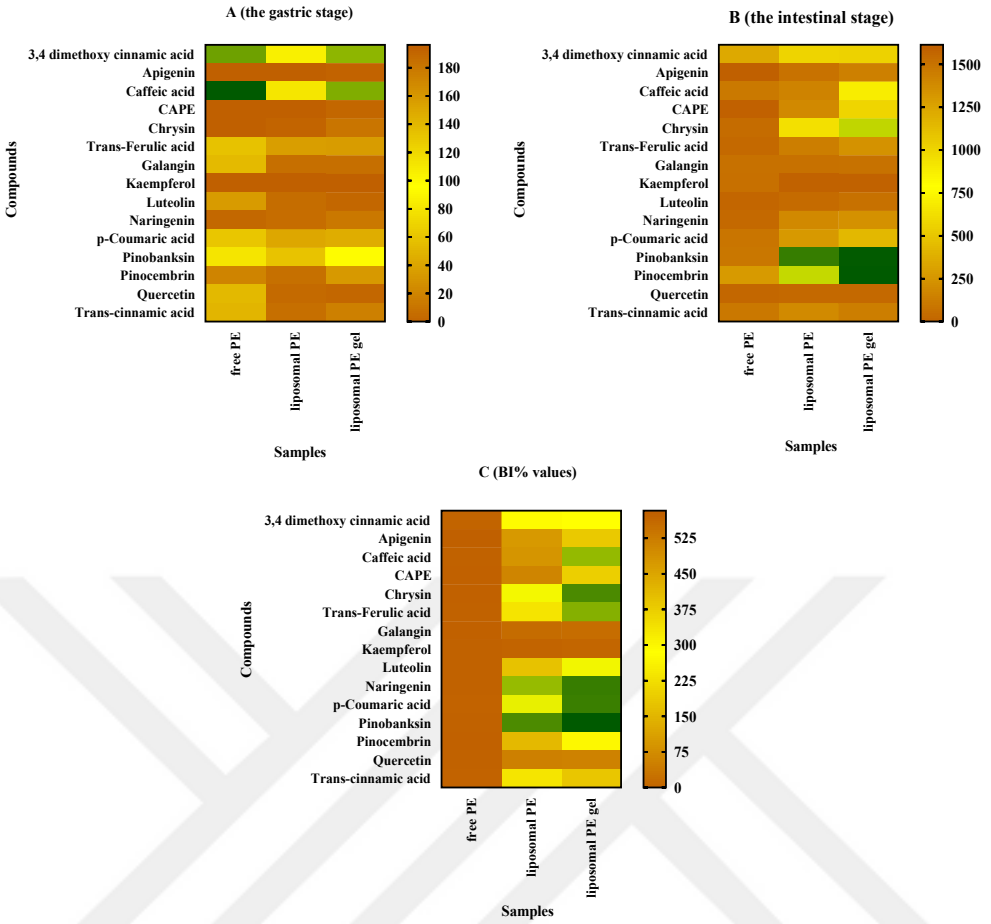

Figure 3. 22 Heat maps showing the concentration profiles of individual phenolic compounds during *in vitro* digestion including the gastric (A) and intestinal (B) phases, as well as their BI (%) values (C).

A heat map was generated to visually compare the change of phenolics at *in vitro* digestion stages, including gastric, and intestinal phases for free PE, liposomal PE and liposomal PE (Figure 3.22). The color intensity indicates the concentration of each compound, with darker tones (brown) representing lower concentrations and yellow to green shades indicating higher concentrations. In the gastric phase, PE exhibited yellowish to light brown tones across most phenolic compounds, indicative of limited release. Both the liposomal PE and liposomal PE gel formulations displayed similar color intensities, suggesting low overall release levels in this phase. However, a relatively higher release was observed for caffeic acid and 3,4-dimethoxycinnamic acid in both formulations, as indicated by lighter colours. In the intestinal stage, PE exhibited low release levels, while both liposomal PE and the liposomal PE gel showed increased release of several

phenolics, particularly pinobanksin and pinocembrin, as indicated by the green color. The BI% heat map (C) supported these trends, indicating improved bioaccessibility in liposomal PE and the liposomal PE gel compared to free PE, with the gel formulation showing the highest bioaccessibility for various compounds, including naringenin, *p*-coumaric acid, pinobanksin, *trans*-ferulic acid, chrysin, and caffeic acid. These results highlight the enhanced stability and controlled release of the AMP-liposomal gel under gastrointestinal conditions, compared to the free compound as well as the liposomal form.

4
CONCLUSION

In this thesis, hybrid encapsulation systems were developed by integrating PE-loaded liposomes into xanthan gum–salep-based hydrogels to enhance the solubility, stability, and bioaccessibility of hydrophobic bioactive compounds. The combination of liposomal encapsulation with a mucoadhesive hydrogel matrix (xanthan gum and salep) offered a multifunctional solution to enhance the performance of PE as a functional ingredient. The study first demonstrated that surfactant-free and surfactant-assisted liposomes could be effectively prepared and embedded within the hydrogel matrix without compromising their structural integrity. Surfactant-free, T80-based, and AMP-based liposomal gels all exhibited solid-like structures, but the strength of this structure varied depending on the formulation. AMP-based liposomes demonstrated stronger interactions with the polysaccharide network, resulting in improved mechanical strength, viscoelastic behavior, and mucoadhesive properties. PE-loaded T80-based liposomal gels, while maintaining a solid-like character, exhibited weaker structural integrity, possibly due to their thermal sensitivity surfactant. Additionally, increasing the salep concentration in the hydrogel matrix contributed to further enhancement of gel strength and elasticity across all formulations. All liposomal gel formulations exhibited shear-thinning behavior, and the addition of liposomes, regardless of the surfactant type, did not significantly impact the overall flow characteristics of the hydrogel matrix. Morphological analyses (SEM, TEM, and Cryo-TEM) revealed that the encapsulation process preserved the spherical shape of liposomes and enabled their uniform distribution within the hydrogel matrix. This outcome supports the physical stability and practical applicability of the developed delivery system. DSC analysis revealed shifts in melting peaks upon PE incorporation, indicating successful entrapment and molecular interactions within the AMP- and

T80-based liposomal gel matrices. Complementary FTIR results supported these findings by showing spectral changes associated with interactions between liposomal components and the polysaccharide-based hydrogel network. The *in vitro* digestion study further demonstrated the effectiveness of the developed system in improving the gastrointestinal stability and bioaccessibility of PE phenolics. While the free extract showed limited recovery, encapsulation within AMP-based liposomes significantly increased their bioaccessibility under simulated digestive conditions. The incorporation of these liposomes into the hydrogel matrix resulted in an even greater enhancement, suggesting that the gel structure contributed to protecting the compounds and enabling their controlled release in the intestinal environment. TEM analysis of digesta confirmed that vesicles remained intact under gastric conditions, whereas partial disruption and vesicle enlargement occurred in the intestinal phase due to bile salts and enzymatic activity. Among the identified phenolic compounds, naringenin, *p*-coumaric acid, pinobanksin, and chrysin exhibited the highest levels of bioaccessibility following digestion of the liposomal hydrogel formulations. These results indicate that the developed delivery system not only improves the overall availability of PE phenolics but also supports their gradual and targeted release during intestinal digestion. Overall, the liposome–hydrogel formulation proved effective in enhancing the intestinal bioaccessibility, aqueous solubility, and structural stability of propolis phenolics throughout the gastrointestinal process. This study highlights the potential of liposomal hydrogels as a robust oral delivery platform for poorly water-soluble natural actives. The use of food-grade materials and the mucoadhesive, soft-gel structure makes the system particularly suitable for functional food and nutraceutical applications. Moreover, it holds promise for special dietary needs, especially in populations with swallowing difficulties, due to its ease of administration and improved retention in the gastrointestinal tract. In future research, *in vivo* and clinical evaluations will be essential for a better understanding of the absorption profile and metabolic behavior of the system, ultimately aiding in its transformation into applicable oral delivery solutions.

REFERENCES

Abduh, M. Y., Shafitri, T. R., & Elfahmi, E. (2024). Chemical profiling, bioactive compounds, antioxidant, and anti-inflammatory activities of Indonesian propolis extract produced by Tetragonula laeviceps. Heliyon, 10(19), e38736. https://doi.org/https://doi.org/10.1016/j.heliyon.2024.e38736

Acar, H., & Kurt, A. (2020). Purified salep glucomannan synergistically interacted with xanthan gum: Rheological and textural studies on a novel pH-/thermo-sensitive hydrogel. *Food Hydrocolloids*, *101*(September 2019), 105463. https://doi.org/10.1016/j.foodhyd.2019.105463

Acemi, A., Çobanoğlu, Ö., & Türker-Kaya, S. (2019). FTIR-based comparative analysis of glucomannan contents in some tuberous orchids, and effects of pre-processing on glucomannan measurement. *Journal of the Science of Food and Agriculture*, *99*(7), 3681–3686. https://doi.org/10.1002/jsfa.9596

Adrar, N., Bahadori, F., Ceylan, F. D., Topçu, G., Bedjou, F., & Capanoglu, E. (2021). Stability evaluation of interdigitated liposomes prepared with a combination of 1,2-distearoyl-sn-glycero-3-phosphocholine and 1,2-dilauroyl-sn-glycero-3-phosphocholine. *Journal of Chemical Technology and Biotechnology*, *96*(9), 2537–2546. https://doi.org/10.1002/jctb.6793

Aguilar-Zárate, M., Macias-Rodriguez, B. A., Toro-Vazquez, J. F., & Marangoni, A. G. (2019). Engineering rheological properties of edible oleogels with ethylcellulose and lecithin. *Carbohydrate Polymers*, *205*(October 2018), 98–105. https://doi.org/10.1016/j.carbpol.2018.10.032

Ahmed, E. M. (2015). Hydrogel: Preparation, characterization, and applications: A review. *Journal of Advanced Research*, *6*(2), 105–121. https://doi.org/https://doi.org/10.1016/j.jare.2013.07.006

Ajeeshkumar, K. K., Aneesh, P. A., Raju, N., Suseela, M., Ravishankar, C. N., & Benjakul, S. (2021). Advancements in liposome technology: Preparation techniques and applications in food, functional foods, and bioactive delivery: A review. *Comprehensive Reviews in Food Science and Food Safety*, *20*(2), 1280–1306. https://doi.org/https://doi.org/10.1111/1541-4337.12725

Alinaghi, A., Rouini, M. R., Johari Daha, F., & Moghimi, H. R. (2013). Hydrogel-embeded vesicles, as a novel approach for prolonged release and delivery of liposome, in vitro and in vivo. *Journal of Liposome Research*, *23*(3), 235–243. https://doi.org/10.3109/08982104.2013.799179

Almgren, M., Edwards, K., & Karlsson, G. (2000). Cryo transmission electron microscopy of liposomes and related structures. *Colloids and Surfaces A: Physicochemical and Engineering Aspects*, *174*(1), 3–21. https://doi.org/https://doi.org/10.1016/S0927-7757(00)00516-1

Alvarenga, L., Cardozo, L. F. M. F., Borges, N. A., Chermut, T. R., Ribeiro, M., Leite, M., Shiels, P. G., Stenvinkel, P., & Mafra, D. (2021). To bee or not to bee? The bee extract propolis as a bioactive compound in the burden of lifestyle diseases. *Nutrition*, *83*, 111094. https://doi.org/https://doi.org/10.1016/j.nut.2020.111094

Álvarez-Diduk, R., Ramírez-Silva, M. T., Galano, A., & Merkoçi, A. (2013). Deprotonation mechanism and acidity constants in aqueous solution of flavonols: A combined experimental and theoretical study. *Journal of Physical Chemistry B*, *117*(41), 12347–12359. https://doi.org/10.1021/jp4049617

Andrews, G. P., Laverty, T. P., & Jones, D. S. (2009). Mucoadhesive polymeric platforms for controlled drug delivery. *European Journal of Pharmaceutics and Biopharmaceutics*, *71*(3), 505–518. https://doi.org/10.1016/j.ejpb.2008.09.028

Anjum, S. I., Ullah, A., Khan, K. A., Attaullah, M., Khan, H., Ali, H., Bashir, M. A., Tahir, M., Ansari, M. J., Ghramh, H. A., Adgaba, N., & Dash, C. K. (2019). Composition and functional properties of propolis (bee glue): A review. *Saudi Journal of Biological Sciences*, *26*(7), 1695–1703. https://doi.org/https://doi.org/10.1016/j.sjbs.2018.08.013

Annabi, N., Nichol, J. W., Zhong, X., Ji, C., Koshy, S., Khademhosseini, A., & Dehghani, F. (2010). Controlling the Porosity and Microarchitecture of Hydrogels for Tissue Engineering. *Tissue Engineering Part B: Reviews*, *16*(4), 371–383. https://doi.org/10.1089/ten.teb.2009.0639

Araújo, D., Alves, V. D., Campos, J., Coelhoso, I., Sevrin, C., Grandfils, C., Freitas, F., & Reis, M. A. M. (2016). Assessment of the adhesive properties of the bacterial polysaccharide FucoPol. *International Journal of Biological Macromolecules*, *92*, 383–389. https://doi.org/10.1016/j.ijbiomac.2016.07.035

Arung, E. T., Syafrizal, Kusuma, I. W., Paramita, S., Amen, Y., Kim, Y.-U., Naibaho, N. M., Ramadhan, R., Ariyanta, H. A., Fatriasari, W., & Shimizu, K. (2023). Antioxidant, anti-inflammatory and anti-acne activities of stingless bee (Tetragonula biroi) propolis. *Fitoterapia*, *164*, 105375. https://doi.org/https://doi.org/10.1016/j.fitote.2022.105375

Atayoglu, A. T., Sözeri Atik, D., Bölük, E., Gürbüz, B., Ceylan, F. D., Çapanoğlu, E., Atayolu, R., Paradkar, A., Fearnley, J., & Palabiyik, I. (2023). Evaluating bioactivity and bioaccessibility properties of the propolis extract prepared with L-lactic acid: An alternative solvent to ethanol for propolis extraction. *Food Bioscience*, *53*(December 2022). https://doi.org/10.1016/j.fbio.2023.102756

Aytekin, A. A., Tuncay Tanrıverdi, S., Aydın Köse, F., Kart, D., Eroğlu, İ., & Özer, Ö. (2020). Propolis loaded liposomes: evaluation of antimicrobial and antioxidant activities. *Journal of Liposome Research*, *30*(2), 107–116. https://doi.org/10.1080/08982104.2019.1599012

Balasubramaniam, A. K., Elangovan, A., Rahman, M. A., Nayak, S., Swain, D., Babu, H. P., Narasimhan, A., & Monga, V. (2025). Propolis: A comprehensive review on the nature's polyphenolic wonder. *Fitoterapia*, *183*, 106526. https://doi.org/https://doi.org/10.1016/j.fitote.2025.106526

Beltrán, J. L., Sanli, N., Fonrodona, G., Barrón, D., Özkan, G., & Barbosa, J.

(2003). Spectrophotometric, potentiometric and chromatographic pKa values of polyphenolic acids in water and acetonitrile-water media. *Analytica Chimica Acta*, *484*(2), 253–264. https://doi.org/10.1016/S0003-2670(03)00334-9

Benzie, F. F. I., & Straint, J. J. (1996). The Ferric Reducing Ability of Plasma (FRAP) as a Measure of "'Antioxidant Power"': The FRAP Assay. *Analytical Biochemistry*, *239*, 70–76.

Berretta, A. A., De Castro, P. A., Cavalheiro, A. H., Fortes, V. S., Bom, V. P., Nascimento, A. P., Marquele-Oliveira, F., Pedrazzi, V., Ramalho, L. N. Z., & Goldman, G. H. (2013). Evaluation of mucoadhesive gels with propolis (EPP-AF) in preclinical treatment of candidiasis vulvovaginal infection. *Evidence-Based Complementary and Alternative Medicine*, *2013*. https://doi.org/10.1155/2013/641480

Bloor, S. J., & Mitchell, K. A. (2021). Metabolic products of European-type propolis. Synthesis and analysis of glucuronides and sulfates. *Journal of Ethnopharmacology*, *274*(March), 114035. https://doi.org/10.1016/j.jep.2021.114035

Brand-Williams, W., Cuvelier, M. E., & Berset, C. (1995). Use of a free radical method to evaluate antioxidant activity. *LWT - Food Science and Technology*, *28*(1), 25–30. https://doi.org/10.1016/S0023-6438(95)80008-5

Brodkorb, A., Egger, L., Alminger, M., Alvito, P., Assunção, R., Ballance, S., Bohn, T., Bourlieu-Lacanal, C., Boutrou, R., Carrière, F., Clemente, A., Corredig, M., Dupont, D., Dufour, C., Edwards, C., Golding, M., Karakaya, S., Kirkhus, B., Le Feunteun, S., … Recio, I. (2019). INFOGEST static in vitro simulation of gastrointestinal food digestion. *Nature Protocols*, *14*(4), 991–1014. https://doi.org/10.1038/s41596-018-0119-1

Busch, V. M., Pereyra-Gonzalez, A., Šegatin, N., Santagapita, P. R., Poklar Ulrih, N., & Buera, M. P. (2017). Propolis encapsulation by spray drying: Characterization and stability. *LWT*, *75*, 227–235. https://doi.org/https://doi.org/10.1016/j.lwt.2016.08.055

Cai, W. Q., Liu, X., Chen, W., Huang, Z., Li, C., Huang, X., Harold, C., Su, B. L., Zhang, B. B., & Yang, Q. Q. (2023). Synergistic effect of lecithin and alginate, CMC, or PVP in stabilizing curcumin and its potential mechanism. *Food Chemistry*, *413*(October 2022), 135634. https://doi.org/10.1016/j.foodchem.2023.135634

Calero, V., Rodrigues, P. M., Dias, T., Ainla, A., Vilaça, A., Pastrana, L., Xavier, M., & Gonçalves, C. (2024). A miniaturised semi-dynamic in-vitro model of human digestion. *Scientific Reports*, *14*(1), 11923. https://doi.org/10.1038/s41598-024-54612-w

Cao, D., Zhang, X., Akabar, M. D., Luo, Y., Wu, H., Ke, X., & Ci, T. (2019). Liposomal doxorubicin loaded PLGA-PEG-PLGA based thermogel for sustained local drug delivery for the treatment of breast cancer. *Artificial Cells, Nanomedicine and Biotechnology*, *47*(1), 181–191. https://doi.org/10.1080/21691401.2018.1548470

Catchpole, O., Mitchell, K., Bloor, S., Davis, P., & Suddes, A. (2018). Anti-gastrointestinal cancer activity of cyclodextrin-encapsulated propolis. *Journal*

of Functional Foods, *41*(December 2017), 1–8. https://doi.org/10.1016/j.jff.2017.12.023

Cea-Pavez, I., Manteca-Bautista, D., Morillo-Gomar, A., Quirantes-Piné, R., & Quiles, J. L. (2024). Influence of the Encapsulating Agent on the Bioaccessibility of Phenolic Compounds from Microencapsulated Propolis Extract during In Vitro Gastrointestinal Digestion. *Foods*, *13*(3). https://doi.org/10.3390/foods13030425

Cevher, E., Taha, M. A. M., Orlu, M., & Araman, A. (2008). Evaluation of mechanical and mucoadhesive properties of clomiphene citrate gel formulations containing carbomers and their thiolated derivatives. *Drug Delivery*, *15*(1), 57–67. https://doi.org/10.1080/10717540701829234

Chai, C., & Park, J. (2024). Food liposomes: Structures, components, preparations, and applications. *Food Chemistry*, *432*, 137228. https://doi.org/https://doi.org/10.1016/j.foodchem.2023.137228

Chandra, M. V., & Shamasundar, B. A. (2015). Texture profile analysis and functional properties of gelatin from the skin of three species of fresh water fish. *International Journal of Food Properties*, *18*(3), 572–584. https://doi.org/10.1080/10942912.2013.845787

Chandrika, K. S. V. P., Singh, A., Rathore, A., & Kumar, A. (2016). Novel cross linked guar gum-g-poly(acrylate) porous superabsorbent hydrogels: Characterization and swelling behaviour in different environments. *Carbohydrate Polymers*, *149*, 175–185. https://doi.org/https://doi.org/10.1016/j.carbpol.2016.04.077

Chen, H., Mou, D., Du, D., Chang, X., Zhu, D., Liu, J., Xu, H., & Yang, X. (2007). Hydrogel-thickened microemulsion for topical administration of drug molecule at an extremely low concentration. *International Journal of Pharmaceutics*, *341*(1–2), 78–84. https://doi.org/10.1016/j.ijpharm.2007.03.052

Chen, J., & Hu, L. (2020). Nanoscale Delivery System for Nutraceuticals: Preparation, Application, Characterization, Safety, and Future Trends. *Food Engineering Reviews*, *12*(1), 14–31. https://doi.org/10.1007/s12393-019-09208-w

Chiu, M. H., & Prenner, E. J. (2011). Differential scanning calorimetry: An invaluable tool for a detailed thermodynamic characterization of macromolecules and their interactions. *Journal of Pharmacy and Bioallied Sciences*, *3*(1). https://journals.lww.com/jpbs/fulltext/2011/03010/differential_scanning_calorimetry__an_invaluable.5.aspx

Cuomo, F., Cofelice, M., & Lopez, F. (2019). Rheological characterization of hydrogels from alginate-based nanodispersion. *Polymers*, *11*(2). https://doi.org/10.3390/polym11020259

Çelekli, A., Akhras, N., & Bozkurt, H. (2024). Improving antimicrobial activity of brown propolis with incorporation of Arthrospira platensis. *Food and Humanity*, *2*, 100191. https://doi.org/https://doi.org/10.1016/j.foohum.2023.11.018

D'Elía, N. L., Rial Silva, R., Sartuqui, J., Ercoli, D., Ruso, J., Messina, P., & Mestres, G. (2020). Development and characterisation of bilayered periosteum-inspired composite membranes based on sodium alginate-hydroxyapatite nanoparticles. *Journal of Colloid and Interface Science*, *572*, 408–420. https://doi.org/10.1016/j.jcis.2020.03.086

da Rosa, C. G., Borges, C. D., Zambiazi, R. C., Nunes, M. R., Benvenutti, E. V., da Luz, S. R., D'Avila, R. F., & Rutz, J. K. (2013). Microencapsulation of gallic acid in chitosan, β-cyclodextrin and xanthan. *Industrial Crops and Products*, *46*, 138–146. https://doi.org/https://doi.org/10.1016/j.indcrop.2012.12.053

Danaei, M., Dehghankhold, M., Ataei, S., Hasanzadeh Davarani, F., Javanmard, R., Dokhani, A., Khorasani, S., & Mozafari, M. R. (2018). Impact of Particle Size and Polydispersity Index on the Clinical Applications of Lipidic Nanocarrier Systems. *Pharmaceutics*, *10*(2). https://doi.org/10.3390/pharmaceutics10020057

Das, D., Pham, H. T. T., Lee, S., & Noh, I. (2019). Fabrication of alginate-based stimuli-responsive, non-cytotoxic, terpolymric semi-IPN hydrogel as a carrier for controlled release of bovine albumin serum and 5-amino salicylic acid. *Materials Science and Engineering C*, *98*(December 2018), 42–53. https://doi.org/10.1016/j.msec.2018.12.127

Dejeu, I. L., Vicaș, L. G., Vlaia, L. L., Jurca, T., Mureșan, M. E., Pallag, A., Coneac, G. H., Olariu, I. V., Muț, A. M., Bodea, A. S., Dejeu, G. E., Maghiar, O. A., & Marian, E. (2022). Study for Evaluation of Hydrogels after the Incorporation of Liposomes Embedded with Caffeic Acid. *Pharmaceuticals*, *15*(2). https://doi.org/10.3390/ph15020175

Díaz-Carballo, D., Malak, S., Bardenheuer, W., Freistuehler, M., & Peter Reusch, H. (2008). The contribution of plukenetione A to the anti-tumoral activity of Cuban propolis. *Bioorganic & Medicinal Chemistry*, *16*(22), 9635–9643. https://doi.org/https://doi.org/10.1016/j.bmc.2008.10.019

Dima, C., Assadpour, E., Dima, S., & Jafari, S. M. (2020). Bioavailability and bioaccessibility of food bioactive compounds; overview and assessment by in vitro methods. *Comprehensive Reviews in Food Science and Food Safety*, *19*(6), 2862–2884. https://doi.org/https://doi.org/10.1111/1541-4337.12623

do Nascimento, T. G., Redondo, G. D. P., de Araújo Abreu, C. T., Silva, V. C., Lira, G. M., Meireles Grillo, L. A., da Conceição, M. M., Freitas, J. D., Souza, J. S., Araújo Júnior, J. X., & Basílio-Júnior, I. D. (2019). Modified release microcapsules loaded with red propolis extract obtained by spray-dryer technique: Phytochemical, thermal and physicochemical characterizations. *Journal of Thermal Analysis and Calorimetry*, *138*(5), 3559–3569. https://doi.org/10.1007/s10973-019-08287-5

Duché, G., Heu, C., & Thordarson, P. (2023). Development and Characterization of Nanoscale Gel-Core Liposomes Using a Short Self-Assembled Peptide Hydrogel: Implications for Drug Delivery. *ACS Applied Nano Materials*, *6*(16), 14745–14755. https://doi.org/10.1021/acsanm.3c02172

Edo, G. I., Mafe, A. N., Akpoghelie, P. O., Gaaz, T. S., Yousif, E., Yusuf, O. S., Isoje, E. F., Igbuku, U. A., Opiti, R. A., Ayinla, J. L., Essaghah, A. E. A., Ahmed, D. S., & Umar, H. (2025). The utilization of biopolymer hydrogels to

encapsulate and protect probiotics in foods. *Process Biochemistry*, *153*, 66–91. https://doi.org/https://doi.org/10.1016/j.procbio.2025.03.008

EFSA. (2015). Scientific Opinion on the re-evaluation of polyoxyethylene sorbitan monolaurate (E 432), polyoxyethylene sorbitan monooleate (E 433), polyoxyethylene sorbitan monopalmitate (E 434), polyoxyethylene sorbitan monostearate (E 435) and polyoxyethylene sorbita. *EFSA Journal*, *13*(7). https://doi.org/10.2903/j.efsa.2015.4152

Eren, B., Tuncay Tanrıverdi, S., Aydın Köse, F., & Özer, Ö. (2019). Antioxidant properties evaluation of topical astaxanthin formulations as anti-aging products. *Journal of Cosmetic Dermatology*, *18*(1), 242–250. https://doi.org/10.1111/jocd.12665

Faria, S., De Oliveira Petkowicz, C. L., De Morais, S. A. L., Terrones, M. G. H., De Resende, M. M., De Frana, F. P., & Cardoso, V. L. (2011). Characterization of xanthan gum produced from sugar cane broth. *Carbohydrate Polymers*, *86*(2), 469–476. https://doi.org/10.1016/j.carbpol.2011.04.063

Ferreira, L. M. de M. C., Cruz, N. F. da, Lynch, D. G., Costa, P. F. da, Salgado, C. G., Silva-Júnior, J. O. C., Rossi, A., & Ribeiro-Costa, R. M. (2024). Hydrogel Containing Propolis: Physical Characterization and Evaluation of Biological Activities for Potential Use in the Treatment of Skin Lesions. *Pharmaceuticals*, *17*(10). https://doi.org/10.3390/ph17101400

Fuguet, E., Ràfols, C., Mañé, M., Ruiz, R., & Bosch, E. (2023). Acidity constants of hydroxyl groups placed in several flavonoids: Two flavanones, two flavones and five flavonols. *Talanta*, *253*(September 2022). https://doi.org/10.1016/j.talanta.2022.124096

Ge, Y., & Ge, M. (2016). Distribution of Melaleuca alternifolia essential oil in liposomes with Tween 80 addition and enhancement of in vitro antimicrobial effect. *Journal of Experimental Nanoscience*, *11*(5), 345–358. https://doi.org/10.1080/17458080.2015.1065013

Ghallab, D. S., Shawky, E., Mohyeldin, M. M., Metwally, A. M., & Reham, S. (2025). Propolis : An update on its chemical diversity , botanical origin and biological activities. *Journal of Advanced Pharmaceutical Sciences*, *2*(1). https://doi.org/10.21608/japs.2025.336494.1032

Gharanjig, H., Gharanjig, K., Hosseinnezhad, M., & Jafari, S. M. (2020). Chapter Ten - Differential scanning calorimetry (DSC) of nanoencapsulated food ingredients. In S. M. Jafari (Ed.), *Characterization of Nanoencapsulated Food Ingredients* (Vol. 4, pp. 295–346). Academic Press. https://doi.org/https://doi.org/10.1016/B978-0-12-815667-4.00010-9

Gibis, M., Vogt, E., & Weiss, J. (2012). Encapsulation of polyphenolic grape seed extract in polymer-coated liposomes. *Food and Function*, *3*(3), 246–254. https://doi.org/10.1039/c1fo10181a

Grijalvo, S., Mayr, J., Eritja, R., & Díaz, D. D. (2016). Biodegradable liposome-encapsulated hydrogels for biomedical applications: a marriage of convenience. *Biomater. Sci.*, *4*(4), 555–574. https://doi.org/10.1039/C5BM00481K

Grundy, M., Deglaire, A., Le Feunteun, S., Reboul, E., Moughan, P. J., Wilde, P.

J., McClements, D. J., & Marze, S. (2025). Bioaccessibility and associated concepts: Terminology in the context of in vitro food digestion studies. *Food Chemistry*, 144424. https://doi.org/https://doi.org/10.1016/j.foodchem.2025.144424

Gul, K., Gan, R.-Y., Sun, C.-X., Jiao, G., Wu, D.-T., Li, H.-B., Kenaan, A., Corke, H., & Fang, Y.-P. (2022). Recent advances in the structure, synthesis, and applications of natural polymeric hydrogels. *Critical Reviews in Food Science and Nutrition*, *62*(14), 3817–3832. https://doi.org/10.1080/10408398.2020.1870034

Guzelmeric, E., Sipahi, H., Özhan, Y., Hamitoğlu, M., Helvacıoğlu, S., Düz, G., Akyıldız, İ. E., Yaman, B. K., Hazar, M., Dilsiz, S. A., Aydın, A., & Yesilada, E. (2023). Comprehensive estrogenic/anti-estrogenic, anticancer, mutagenic/anti-mutagenic, and genotoxic/anti-genotoxic activity studies on chemically characterized black poplar and Eurasian aspen propolis types. *Journal of Pharmaceutical and Biomedical Analysis*, *226*(January), 1–13. https://doi.org/10.1016/j.jpba.2023.115241

Han, X., Huang, J., To, A. K. W., Lai, J. H. C., Xiao, P., Wu, E. X., Xu, J., & Chan, K. W. Y. (2020). CEST MRI detectable liposomal hydrogels for multiparametric monitoring in the brain at 3T. *Theranostics*, *10*(5), 2215–2228. https://doi.org/10.7150/thno.40146

Hegazi, A. G., Abd El Hady, F. K., & Abd Allah, F. A. M. (2000). Chemical Composition and Antimicrobial Activity of European Propolis. *Zeitschrift Für Naturforschung*, *55*(1–2), 70–75. https://doi.org/10.1007/s10600-016-1566-y

Hu, Y., Zhang, L., Wei, L. feng, Lu, F. yan, Wang, L. huai, Ding, Q., Chen, M. shun, & Tu, Z. cai. (2023). Liposomes encapsulation by pH driven improves the stability, bioaccessibility and bioavailability of urolithin A: A comparative study. *International Journal of Biological Macromolecules*, *253*(P7), 127554. https://doi.org/10.1016/j.ijbiomac.2023.127554

Hurler, J., Engesland, A., Poorahmary Kermany, B., & Škalko-Basnet, N. (2012). Improved texture analysis for hydrogel characterization: Gel cohesiveness, adhesiveness, and hardness. *Journal of Applied Polymer Science*, *125*(1), 180–188. https://doi.org/https://doi.org/10.1002/app.35414

Hurler, J., Žakelj, S., Mravljak, J., Pajk, S., Kristl, A., Schubert, R., & Škalko-Basnet, N. (2013). The effect of lipid composition and liposome size on the release properties of liposomes-in-hydrogel. *International Journal of Pharmaceutics*, *456*(1), 49–57. https://doi.org/10.1016/j.ijpharm.2013.08.033

Iqbal, M., Fan, T., Watson, D., Alenezi, S., Saleh, K., & Sahlan, M. (2019). Preliminary studies: the potential anti-angiogenic activities of two Sulawesi Island (Indonesia) propolis and their chemical characterization. *Heliyon*, *5*(7), e01978. https://doi.org/https://doi.org/10.1016/j.heliyon.2019.e01978

Irigoiti, Y., Navarro, A., Yamul, D., Libonatti, C., Tabera, A., & Basualdo, M. (2021). The use of propolis as a functional food ingredient: A review. *Trends in Food Science & Technology*, *115*, 297–306. https://doi.org/https://doi.org/10.1016/j.tifs.2021.06.041

Jang, E., Jeong, J., Yim, J. H., Kim, Y., Lee, C. H., Choi, D., & Chung, H. (2019). Improved infrared spectroscopic discrimination between gall bladder (GB)

polyps and GB cancer using component-descriptive spectral features of separated phases from bile. *Analyst*, *144*(16), 4826–4834. https://doi.org/10.1039/c9an00878k

Jia, H., Ren, F., & Liu, H. (2024). Evaluation of bioaccessibility and bioavailability of dietary bioactives and their application in food systems. *Food Bioscience*, *62*, 105428. https://doi.org/https://doi.org/10.1016/j.fbio.2024.105428

Jøraholmen, M. W., Johannessen, M., Gravningen, K., Puolakkainen, M., Acharya, G., Basnet, P., & Škalko-Basnet, N. (2020). Liposomes-in-hydrogel delivery system enhances the potential of resveratrol in combating vaginal chlamydia infection. *Pharmaceutics*, *12*(12), 1–14. https://doi.org/10.3390/pharmaceutics12121203

Jurasekova, Z., Domingo, C., Garcia-Ramos, J. V., & Sanchez-Cortes, S. (2014). Effect of pH on the chemical modification of quercetin and structurally related flavonoids characterized by optical (UV-visible and Raman) spectroscopy. *Physical Chemistry Chemical Physics*, *16*(25), 12802–12811. https://doi.org/10.1039/c4cp00864b

Kadri, R., Bacharouch, J., Elkhoury, K., Ben Messaoud, G., Kahn, C., Desobry, S., Linder, M., Tamayol, A., Francius, G., Mano, J. F., Sánchez-González, L., & Arab-Tehrany, E. (2020). Role of active nanoliposomes in the surface and bulk mechanical properties of hybrid hydrogels. *Materials Today Bio*, *6*, 100046. https://doi.org/https://doi.org/10.1016/j.mtbio.2020.100046

Kaplan, M., Tuğcu-Demiröz, F., Vural, İ., & Çelebi, N. (2018). Development and characterization of gels and liposomes containing ovalbumin for nasal delivery. *Journal of Drug Delivery Science and Technology*, *44*(July 2017), 108–117. https://doi.org/10.1016/j.jddst.2017.12.006

Karakas, C. Y., Ustundag, C. B., Sahin, A., & Karadag, A. (2023). Co-axial electrospinning of liposomal propolis loaded gelatin-zein fibers as a potential wound healing material. *Journal of Applied Polymer Science*, *July*, 1–20. https://doi.org/10.1002/app.54683

Karaz, S., Han, M., Akay, G., Onal, A., Nizamoglu, S., Kizilel, S., & Senses, E. (2022). Multiscale Dynamics of Lipid Vesicles in Polymeric Microenvironment. *Membranes*, *12*(7). https://doi.org/10.3390/membranes12070640

Kashyap, P., Shikha, D., Thakur, M., & Aneja, A. (2022). Functionality of apigenin as a potent antioxidant with emphasis on bioavailability, metabolism, action mechanism and in vitro and in vivo studies: A review. *Journal of Food Biochemistry*, *46*(4), 1–23. https://doi.org/10.1111/jfbc.13950

Khoobbakht, F., Khorshidi, S., Bahmanyar, F., Hosseini, S. M., Aminikhah, N., Farhoodi, M., & Mirmoghtadaie, L. (2024). Modification of mechanical, rheological and structural properties of agar hydrogel using xanthan and locust bean gum. *Food Hydrocolloids*, *147*(PA), 109411. https://doi.org/10.1016/j.foodhyd.2023.109411

Klein, M., & Poverenov, E. (2020). Natural biopolymer-based hydrogels for use in food and agriculture. *Journal of the Science of Food and Agriculture*, *100*(6), 2337–2347. https://doi.org/10.1002/jsfa.10274

Kouidhi, B., Zmantar, T., & Bakhrouf, A. (2010). Anti-cariogenic and anti-biofilms activity of Tunisian propolis extract and its potential protective effect against cancer cells proliferation. *Anaerobe*, *16*(6), 566–571. https://doi.org/https://doi.org/10.1016/j.anaerobe.2010.09.005

Koynova, R., & Caffrey, M. (1998). Phases and phase transitions of the phosphatidylcholines. *Biochimica et Biophysica Acta - Reviews on Biomembranes*, *1376*(1), 91–145. https://doi.org/10.1016/S0304-4157(98)00006-9

Kuligowski, J., Quintás, G., Esteve-Turrillas, F. A., Garrigues, S., & de la Guardia, M. (2008). On-line gel permeation chromatography-attenuated total reflectance-Fourier transform infrared determination of lecithin and soybean oil in dietary supplements. *Journal of Chromatography A*, *1185*(1), 71–77. https://doi.org/10.1016/j.chroma.2008.01.048

Kurt, A. (2018). *Modulating hydrogel characteristics of deacetylated salep glucomannan by blending xanthan gum.* 15.

Kurt, A., & Kahyaoglu, T. (2017). Purification of glucomannan from salep: Part 2. Structural characterization. *Carbohydrate Polymers*, *169*, 406–416. https://doi.org/10.1016/j.carbpol.2017.04.052

Lemańska, K., Szymusiak, H., Tyrakowska, B., Zieliński, R., Soffers, A. E. M. F., & Rietjens, I. M. C. M. (2001). The influence of pH on antioxidant properties and the mechanism of antioxidant action of hydroxyflavones. *Free Radical Biology and Medicine*, *31*(7), 869–881. https://doi.org/10.1016/S0891-5849(01)00638-4

Leyva-Porras, C., Cruz-Alcantar, P., Espinosa-Solís, V., Martínez-Guerra, E., Piñón-Balderrama, C. I., Compean Martínez, I., & Saavedra-Leos, M. Z. (2020). Application of Differential Scanning Calorimetry (DSC) and Modulated Differential Scanning Calorimetry (MDSC) in Food and Drug Industries. *Polymers*, *12*(1). https://doi.org/10.3390/polym12010005

Li, C., Bai, M., Chen, X., Hu, W., Cui, H., & Lin, L. (2022). Controlled release and antibacterial activity of nanofibers loaded with basil essential oil-encapsulated cationic liposomes against Listeria monocytogenes. *Food Bioscience*, *46*(January), 101578. https://doi.org/10.1016/j.fbio.2022.101578

Li, C. X., Wang, F. R., Zhang, B., Deng, Z. Y., & Li, H. Y. (2023). Stability and antioxidant activity of phenolic compounds during in vitro digestion. *Journal of Food Science*, *88*(2), 696–716.

Li, J., Jia, X., & Yin, L. (2021). Hydrogel: Diversity of Structures and Applications in Food Science. *Food Reviews International*, *37*(3), 313–372. https://doi.org/10.1080/87559129.2020.1858313

Li, P., Li, T., Zeng, Y., Li, X., Jiang, X., Wang, Y., Xie, T., & Zhang, Y. (2016). Biosynthesis of xanthan gum by Xanthomonas campestris LRELP-1 using kitchen waste as the sole substrate. *Carbohydrate Polymers*, *151*, 684–691. https://doi.org/10.1016/j.carbpol.2016.06.017

Lin, X., Zhao, X., Xu, C., Wang, L., & Xia, Y. (2022). Progress in the mechanical enhancement of hydrogels: Fabrication strategies and underlying mechanisms. *Journal of Polymer Science*, *60*(17), 2525–2542.

https://doi.org/https://doi.org/10.1002/pol.20220154

Liu, C., Cheng, X., Wu, Y., Xu, W., Xia, H., Jia, R., Liu, Y., Shen, S., Xu, Y., & Cheng, Z. (2023). Antioxidant Activity of Quercetin-Containing Liposomes-in-Gel and Its Effect on Prevention and Treatment of Cutaneous Eczema. *Pharmaceuticals*, *16*(8). https://doi.org/10.3390/ph16081184

Liu, W., Kong, Y., Ye, A., Shen, P., Dong, L., Xu, X., Hou, Y., Wang, Y., Jin, Y., & Han, J. (2020). Preparation, formation mechanism and in vitro dynamic digestion behavior of quercetin-loaded liposomes in hydrogels. *Food Hydrocolloids*, *104*(February), 105743. https://doi.org/10.1016/j.foodhyd.2020.105743

Liu, W., Ye, A., Liu, C., Liu, W., & Singh, H. (2012). Structure and integrity of liposomes prepared from milk- or soybean-derived phospholipids during in vitro digestion. *Food Research International*, *48*(2), 499–506. https://doi.org/10.1016/j.foodres.2012.04.017

Liu, W., Ye, A., Liu, W., Liu, C., Han, J., & Singh, H. (2015). Behaviour of liposomes loaded with bovine serum albumin during in vitro digestion. *Food Chemistry*, *175*, 16–24. https://doi.org/10.1016/j.foodchem.2014.11.108

Liu, W., Ye, A., & Singh, H. (2015). Chapter 8 - Progress in Applications of Liposomes in Food Systems. In L. M. C. Sagis (Ed.), *Microencapsulation and Microspheres for Food Applications* (pp. 151–170). Academic Press. https://doi.org/https://doi.org/10.1016/B978-0-12-800350-3.00025-X

Liu, X., Wang, P., Zou, Y. X., Luo, Z. G., & Tamer, T. M. (2020). Co-encapsulation of Vitamin C and β-Carotene in liposomes: Storage stability, antioxidant activity, and in vitro gastrointestinal digestion. *Food Research International*, *136*(July), 109587. https://doi.org/10.1016/j.foodres.2020.109587

Liu, Y., & Liang, D. (2011). Hydrogel integrated with liposome: A two-stage drug delivery system. *Journal of Controlled Release*, *152*, e63–e64. https://doi.org/https://doi.org/10.1016/j.jconrel.2011.08.124

Liu, Y., Ling, S., Chen, Z., & Xu, J. (2025). Recent advances of macroporous hydrogel microparticles: Fabrication and applications. *Chemical Engineering Journal*, *510*, 161435. https://doi.org/https://doi.org/10.1016/j.cej.2025.161435

Machado, A. R., Pinheiro, A. C., Vicente, A. A., Souza-Soares, L. A., & Cerqueira, M. A. (2019). Liposomes loaded with phenolic extracts of Spirulina LEB-18: Physicochemical characterization and behavior under simulated gastrointestinal conditions. *Food Research International*, *120*(June 2018), 656–667. https://doi.org/10.1016/j.foodres.2018.11.023

Maja, L., Željko, K., & Mateja, P. (2020). Sustainable technologies for liposome preparation. *The Journal of Supercritical Fluids*, *165*, 104984. https://doi.org/https://doi.org/10.1016/j.supflu.2020.104984

Mariana Kustiawan, P., Siregar, K. A. A. K., Syaifie, P. H., Zein Muttaqin, F., Ibadillah, D., Miftah Jauhar, M., Djamas, N., Mardliyati, E., & Taufiqu Rochman, N. (2024). Uncovering the anti-breast cancer activity potential of east Kalimantan propolis by In vitro and bioinformatics analysis. *Heliyon*, *10*(13), e33636. https://doi.org/https://doi.org/10.1016/j.heliyon.2024.e33636

Martín-Saavedra, F., Ruiz-Hernández, E., Escudero-Duch, C., Prieto, M., Arruebo, M., Sadeghi, N., Deckers, R., Storm, G., Hennink, W. E., Santamaría, J., & Vilaboa, N. (2017). Lipogels responsive to near-infrared light for the triggered release of therapeutic agents. *Acta Biomaterialia*, *61*, 54–65. https://doi.org/10.1016/j.actbio.2017.08.010

Mendez-Pfeiffer, P., Juarez, J., Hernandez, J., Taboada, P., Virués, C., Valencia, D., & Velazquez, C. (2021). Nanocarriers as drug delivery systems for propolis: A therapeutic approach. *Journal of Drug Delivery Science and Technology*, *65*, 102762. https://doi.org/https://doi.org/10.1016/j.jddst.2021.102762

Mergen Duymaz, G., Duz, G., Ozkan, K., Karadag, A., Yilmaz, O., Karakus, A., Cengiz, O., Akyildiz, I. E., Basdogan, G., Damarlı, E., & Sagdic, O. (2024). The evaluation of L-arginine solution as a solvent for propolis extraction: The phenolic profile, antioxidant, antibacterial activity, and in vitro bioaccessibility. *Food Science and Nutrition*, *December 2023*, 2724–2735. https://doi.org/10.1002/fsn3.3953

Midekessa, G., Godakumara, K., Ord, J., Viil, J., Lättekivi, F., Dissanayake, K., Kopanchuk, S., Rinken, A., Andronowska, A., Bhattacharjee, S., Rinken, T., & Fazeli, A. (2020). Zeta Potential of Extracellular Vesicles: Toward Understanding the Attributes that Determine Colloidal Stability. *ACS Omega*, *5*(27), 16701–16710. https://doi.org/10.1021/acsomega.0c01582

Minekus, M., Alminger, M., Alvito, P., Ballance, S., Bohn, T., Bourlieu, C., Carrière, F., Boutrou, R., Corredig, M., Dupont, D., Dufour, C., Egger, L., Golding, M., Karakaya, S., Kirkhus, B., Le Feunteun, S., Lesmes, U., MacIerzanka, A., MacKie, A., … Brodkorb, A. (2014). A standardised static in vitro digestion method suitable for food-an international consensus. *Food and Function*, *5*(6), 1113–1124. https://doi.org/10.1039/c3fo60702j

Mirbagheri, M. S., Akhavan-Mahdavi, S., Hasan, A., Kharazmi, M. S., & Jafari, S. M. (2023). Propolis-loaded nanofiber scaffolds based on polyvinyl alcohol and polycaprolactone. *International Journal of Pharmaceutics*, *642*, 123186. https://doi.org/https://doi.org/10.1016/j.ijpharm.2023.123186

Mkam Tsengam, I. K., Omarova, M., Kelley, E. G., McCormick, A., Bothun, G. D., Raghavan, S. R., & John, V. T. (2022). Transformation of Lipid Vesicles into Micelles by Adding Nonionic Surfactants: Elucidating the Structural Pathway and the Intermediate Structures. *Journal of Physical Chemistry B*, *126*(11), 2208–2216. https://doi.org/10.1021/acs.jpcb.1c09685

Moreira, H. R., Munarin, F., Gentilini, R., Visai, L., Granja, P. L., Tanzi, M. C., & Petrini, P. (2014). Injectable pectin hydrogels produced by internal gelation: PH dependence of gelling and rheological properties. *Carbohydrate Polymers*, *103*(1), 339–347. https://doi.org/10.1016/j.carbpol.2013.12.057

Mortensen, A., Aguilar, F., Crebelli, R., Domenico, A. Di, Dusemund, B., Frutos, M. J., Galtier, P., Gott, D., Gundert-Remy, U., Leblanc, J., Lindtner, O., Moldeus, P., Mosesso, P., Parent-Massin, D., Oskarsson, A., Stankovic, I., Waalkens-Berendsen, I., Woutersen, R. A., Wright, M., … Lambré, C. (2016). Re-evaluation of ammonium phosphatides (E 442) as a food additive. *EFSA Journal*, *14*(11). https://doi.org/10.2903/j.efsa.2016.4597

Mourtas, S., Haikou, M., Theodoropoulou, M., Tsakiroglou, C., & Antimisiaris, S. G. (2008). The effect of added liposomes on the rheological properties of a hydrogel: A systematic study. *Journal of Colloid and Interface Science*, *317*(2), 611–619. https://doi.org/10.1016/j.jcis.2007.09.070

Mousavi, S. F., Koocheki, A., Ghorani, B., & Mohebbi, M. (2025). Physicochemical characteristics of liposomal curcumin immobilized in hybrid alginate/ Alyssum homocarpum seed gum hydrogels by electro-hydrodynamic atomization. *Food Hydrocolloids*, *163*, 111081. https://doi.org/https://doi.org/10.1016/j.foodhyd.2025.111081

Nair, R., & Roy Choudhury, A. (2020). Synthesis and rheological characterization of a novel shear thinning levan gellan hydrogel. *International Journal of Biological Macromolecules*, *159*, 922–930. https://doi.org/10.1016/j.ijbiomac.2020.05.119

Naji-Tabasi, S., Shahidi-Noghabi, M., & Dovom, A. M. (2023). Investigating the fabrication and functional properties of new composite hydrogels containing gellan/ alginate/ xanthan gum. *Journal of Sol-Gel Science and Technology*, *105*(3), 637–649. https://doi.org/10.1007/s10971-022-06014-5

Nakamura, F., Ohta, R., Machida, Y., & Nagai, T. (1996). In vitro and in vivo nasal mucoadhesion of some water-soluble polymers. *International Journal of Pharmaceutics*, *134*(1–2), 173–181. https://doi.org/10.1016/0378-5173(95)04416-7

Nascimento, L. G. L., Casanova, F., Silva, N. F. N., Teixeira, A. V. N. de C., & de Carvalho, A. F. (2020). Casein-based hydrogels: A mini-review. *Food Chemistry*, *314*, 126063. https://doi.org/10.1016/j.foodchem.2019.126063

Németh, Z., Csóka, I., Semnani Jazani, R., Sipos, B., Haspel, H., Kozma, G., Kónya, Z., & Dobó, D. G. (2022). Quality by Design-Driven Zeta Potential Optimisation Study of Liposomes with Charge Imparting Membrane Additives. *Pharmaceutics*, *14*(9). https://doi.org/10.3390/pharmaceutics14091798

Nna, V. U., Abu Bakar, A. B., Md Lazin, M. R. M. L., & Mohamed, M. (2018). Antioxidant, anti-inflammatory and synergistic anti-hyperglycemic effects of Malaysian propolis and metformin in streptozotocin–induced diabetic rats. *Food and Chemical Toxicology*, *120*, 305–320. https://doi.org/https://doi.org/10.1016/j.fct.2018.07.028

Nori, M. P., Favaro-Trindade, C. S., Matias de Alencar, S., Thomazini, M., de Camargo Balieiro, J. C., & Contreras Castillo, C. J. (2011). Microencapsulation of propolis extract by complex coacervation. *Lwt*, *44*(2), 429–435. https://doi.org/10.1016/j.lwt.2010.09.010

Norn, V. (2014). *"Ammonium phosphatides." Emulsifiers in Food Technology*. 61–72. https://doi.org/10.1111/j.1471-0307.2006.00224.x

Ortan, A., Parvu, C. D., Ghica, M. V., Popescu, L. M., & Ionita, L. (2011). Rheological study of a liposomal hydrogel based on carbopol. *Romanian Biotechnological Letters*, *16*(1 SUPPL.), 47–54.

Owczarz, P., Rył, A., & Wichłacz, Ż. (2019). Application of texture profile analysis to investigate the mechanical properties of thermosensitive injectable chitosan

hydrogels. *Progress on Chemistry and Application of Chitin and Its Derivatives*, *24*, 151–163. https://doi.org/10.15259/PCACD.24.014

Ozdal, T., Ceylan, F. D., Eroglu, N., Kaplan, M., Olgun, E. O., & Capanoglu, E. (2019). Investigation of antioxidant capacity, bioaccessibility and LC-MS/MS phenolic profile of Turkish propolis. *Food Research International*, *122*(May), 528–536. https://doi.org/10.1016/j.foodres.2019.05.028

Pamunuwa, G. K., & Karunaratne, D. N. (2022). Liposomal Delivery of Plant Bioactives Enhances Potency in Food Systems: A Review. *Journal of Food Quality*, *2022*(1), 5272592. https://doi.org/https://doi.org/10.1155/2022/5272592

Pasarin, D., Ghizdareanu, A.-I., Enascuta, C. E., Matei, C. B., Bilbie, C., Paraschiv-Palada, L., & Veres, P.-A. (2023). Coating Materials to Increase the Stability of Liposomes. *Polymers*, *15*(3). https://doi.org/10.3390/polym15030782

Patel, D., & Patel, N. (2020). Fabrication and characterization of sterically stabilized liposomes of topotecan. *Future Journal of Pharmaceutical Sciences*, *6*(1). https://doi.org/10.1186/s43094-020-00089-z

Paun, V. A., Popa, M., Desbrieres, J., Peptu, C. A., Dragan, S. V., Zegan, G., & Cioca, G. (2016). Liposome loaded chitosan hydrogels, a promising way to reduce the burst effect in drug release a comparativ analysis. *Materiale Plastice*, *53*(4), 590–593.

Pippa, N., Perinelli, D. R., Pispas, S., Bonacucina, G., Demetzos, C., Forys, A., & Trzebicka, B. (2018). Studying the colloidal behavior of chimeric liposomes by cryo-TEM, micro-differential scanning calorimetry and high-resolution ultrasound spectroscopy. *Colloids and Surfaces A: Physicochemical and Engineering Aspects*, *555*(June), 539–547. https://doi.org/10.1016/j.colsurfa.2018.07.025

Qu, Y., Tang, J., Liu, L., Song, L., Chen, S., & Gao, Y. (2019). α-Tocopherol liposome loaded chitosan hydrogel to suppress oxidative stress injury in cardiomyocytes. *International Journal of Biological Macromolecules*, *125*, 1192–1202. https://doi.org/https://doi.org/10.1016/j.ijbiomac.2018.09.092

Rahman Khan, M. A., Amin, M. R., Rahman, M., Abdul Rub, M., Hoque, M. A., Khan, M. A., & Asiri, A. M. (2019). Influence of Different Additives on the Clouding Nature and Thermodynamic Behavior of Tween 80 Solution in the Absence and Presence of the Amikacin Sulfate Drug. *Journal of Chemical and Engineering Data*, *64*(2), 668–675. https://doi.org/10.1021/acs.jced.8b00897

Rahman, M. S., & Al-Mahrouqi, A. I. (2009). Instrumental texture profile analysis of gelatin gel extracted from grouper skin and commercial (bovine and porcine) gelatin gels. *International Journal of Food Sciences and Nutrition*, *60*(SUPPL. 7), 229–242. https://doi.org/10.1080/09637480902984414

Ramesh, S., Kovelakuntla, V., & Meyer, A. S. (2021). Three-dimensional printing of stimuli-responsive hydrogel with antibacterial activity. *Bioprinting*, *24*(October 2020), e00106. https://doi.org/10.1016/j.bprint.2020.e00106

Ramli, N. A., Ali, N., Hamzah, S., & Yatim, N. I. (2021). Physicochemical characteristics of liposome encapsulation of stingless bees' propolis. *Heliyon*, *7*(4), e06649. https://doi.org/10.1016/j.heliyon.2021.e06649

Re, R., Pellegrini, N., Proteggente, A., Pannala, A., Yang, M., & Catherina, R.-E. (1999). Antioxidant activity applying an improved ABTS radical cation decolorization assay. *Free Radical Biology & Medicine*, *26*, 1231–1237.

Refaat, H., Mady, F. M., Sarhan, H. A., Rateb, H. S., & Alaaeldin, E. (2021). Optimization and evaluation of propolis liposomes as a promising therapeutic approach for COVID-19. *International Journal of Pharmaceutics*, *592*(September 2020), 120028. https://doi.org/10.1016/j.ijpharm.2020.120028

Righi, A. A., Negri, G., & Salatino, A. (2013). Comparative chemistry of propolis from eight brazilian localities. *Evidence-Based Complementary and Alternative Medicine*, *2013*. https://doi.org/10.1155/2013/267878

Ruozi, B., Belletti, D., Tombesi, A., Tosi, G., Bondioli, L., Forni, F., & Vandelli, M. A. (2011). AFM, ESEM, TEM, and CLSM in liposomal characterization: a comparative study. *International Journal of Nanomedicine*, *6*, 557–563. https://doi.org/10.2147/ijn.s14615

Russo, A., Cardile, V., Sanchez, F., Troncoso, N., Vanella, A., & Garbarino, J. A. (2004). Chilean propolis: antioxidant activity and antiproliferative action in human tumor cell lines. *Life Sciences*, *76*(5), 545–558. https://doi.org/https://doi.org/10.1016/j.lfs.2004.07.019

Sarabandi, K., Mahoonak, A. S., Hamishehkar, H., Ghorbani, M., & Jafari, S. M. (2019). Protection of casein hydrolysates within nanoliposomes: Antioxidant and stability characterization. *Journal of Food Engineering*, *251*(January), 19–28. https://doi.org/10.1016/j.jfoodeng.2019.02.004

Saroglu, O., Atalı, B., Yıldırım, R. M., & Karadag, A. (2022). Characterization of nanoliposomes loaded with saffron extract: in vitro digestion and release of crocin. *Journal of Food Measurement and Characterization*, *16*(6), 4402–4415. https://doi.org/10.1007/s11694-022-01526-8

Seibert, J. B., Bautista-Silva, J. P., Amparo, T. R., Petit, A., Pervier, P., dos Santos Almeida, J. C., Azevedo, M. C., Silveira, B. M., Brandão, G. C., de Souza, G. H. B., de Medeiros Teixeira, L. F., & dos Santos, O. D. H. (2019). Development of propolis nanoemulsion with antioxidant and antimicrobial activity for use as a potential natural preservative. *Food Chemistry*, *287*, 61–67. https://doi.org/https://doi.org/10.1016/j.foodchem.2019.02.078

Sevinç-Özakar, R., Seyret, E., Özakar, E., & Adıgüzel, M. C. (2022). Nanoemulsion-Based Hydrogels and Organogels Containing Propolis and Dexpanthenol: Preparation, Characterization, and Comparative Evaluation of Stability, Antimicrobial, and Cytotoxic Properties. *Gels*, *8*(9). https://doi.org/10.3390/gels8090578

Shahab-Navaei, F., & Asoodeh, A. (2023). Synthesis of optimized propolis solid lipid nanoparticles with desirable antimicrobial, antioxidant, and anti-cancer properties. *Scientific Reports*, *13*(1), 18290. https://doi.org/10.1038/s41598-023-45768-y

Shakoury, N., Aliyari, M. A., Salami, M., Emam-Djomeh, Z., Vardhanabhuti, B., & Moosavi-Movahedi, A. A. (2022). Encapsulation of propolis extract in whey protein nanoparticles. *Lwt*, *158*(September 2021), 113138. https://doi.org/10.1016/j.lwt.2022.113138

Shen, W., Ye, Q., Zhang, H., Xie, S., Xie, S., Chen, C., Liu, J., Huang, Z., Luo, H.-B., & Guo, L. (2025). A Tea Polyphenol-Infused Sprayable Thermosensitive Liposomal Hydrogel for Enhanced Anti-Inflammatory and Antibacterial Psoriasis Treatment. *Journal of Functional Biomaterials*, *16*(4). https://doi.org/10.3390/jfb16040124

Singleton, V. L., & Rossi, J. A. (1965). Colorimetry of Total Phenolics with Phosphomolybdic-Phosphotungstic Acid Reagents. *American Journal of Enology and Viticulture*, *16*(3), 144 LP – 158.

Stalmach, A. (2014). Chapter 42 - Bioavailability of Dietary Anthocyanins and Hydroxycinnamic Acids. In R. R. Watson, V. R. Preedy, & S. Zibadi (Eds.), *Polyphenols in Human Health and Disease* (pp. 561–576). Academic Press. https://doi.org/https://doi.org/10.1016/B978-0-12-398456-2.00042-6

Stevens, J. F., & Maier, C. S. (2016). The chemistry of gut microbial metabolism of polyphenols. *Phytochemistry Reviews*, *15*(3), 425–444. https://doi.org/10.1007/s11101-016-9459-z

Šturm, L., Osojnik Črnivec, I. G., Istenič, K., Ota, A., Megušar, P., Slukan, A., Humar, M., Levic, S., Nedović, V., Kopinč, R., Deželak, M., Pereyra Gonzales, A., & Poklar Ulrih, N. (2019). Encapsulation of non-dewaxed propolis by freeze-drying and spray-drying using gum Arabic, maltodextrin and inulin as coating materials. *Food and Bioproducts Processing*, *116*, 196–211. https://doi.org/10.1016/j.fbp.2019.05.008

Sun, C., Wu, Z., Wang, Z., & Zhang, H. (2015). Effect of ethanol/water solvents on phenolic profiles and antioxidant properties of Beijing propolis extracts. *Evidence-Based Complementary and Alternative Medicine*, *2015*. https://doi.org/10.1155/2015/595393

Szczesniak, A. S. (2002). Texture is a sensory property. *Food Quality and Preference*, *13*(4), 215–225. https://doi.org/https://doi.org/10.1016/S0950-3293(01)00039-8

Tai, K., He, X., Yuan, X., Meng, K., Gao, Y., & Yuan, F. (2017). A comparison of physicochemical and functional properties of icaritin-loaded liposomes based on different surfactants. *Colloids and Surfaces A: Physicochemical and Engineering Aspects*, *518*(17), 218–231. https://doi.org/10.1016/j.colsurfa.2017.01.019

Tan, C., Xue, J., Abbas, S., Feng, B., Zhang, X., & Xia, S. (2014). Liposome as a delivery system for carotenoids: Comparative antioxidant activity of carotenoids as measured by ferric reducing antioxidant power, DPPH assay and lipid peroxidation. *Journal of Agricultural and Food Chemistry*, *62*(28), 6726–6735. https://doi.org/10.1021/jf405622f

Tantipolphan, R., Rades, T., & Medlicott, N. J. (2009). Swelling lecithin: Cholesterol implants for the controlled release of proteins. *Journal of Liposome Research*, *19*(1), 37–48. https://doi.org/10.1080/08982100802636434

Tasi, L. M., Liu, D. Z., & Chen, W. Y. (2003). Microcalorimetric investigation of the interaction of polysorbate surfactants with unilamellar phosphatidylcholines liposomes. *Colloids and Surfaces A: Physicochemical and Engineering Aspects*, *213*(1), 7–14. https://doi.org/10.1016/S0927-

7757(02)00287-X

Tavares, L., Smaoui, S., Lima, P. S., de Oliveira, M. M., & Santos, L. (2022). Propolis: Encapsulation and application in the food and pharmaceutical industries. *Trends in Food Science & Technology*, *127*, 169–180. https://doi.org/https://doi.org/10.1016/j.tifs.2022.06.003

Thirawong, N., Nunthanid, J., Puttipipatkhachorn, S., & Sriamornsak, P. (2007). Mucoadhesive properties of various pectins on gastrointestinal mucosa: An in vitro evaluation using texture analyzer. *European Journal of Pharmaceutics and Biopharmaceutics*, *67*(1), 132–140. https://doi.org/10.1016/j.ejpb.2007.01.010

Toker, O. S., Karasu, S., Yilmaz, M. T., & Karaman, S. (2015). Three interval thixotropy test (3ITT) in food applications: A novel technique to determine structural regeneration of mayonnaise under different shear conditions. *Food Research International*, *70*, 125–133. https://doi.org/10.1016/j.foodres.2015.02.002

Toro-Uribe, S., Ibáñez, E., Decker, E. A., McClements, D. J., Zhang, R., López-Giraldo, L. J., & Herrero, M. (2018). Design, Fabrication, Characterization, and in Vitro Digestion of Alkaloid-, Catechin-, and Cocoa Extract-Loaded Liposomes. *Journal of Agricultural and Food Chemistry*, *66*(45), 12051–12065. https://doi.org/10.1021/acs.jafc.8b04735

Tu, Y., Ning, Y., Wang, H., Li, Y., Yao, Z., Tao, S., Yang, W., Li, B., Li, X., He, H., & Li, S. (2025). Liposomal nano-encapsulation of bFGF combined with injectable BSA hydrogel for efficient burn wound healing. *Colloids and Surfaces B: Biointerfaces*, *245*, 114263. https://doi.org/https://doi.org/10.1016/j.colsurfb.2024.114263

Ubeyitogullari, A., Ahmadzadeh, S., Kandhola, G., & Kim, J.-W. (2022). Polysaccharide-based porous biopolymers for enhanced bioaccessibility and bioavailability of bioactive food compounds: Challenges, advances, and opportunities. *Comprehensive Reviews in Food Science and Food Safety*, *21*(6), 4610–4639. https://doi.org/https://doi.org/10.1111/1541-4337.13049

Ucar, T. M., & Karadag, A. (2019). The effects of vacuum and freeze-drying on the physicochemical properties and in vitro digestibility of phenolics in oyster mushroom (Pleurotus ostreatus). *Journal of Food Measurement and Characterization*, *13*(3), 2298–2309. https://doi.org/10.1007/s11694-019-00149-w

Ulrich, A. S. (2002). Biophysical Aspects of Using Liposomes as Delivery Vehicles. *Bioscience Reports*, *22*(2), 129–150. https://doi.org/10.1023/A:1020178304031

Vargas Villanueva, J. G., Sarmiento Huertas, P. A., Galan, F. S., Esteban Rueda, R. J., Briceño Triana, J. C., & Casas Rodriguez, J. P. (2019). Bio-adhesion evaluation of a chitosan-based bone bio-adhesive. *International Journal of Adhesion and Adhesives*, *92*, 80–88. https://doi.org/https://doi.org/10.1016/j.ijadhadh.2019.04.009

Wang, A., Leible, M., Lin, J., Weiss, J., & Zhong, Q. (2020). Caffeic Acid Phenethyl Ester Loaded in Skim Milk Microcapsules: Physicochemical Properties and Enhanced in Vitro Bioaccessibility and Bioactivity against

Colon Cancer Cells. *Journal of Agricultural and Food Chemistry*, *68*(50), 14978–14987. https://doi.org/10.1021/acs.jafc.0c05143

Wei, X., Dai, J., Zhong, Y., Zhang, D., Liu, L., Wang, L., Huang, Y. K., Chen, P., Zhou, Z., Chen, X., Yang, X., & Wang, Q. (2021). Caffeic acid phenethyl ester loaded in nano-targeted delivery system with casein: Physicochemical characterization, in vitro release, and binding mechanisms. *Lwt*, *150*(April), 111938. https://doi.org/10.1016/j.lwt.2021.111938

Xavier, A. A. O., & Mariutti, L. R. B. (2021). Static and semi-dynamic in vitro digestion methods: state of the art and recent achievements towards standardization. *Current Opinion in Food Science*, *41*, 260–273. https://doi.org/https://doi.org/10.1016/j.cofs.2021.08.002

Xia, S., & Xu, S. (2005). Ferrous sulfate liposomes: Preparation, stability and application in fluid milk. *Food Research International*, *38*(3), 289–296. https://doi.org/10.1016/j.foodres.2004.04.010

Xiu, A., Zhou, M., Zhu, B., Wang, S., & Zhang, J. (2011). Rheological properties of Salecan as a new source of thickening agent. *Food Hydrocolloids*, *25*(7), 1719–1725. https://doi.org/10.1016/j.foodhyd.2011.03.013

Xu, P., Song, J., Dai, Z., Xu, Y., Li, D., & Wu, C. (2021). Effect of Ca2+ cross-linking on the properties and structure of lutein-loaded sodium alginate hydrogels. *International Journal of Biological Macromolecules*, *193*(PA), 53–63. https://doi.org/10.1016/j.ijbiomac.2021.10.114

Xu, X., Tian, M., Deng, L., Jiang, H., Han, J., Zhen, C., Huang, L., & Liu, W. (2023). Structural degradation and uptake of resveratrol-encapsulated liposomes using an in vitro digestion combined with Caco-2 cell absorption model. *Food Chemistry*, *403*(January 2022), 133943. https://doi.org/10.1016/j.foodchem.2022.133943

Yang, Z., McClements, D. J., Li, C., Sang, S., Chen, L., Long, J., Qiu, C., & Jin, Z. (2023). Targeted delivery of hydrogels in human gastrointestinal tract: A review. *Food Hydrocolloids*, *134*, 108013. https://doi.org/https://doi.org/10.1016/j.foodhyd.2022.108013

Yen, C. H., Chiu, H. F., Wu, C. H., Lu, Y. Y., Han, Y. C., Shen, Y. C., Venkatakrishnan, K., & Wang, C. K. (2017). Beneficial efficacy of various propolis extracts and their digestive products by in vitro simulated gastrointestinal digestion. *Lwt*, *84*, 281–289. https://doi.org/10.1016/j.lwt.2017.05.074

Yesiltas, B., Capanoglu, E., Firatligil-Durmus, E., Sunay, A. E., Samanci, T., & Boyacioglu, D. (2014). Investigating the in-vitro bioaccessibility of propolis and pollen using a simulated gastrointestinal digestion System. *Journal of Apicultural Research*, *53*(1), 101–108. https://doi.org/10.3896/IBRA.1.53.1.10

Yun, P., Devahastin, S., & Chiewchan, N. (2021). Microstructures of encapsulates and their relations with encapsulation efficiency and controlled release of bioactive constituents: A review. *Comprehensive Reviews in Food Science and Food Safety*, *20*(2), 1768–1799. https://doi.org/https://doi.org/10.1111/1541-4337.12701

Zhang, J., Han, J., Ye, A., Liu, W., Tian, M., Lu, Y., Wu, K., Liu, J., & Lou, M. P. (2019). Influence of Phospholipids Structure on the Physicochemical Properties and In Vitro Digestibility of Lactoferrin-Loaded Liposomes. *Food Biophysics*, *14*(3), 287–299. https://doi.org/10.1007/s11483-019-09581-3

Zheng, Y. Z., Deng, G., Chen, D. F., Liang, Q., Guo, R., & Fu, Z. M. (2018). Theoretical studies on the antioxidant activity of pinobanksin and its ester derivatives: Effects of the chain length and solvent. *Food Chemistry*, *240*(May 2017), 323–329. https://doi.org/10.1016/j.foodchem.2017.07.133

Zhishen, J., Mengcheng, T., & Jianming, W. (1999). The determination of flavonoid contents in mulberry and their scavenging effects on superoxide radicals. In *Food Chemistry* (Vol. 64, Issue 4, pp. 555–559). https://doi.org/10.1016/S0308-8146(98)00102-2

Zhu, L., Qiu, J., Sakai, E., & Ito, K. (2017). Rapid Recovery Double Cross-Linking Hydrogel with Stable Mechanical Properties and High Resilience Triggered by Visible Light. *ACS Applied Materials & Interfaces*, *9*(15), 13593–13601. https://doi.org/10.1021/acsami.7b01003

PUBLICATIONS FROM THE THESIS

Conference Papers

1. Saroğlu, Ö., Karadağ, A., Tekin Çakmak, Z. H., & Karasu, S., (2024). Investigating the Rheological, Microstructural, and Textural Properties of Liposomal Gels Derived from Salep and Xanthan Gum . International Food Innovation and Sustainability Congress (pp.118-119). İstanbul, Turkey

Papers

1. Saroğlu, Ö., Karadağ, A., Cakmak, Z. H., & Karasu, S., (2023). The formulation and microstructural, rheological, and textural characterization of salep-xanthan gum-based liposomal gels. POLYMER BULLETIN , vol.80, no.9, 9941-9962.

2. Saroglu, O., Karakas, C. Y., Yildirim, R. M., Erdem, O., Karasu, S., Sagdic, O., & Karadag, A. (2025). Liposomal propolis loaded xanthan gum-salep hydrogels: Preparation, characterization, and in vitro bioaccessibility of phenolics. International Journal of Biological Macromolecules, 140323.

3. Saroglu, Ö & Karadağ, A., (2024). Propolis-loaded liposomes: characterization and evaluation of the in vitro bioaccessibility of phenolic compounds. ADMET and DMPK , vol.12, no.1, 209-224.